Dissertation zur Erlangung des Doktorgrades

der Fakultät für Chemie und Pharmazie

der Ludwig-Maximilians-Universität München

Functional characterization of HCN2 channels in the septo-hippocampal system

Saskia Christina Spahn

aus

Würzburg

Deutschland

2015

Für meine Familie

Erklärung

Diese Dissertation wurde im Sinne von § 7 der Promotionsordnung vom 28. November 2011 von Herrn Prof. Dr. Christian Wahl-Schott betreut.

Eidesstattliche Versicherung

Diese Dissertation wurde eigenständig und ohne unerlaubte Hilfe erarbeitet.

München, den 11. Juni 2015

Saskia Spahn

Dissertation eingereicht am	19.06.2015
1. Gutachter	Prof. Dr. Christian Wahl-Schott
2. Gutachter	Prof. Dr. Martin Biel
Mündliche Prüfung am	28.07.2015

Table of contents

1 Introduction

'How can I find my way through a complex environment?' – The work of last year's Nobel laureates, John O'Keefe, May-Britt and Edvard Moser contributed substantially to clarify this essential issue. These scientists discovered a positioning system in the brain that constitutes the basis for orientation in space. The hippocampal formation, including the hippocampus and the entorhinal cortex (EC), is an important brain area involved in this orientation system. Specialized neuronal cells, called place cells and grid are crucially involved in spatial navigation (Fig. 1).

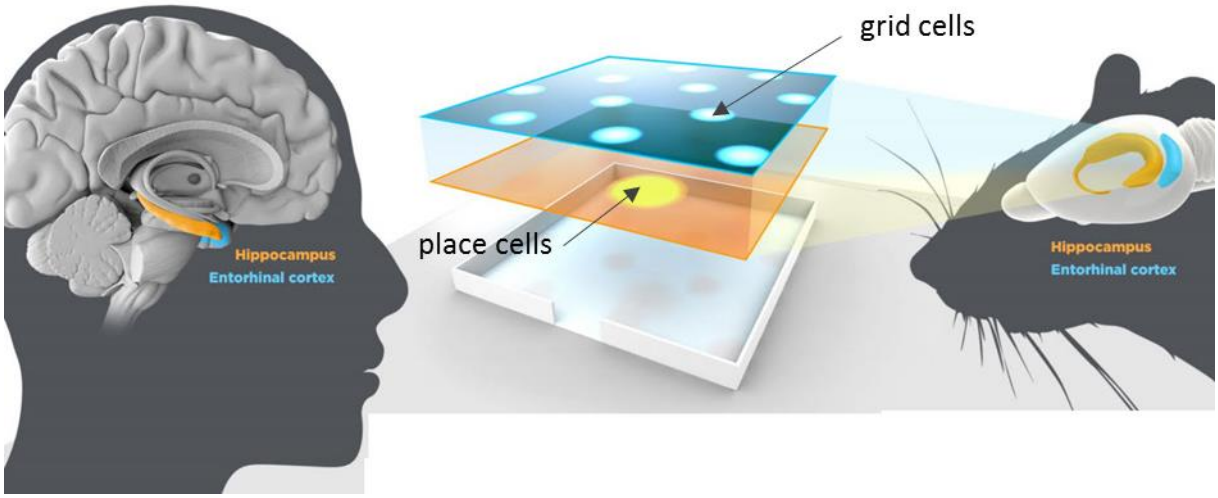

Figure 1 Function of place and grid cells

A schema of the function of place cells in the hippocampus (yellow) and grid cells in the EC (blue). Place cells fire at particular locations in the environment. Every place cell is activated at a different place. A single grid cell fires when the animal or human reaches particular locations and these locations are arranged in a hexagonal pattern.

Adapted from © 2014 The Nobel Committee for Physiology or Medicine; Illustration and layout: Mattias Karlén

The firing of these neurons is strongly modulated by the theta rhythm, one of the most important oscillations in the mammalian brain firing in the frequency range of 4 to 12Hz [4-6]. These oscillations are critically involved in the controlling of neuronal networks and the communication between different brain areas. Theta waves are particularly present during wake, especially during activity states, such as walking or exploratory sniffing and also during

rapid eye movement (REM) sleep [1]. At REM sleep onset, waves characteristic for non-rapid eye movement (NREM) sleep (sharp ripple waves) are terminated and the oscillation pattern is switched to theta waves within the hippocampus. This theta band is maintained during the whole REM sleep episode (Fig. 2).

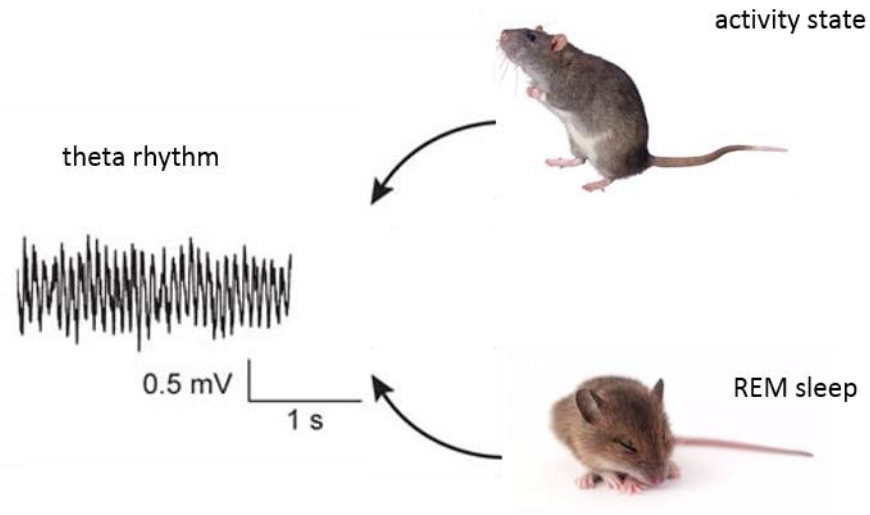

Figure 2 Exemplary theta trace and behaviors associated with this oscillation

The trace shows theta waves in the frequency range of 4 to 12Hz recorded from the hippocampus occurring primarily during activity states and REM sleep.

Modified from [2] and images from: http://mentalfloss.com and http://www.shutterstock.com

Theta rhythm generation and modulation originates from brainstem (BS) nuclei and depends critically on projections from medial septum (MS). MS receives input from deeper brain areas via two different pathways. The direct pathway which projects directly from BS to MS [58, 59] and the indirect one which passes the hypothalamus (HT) [60] (Fig. 3). MS GABAergic neurons inhibit hippocampal GABAergic (inhibitory) interneurons, which in turn target principal neurons of the hippocampal formation. Thus MS GABAergic neurons contribute to induce theta rhythms within the hippocampus by transmitting a disinhibitory signal to hippocampal pyramidal cells [3]. In previous studies it could be shown that stimulation of MS neurons drives theta rhythm [2] and MS lesions eliminate theta rhythm in the hippocampal formation [3, 4]. Consequently MS has been designated as pacemaker for the theta rhythm [5].

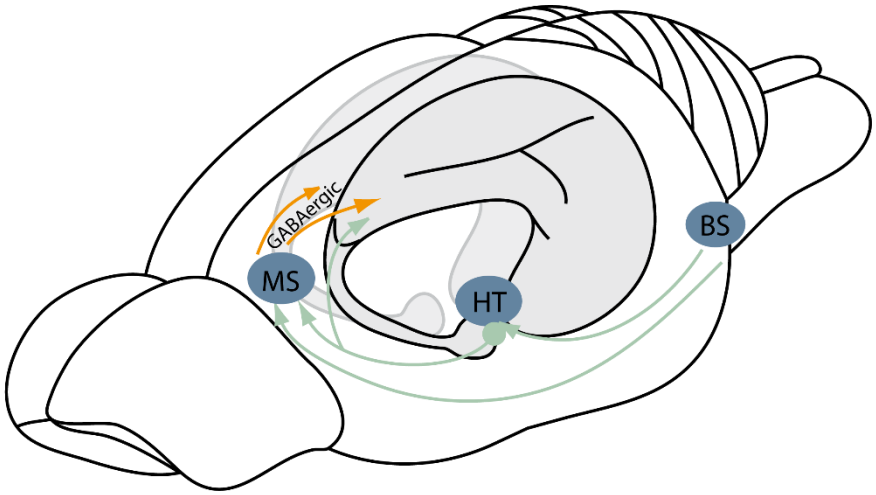

Figure 3 Pathways regulating theta oscillations

Direct and indirect pathways mediating the activation of medial septum (MS). Both pathways originate from the brainstem (BS), the indirect one passes the hypothalamus (HT), the direct one goes directly to MS. GABAergic neurons in MS project to the hippocampal formation.

Modified from [4]

The circuits involved in generating theta rhythm are well studied, but it is little known how ion channels contribute to the electrical activity pattern of single cells involved in the regulation mechanism. In this context the expression of hyperpolarization-activated cyclic nucleotide-gated cation (HCN) channels within the MS could be highly relevant, since it is known that they contribute to the regulation of rhythmic bursting and network oscillations in various brain areas [5-8]. Consistent with this hypothesis, preliminary evidence suggests that selective blocking of HCN channels within MS neurons reduces the firing activity of septo-hippocampal GABAergic neurons *in vivo* [9]. As septo-hippocampal GABAergic neurons projections lead to an induction of brain activity in hippocampal pyramidal cells, a HCN channel blockade could lead to an inhibition of these cells and thus to a reduction of the theta rhythm.

HCN channels belong to the superfamily of voltage gated pore-loop cation channels and are activated by hyperpolarization [10, 11]. The current produced by HCN channels, I_h has been termed as pacemaker current because of its importance for controlling the rhythmic activity of cardiac cells and neurons [12-20]. I_h is a mixed cationic current carried by Na^+ and K^+ and its activation is modulated by cAMP [21, 22].

It is known that HCN channels contribute via several mechanisms to the regulation of excitability and electrical activity of neurons. HCN channels are constitutively open at rest and pass a depolarizing inward current, playing a role in determining the membrane potential in many neurons. Furthermore HCN channels may counteract both, membrane hyperpolarization by conducting a depolarizing inward current (caused by I_h channel activation) and depolarization by facilitating hyperpolarization (due to I_h channel deactivation), thus HCN channels demonstrate a negative-feedback property [11]. As a consequence HCN channels are able to reduce inhibitory and excitatory stimuli leading to a stabilization of the membrane potential. The relation between the activation curve and the reversal potential of I_h is responsible for this characteristic because the reversal potential of I_h declines close to the base of its activation curve. Hyperpolarization augments the number of open HCN channels and the depolarizing inward current causes a membrane potential of initial values near the resting membrane potential (depolarizing voltage sag). In contrast depolarization leads to deactivation of the I_h and thereby causes a loss of the tonic depolarizing current (hyperpolarizing voltage sag) and returns membrane potential back to rest [11]. In addition there is evidence that I_h facilitates resonance and network oscillations crucially involved in information processing in neuronal circuits. The most extensively studied system regarding neuronal oscillations is the thalamo-cortical system, which operates in two distinct firing modes, transmission mode and burst mode (Fig. 4A). During burst mode there is an interaction of a low-threshold Ca^{2+} current (I_T), conferred by T-Type Ca^{2+} channels, and I_h. Hyperpolarization activates I_h leading to a depolarization of the membrane potential and causes an activation of I_T. Further membrane depolarization facilitates a threshold for a burst of Na^+ and K^+ dependent action potentials. Repolarization, caused by I_T deactivation, is followed again by hyperpolarization and by an activation of I_h. The cycle repeats again and continuous rhythmic burst firing is sustained (Fig. 4B) [11]. The time course of activation of HCN channels determines the frequency of membrane potential rhythms [7, 8] and the sensitivity is adjusted by neurotransmitters modulating cAMP levels. The transition between burst mode and transition mode is highly controlled by neurotransmitters and neuropeptides that elevate cAMP levels leading to an enhancement of I_h activity [23]. Pathological alterations in this process are associated with the generation of epileptic seizures [24]. It could be demonstrated previously that an absence of HCN channels leads to an increased oscillatory

activity in the thalamo-cortical network and thus to spike and wave discharges (SWDs), the major feature of absence epilepsy [25].

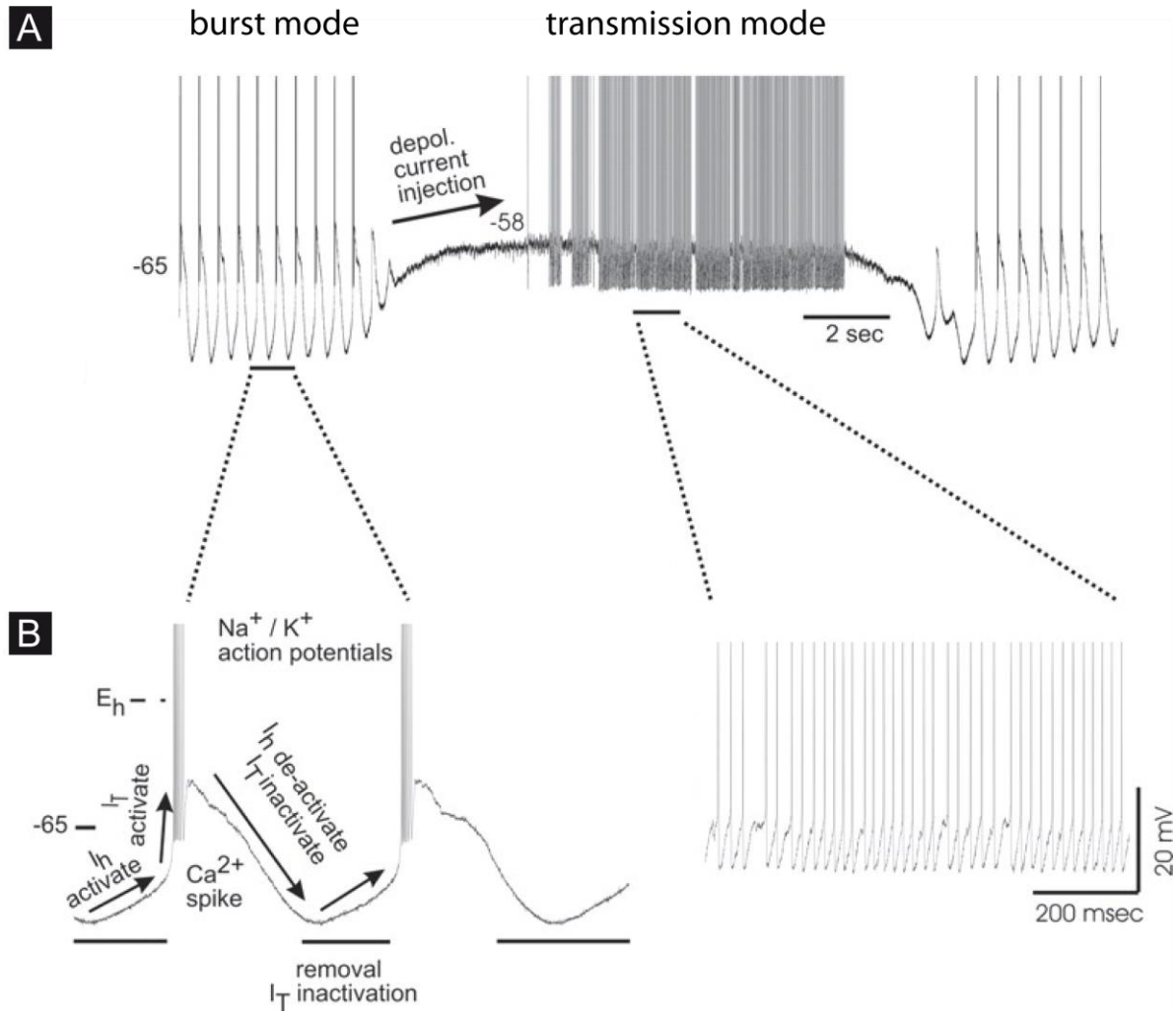

Figure 4 The involvement of I_h in the generation of thalamic oscillations

(A) Thalamic neurons generate spontaneously rhythmic bursts of action potentials due to the interaction of I_T and I_h. Depolarizing the neuron leads to a change of the firing mode from rhythmic burst firing to tonic action potential generation. Removal of the depolarization leads again to rhythmic burst firing. (B) Detailed view of rhythmic burst firing mode (left panel) and tonic firing mode (right panel).

Adapted from [11]

HCN channels consist of four subunits forming homotetramers or heterotetramers. Each HCN channel subunit is composed of the transmembrane core, the cytosolic N-terminal and the C-terminal domain. The transmembrane channel core consists of six α-helical segments (S1-S6)

and an ion-conducting pore loop between S5 and S6. The pore contains the glycine-tyrosine-glycine (GYG) motif that represents the characteristic selectivity filter in K^+ channels [26]. The C-terminus contains a cyclic nucleotide binding domain (CNBD), which is connected to the S6 segment via the C-Linker [27]. Direct cAMP binding to the CNBD affects the voltage dependent activation of HCN channels. The C-linker of the CNBD is an autoinhibitory domain that lowers open probability in the absence of cAMP. Binding of cAMP increases channel activity by removing tonic channel inhibition that is conferred by this domain. That means the binding of cAMP leads to a shift of the voltage dependence of activation towards more positive values. For the voltage sensitivity of HCN channels the positively charged S4 segment is responsible. It carries nine arginine or lysine residues regularly spaced at every third position [28, 29] (Fig. 5).

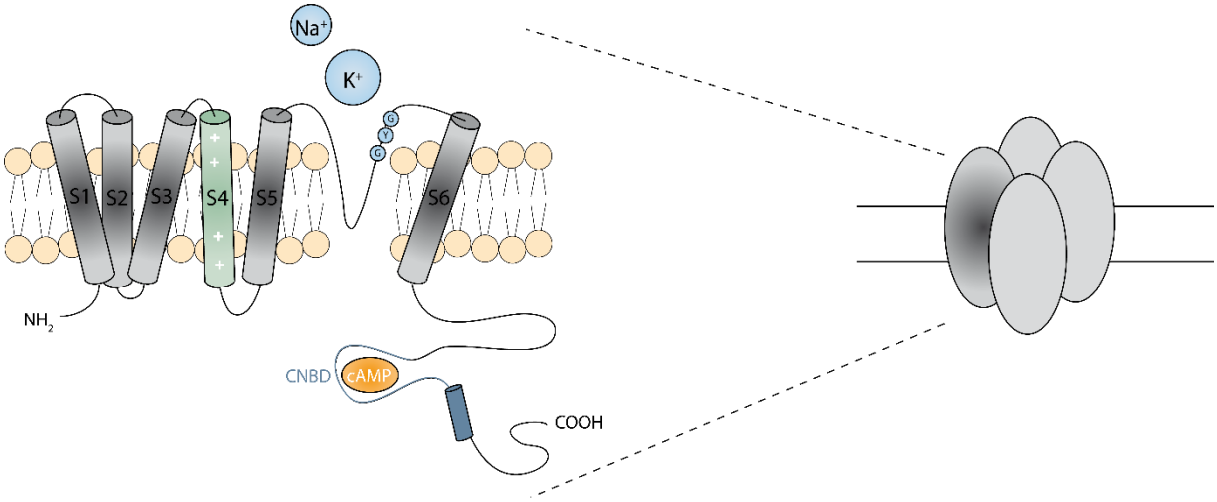

Figure 5 Structure of HCN channels

HCN channels consist of four homologous subunits. Each subunit consists of six α-helical transmembrane segments (S1-S6) containing the voltage sensor (S4) and the pore between segment S5 and S6, including the selectivity filter (GYG). N- and C-terminus are localized intracellularly. The C-Terminus consists of three parts, the C-Linker, the CNBD and the sequence downstream of the CNBD.

There is evidence that HCN channels contain auxiliary proteins in addition to the principal pore-forming subunits. These auxiliary proteins are required for modifying electrophysiological properties, the functional coupling to signaling pathways and trafficking to specific cellular compartments. An important auxiliary protein is the MinK-related protein

MiRP1. It interacts with several HCN channel types and increases current densities. The transmembrane protein KCR1 was reported to interact with HCN2. It acts as an inhibitory auxiliary subunit of HCN channels and serves as a regulator of cardiac automaticity. An important neuronal auxiliary subunit of HCN1 channels is TRIP8b (TPR-containing Rab8b-interacting protein), an accessory protein that determines the cell surface expression and dendritic localization of the channel and reduces the cyclic nucleotide dependence of HCN1 channels [30]

The HCN channel family comprises four isoforms (HCN1-4). The members of the family are characterized by different biophysical properties. HCN1 channels activate quickly on hyperpolarization and are modulated barely by cAMP [31]. HCN2 channels activate more slowly and respond strongly to cAMP [32]. HCN3 has also a moderate activation kinetic and is only weakly affected by cAMP [10] while HCN4 is the slowest channel and shows strong response to cAMP [33, 34].

HCN channels in general are expressed in cardiac cells and in a variety of peripheral and central neurons [35, 36]. Studies examining the mRNA distribution reveal that all four HCN isoforms are expressed throughout the brain, with different distributions and levels. HCN1 mRNA is especially expressed in cortical areas, HCN2 shows a ubiquitous expression at a high level, HCN3 is weakly expressed throughout the brain with higher expression levels in the hypothalamus and olfactory bulb [37] and HCN4 is particularly expressed in subcortical areas [31, 32, 38]. As HCN2 is the dominant subunit expressed in MS neurons, an important structure involved in control and generation of the theta rhythm, it is possible that HCN2 channels are involved in theta rhythm generation [39, 40]. Further initial data reveal that elevation of cAMP in MS neurons results in an increase of hippocampal theta frequency [41] or induction of theta burst firing [42] while a decrease of cAMP levels leads to a reduction of firing activity and theta bursting [43]. As HCN2 is highly regulated by cAMP it is interesting to investigate whether the theta modulating effect in MS neurons via cAMP is HCN2-mediated. So it is essential to clarify which impact a cAMP insensitivity of HCN2 channels would have on theta regulation mechanisms.

It was shown in previous studies that HCN1 has also a slight effect in theta regulating mechanisms. Deletion of HCN1 increases the power of theta oscillations slightly and enhances hippocampal-dependent learning and memory [44]. These findings suggest a direct

involvement of HCN1 channels in suppressing theta frequency activity. It is likely that the theta augmentation is not due to the absence of HCN1 in MS, as HCN1 expression is low in this area and I_h block leads to a reduction of theta power [9]. Possibly its expression within the hippocampus, which may contribute partly to theta regulation, is responsible for this effect.

Furthermore HCN1 has been identified as a determinant of spatial scale in the EC. It is known that the grid cell firing field expanses from dorsal to ventral EC. It was demonstrated that entorhinal cells in HCN1 KO mice show an increased grid field size [45]. However, *in vitro* data of a HCN1 KO model predict an increase in grid cell spacing that is far larger than what was observed *in vivo*. This suggests that the grid spacing *in vivo* is maintained by residual I_h [45-47]. The increase of the grid field size occurs simultaneously with an augmentation in the size of place fields within the hippocampus [48], indicating that the same mechanisms play a role in influencing the scales of grid and place cells. It needs to be determined whether the scale change is induced locally or if it results from a HCN deficiency upstream of the EC and hippocampal region. A promising nucleus could be MS, which has projecting neurons to the hippocampus and EC influencing the theta rhythm. As the HCN2 subunit is highest expressed in MS [39] it can be assumed that this isoform could have a major impact on determining theta frequency within the hippocampal formation.

2 Aim of this study

In this study, the contribution of HCN2 channels to the regulation and control of neuronal oscillations should be investigated. The main focus of this work was to investigate the role of HCN2 within the MS, the pacemaker nucleus for theta regulation. Firstly, the protein expression of HCN2 in the MS should be examined by performing immunohistochemistry staining. To estimate the impact of HCN2 on neuronal rhythms *in vivo* electroencephalography (EEG) measurements should be established and performed. Both, global and MS-restricted HCN2 KO animals should be used for EEG recordings. The MS-selective KO was generated by using an *in vivo* AAV-mediated cre-dependent gene silencing approach in floxed HCN2 mice. To estimate the effect of cAMP-insensitive HCN2 channels on neuronal oscillations, EEG measurements should be performed with HCN2 FEA and EA mutant mice. Both mutants are insensitive to cAMP while the FEA mutant is additionally activated at more positive values in comparison to WT in systems with low basal cAMP levels. The behavioral phenotype of a HCN2 loss in MS neurons should be assessed by conducting the water cross maze (WCM), a behavioral test for assessing spatial memory capabilities. Another important question addressed by this study was to investigate the contribution of HCN2 to the occurrence of absence seizures by performing EEG measurements in global HCN2 KO, FEA and EA animals.

3 Material and methods

3.1 Chemicals, solutions and buffers

Unless indicated otherwise, all used chemicals were obtained from Merck, Roth and Sigma-Aldrich. The quality used standard was pro analysi or for molecular biological use. For all working solutions high pure and deionized water was used (high pure water system Easypure UV/UF, Werner GmbH). Solutions for sensitive applications (e.g. PCR) or solutions for long-term use were autoclaved or sterile filtered.

3.2 Mouse lines

In the present thesis HCN2 knockout (KO,L1) and HCN2 floxed (L2) male mice as well as male mice of the HCN2 mutant lines HCN2 EA and HCN2 FEA including corresponding WT littermates were used. Unlike WT mice, HCN2 L2 mice possess two loxP sites, which flank exon 2 and 3 of the HCN2 gene. In the HCN2-deficient mouse line exon 2 and 3 encoding for the transmembrane segments 2 to 6 and the pore were eliminated via cre-mediated deletion [25]. The HCN2 EA mutant displays an insensitivity to cAMP. It shows two point mutations (R591E and T592A) in Exon 7 in the CNBD of the HCN2 channel. The resulting change in the CNBD abolishes high affinity binding of cAMP leading to a suppression of the coactivaton of the channel. The HCN2 FEA mutant is additionally activated at voltages that are more positive. In native cells HCN channels are possibly preactivated to some extent by basal cAMP levels [49]. To imitate this conceivable preactivation an additional third mutation (Y449F) in Exon 4, which encodes for the C-Linker of the channel was inserted. This mutation leads to an activation curve shift to more positive values (Fig. 6).

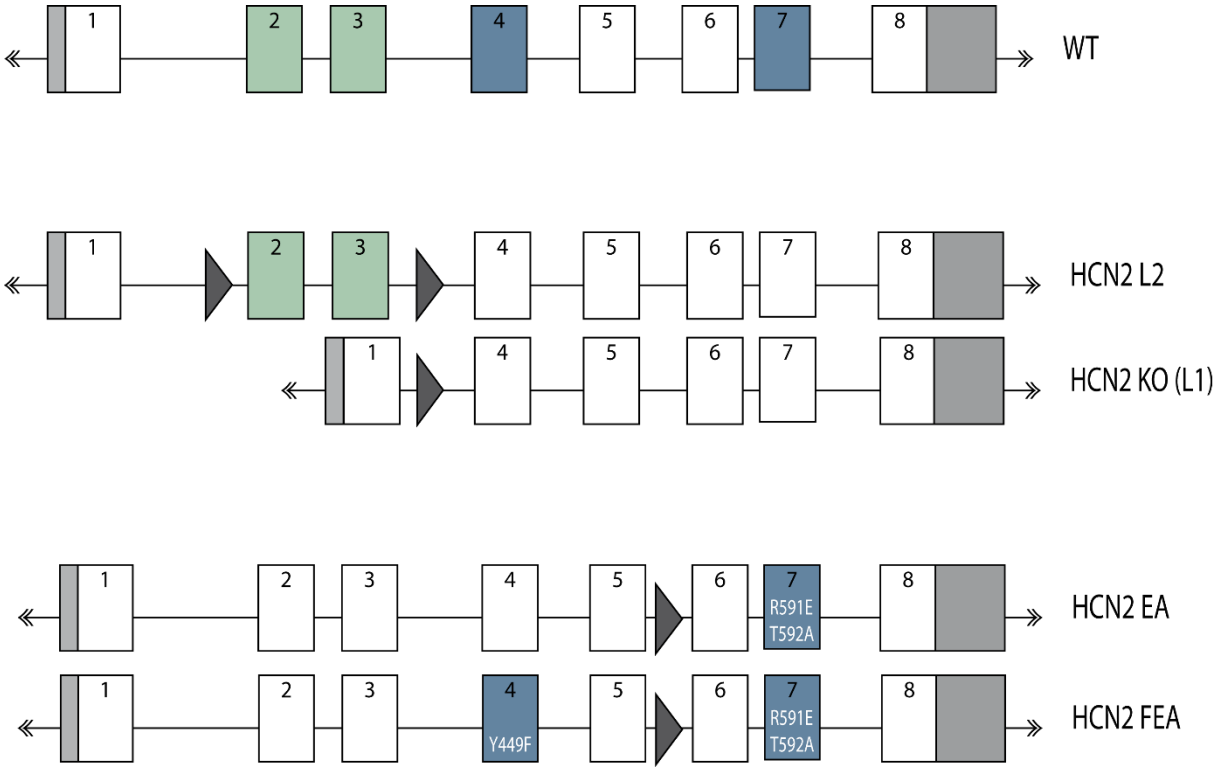

Figure 6 Schematic illustration of HCN2 mutant alleles

Schematic illustration of WT, HCN2 floxed (L2), HCN2 KO (L1), HCN2 EA and HCN2 FEA alleles. Numbered boxes are exons, mutated exons are marked by blue and green boxes respectively, dark gray triangles indicate loxP sites, UTRs are light gray boxes.

The mating of HCN2 KO, HCN2 EA and HCN2 FEA mouse lines was heterozygous, the mating of HCN2 floxed was homozygous. The HCN2 KO mouse was bred on a mixed background of 129SvJ and C57-Bl6/N strains and all other used mouse lines were on a background of the C57-Bl6/N strain. All animals received food (Ssniff; regular feed: R/M-H, breeding feed: M-Z Extrudat) and water ad libitum and were maintained under a 12h light/dark cycle.

3.3 Immunohistochemistry

Mouse brains were removed due to legal regulations. They were directly frozen and dehydrated in 2-methylbuatnol for 5min. To evaporate the mouse brains they were maintained on dry ice for approx. 30min and then stored at -80°C. The brains were sectioned with a cryostat (Leica CM3050S) into 30µm thick coronal sections.

Brain tissues were rehydrated 10min in PBS. Sections were fixed and permeabilized in ice cold 100% Methanol at -80°C for 30 min, incubated 1h with PBS and washed 3x with PBS for 10min. Sections were blocked with 10% normal goat serum (NGS) (Sigma), 0.1% Triton-X100 for 1h. The incubation with αHCN2 primary antibody (1:1000) (#APC-030, Alamone labs), diluted in 1%NGS, 0.1% Triton-X100 was accomplished for 2h, followed by extensive washing with PBS and secondary antibody Cy3 (1:400) (Jackson ImmunoResearch) incubation for 1h. After washing with PBS for 10min a Hoechst staining (5µg/ml) (Hoechst 33342) was performed. Sections were embedded in Mowiol mounting medium. All chemicals were diluted in ice cold PBS. Images were captured and analyzed using Leica SP8 SMD Confocal Microscope. Figures were prepared using ImageJ software. Manipulation of images were restricted to threshold and brightness adjustments applied to the entire image.

PBS 10x (1M)

100	mM	Na_2HPO_4
1.37	M	NaCl
27	mM	KCl
18	mM	KH_2PO_4

3.4 Electroencephalography (EEG)

3.4.1 EEG surgery

The appropriate surgical anesthesia was administered and eye ointment was applied to each eye. The body hair was removed liberally from all intended incision sites. The incision sites were disinfected. A 2-3cm incision through the skin along the neck was made. A subcutaneous pocket was formed by blunt dissection from the neck incision across the back and down along the animal's flank. The tunnel was irrigated with sterile saline and the transmitter **(**F20-EET Mouse Telemetry for CNS Research, DSI) was inserted into the subcutaneous pocket with the biopotential leads orientated cranially.

The lead pair of channel 2 (orange) was used to monitor postural muscle electromyography (EMG). The cervical trapezius muscle in the dorsal region of the neck was located and an area of the muscle that can accommodate lead attachment was selected. One of the leads was cut

to length and 4-5mm of the insulation from the terminal end of the lead was stripped. Using a 21-gauge needle, it was tunneled through approx. 3mm of muscle tissue perpendicular to the long axis of the fiber bundles. The bare lead wire was passed into the lumen of the needle so that, as the needle was withdrawn, the lead wire was left embedded in the muscle. The saved piece of insulation was put onto the terminal end of the lead wire, secured with several suture ties. This procedure was repeated for the other lead. Both leads were placed 1-2mm apart along the same group of muscle fibers.

The mouse was fixed in a stereotaxic apparatus (Model 902 Dual Small Animal Stereotaxic Instrument, TSE). in sternal recumbence. An approx. 2cm incision was made through the skin along the dorsal midline from the posterior margin of the eyes to a point midway between the scapulae. The skull was cleared of tissue down to the bone by using a cotton bud soaked in 3% hydrogen peroxide. The bone was dehydrated again with application of sterile saline. The correct positions (ML 1.8; AP 2.0 recording electrode and ML -0.5; AP 1.0 reference electrode) were identified and marked by using lambda/ bregma as a reference. If the lambda to bregma distance was less than 4.0mm, the coordinates were adjusted. Using a 1.0mm micro drill bit (K-control 4970 with K5 plus-tool holder, KaVo), the skull was perforated at the marked locations. The holes passed completely through the skull but did not perforate the dura membrane.

The channel 1 (blue) EEG leads were pervaded subcutaneously from the neck incision to the cranial one. The leads were cut to length. 1mm of the insulation was stripped from the terminal end of the leads. The wire coil were grasped between two pairs of fine forceps and the coil was gently stretched to a length of 3mm. With fine forceps, the lead wire was bent to a U-form. The bent loop portion of the wire was compressed and inserted into the skull perforation. The wire loop was advanced into the hole until the wire was in contact with the dura membrane. The compressed loop needed to expand and the spring tension held temporarily the bent wire in place. The procedure was repeated using the other lead from channel 1. The skull was dried with a cotton tip. The dental acrylic was applied sparingly to the lead entry holes and the surrounding bone. The dental acrylic covered all bare wire and incorporate the insulation of both lead wires. Once the dental acrylic was cured, the remaining leads were stored and the incisions were sutured and/or clipped.

Post-surgical analgesia and antiseptic PVP-iodine ointment were administered. The mouse was monitored closely for the return of normal postures and behaviors. In addition, mice were maintained under a 12h light/dark cycle, with the light cycle beginning at 7pm. Animals were allowed approx. 14 days of recovery from surgery and habituation before the recording started.

The animals were placed into a separate housing cage with free access to food and water several days before the recording started. The same number of WT and mutant mice were included in one recording session to equally distribute the environmental variations. Four animals were recorded simultaneously in one session with the Dataquest A.R.T. ™ system (Data Sciences International). In each session, EEG, EMG, activity and video signals were recorded continuously for at least 24h that means at least a full 12h light period and a full 12h dark period without any disturbance. Before each recording every transmitter had to be configured within the Dataquest A.R.T. ™ system. The EMG and the EEG signal were sampled at 2 kHz while activity data was sampled at 0.1Hz. Before starting the recording, the transmitters had to be turned on by a magnet. An AM radio tuned to 550 kHz served as an audible function control.

3.4.2 EEG analysis

NeuroScore™ analysis software and Matlab™ were used to analyze the neurophysiology data collected in Dataquest A.R.T.™. Recordings were analyzed with focus on seizures, oscillations and sleep staging. Vigilance states were scored by the manual, visual inspection of the traces. The whole recording was divided into 4s epochs. Each of these 4s epochs was scored as wake, NREM or REM sleep on the basis of the video, EEG, EMG and activity data due to general approved criteria. Wake state includes a broad variety of behaviors (e.g. drowsiness, exploratory behavior, grooming), therefore it is characterized by an EEG pattern of various frequency contents and a low-amplitude. Not only lower frequency components (delta waves during drowsiness) but also higher ones (theta waves during exploratory behavior) contribute. Muscle tone is present and can be highly variable and the animal can be active. REM sleep is characterized by regular low-amplitude theta waves (4-12Hz) in the EEG. To clearly identify a REM sleep period, the theta ratio (quotient of theta power to delta power) was calculated.

The theta ratio greater than approx. 3.2 indicates a REM sleep episode. Further hallmarks of a REM sleep period are muscle atonia and no activity. NREM sleep is dominated by high-amplitude slow waves in the delta frequency range (1-4Hz). The muscle tone is low-mid and there is no activity recognizable [51].

Each 4s epoch of the 24h recording was visually scored as wake, NREM and REM. Artifacts were excluded from further analysis. All scoring data was saved in the database. The spectrum including EEG and EMG signal, time stamps, sleep stages in the frequency range 0.75-25Hz was exported into Excel using Discrete Fourier Transform (DFT) and signal window Hamming.

To investigate the time the mice spent in the different behavioral states, all the epochs that had been scored as wake, NREM or REM were summed up into three separate categories. The total recording time minus the artifact periods was calculated. The total time spent in each behavioral state in the light period, the dark period and/or the total recording time was calculated and normalized to the total recording time.

To calculate the mean episode duration, the artifacts were removed and then the mean of all individual bouts scored as wake, NREM or REM were calculated in three separate categories.

The number of transitions from one behavioral state to another was determined and normalized to the total number of transitions within the total recording time.

For determining the power change of each frequency bin over time, a 3-dimensional plot was created. The power intensity is visualized by a color code while the time is plotted (x-axis) against the frequency (y-axis). The power intensity was calculated by using Fast Fourier Transform (FFT).

For power spectra analysis, the raw EEG data was imported into Matlab™ (see appendix for scripts). For determining power spectra, every single 4s epoch of the EEG recording was subjected to DFT between 0.75 and 25Hz (0.25Hz bins, 4s epoch, signal window Hamming). If a 4s epoch of one vigilance state was adjacent to an epoch scored as a different state, it was excluded from spectral analysis. The mean power spectrum was calculated in total and separately for each vigilance state. To correct interindividual variations in overall EEG signal amplitude, absolute spectral values were normalized to the mean total EEG power for all frequency bins of the three vigilance states. The relative EEG spectral power was averaged

over all mice. The relative spectral EEG power was plotted against the frequency in total and for each vigilance state.

The EEG dynamics at state transition reveals the time course of the EEG changes immediately before and after a transition from one behavioral state to another. Based on the vigilance state scoring, at least 8 consecutive episodes of one behavioral state followed by at least 8 consecutive episodes of another vigilance state were identified using a Matlab™ based script (see appendix). All characteristic power values of selected transitions are aligned with respect to the time of transition (=time 0). The power values of selected frequency ranges of corresponding 4s-epochs were averaged and expressed as percentage of mean power scored as NREM 2min before or after the transition. The power values of the particular frequency range were plotted against the time.

3.5 Viral injection

Adult mice were anesthetized with inhaled isoflourane and virus was delivered to MS area by stereotactic injection. Before starting the surgery, the surgical area and all tools and reagents were cleaned by wiping with 70% ethanol. The fur on the skull was shaved and the animal was put in the stereotaxic apparatus (Model 902 Dual Small Animal Stereotaxic Instrument, TSE). A dissecting microscope (OPMI 1 FR pro, Zeiss) was used to visualize the top of the animal's skull. A midline incision with small surgical scissors was made and the subcutaneous and muscle tissue was removed. The bregma and lambda areas were cleaned using a cotton bud soaked in 3% hydrogen peroxide and the skull is kept moist with sterile PBS throughout the surgery. The position of the coordinates of bregma were measured and the coordinates of MS area were calculated (AP 0.7; ML 0.0; DV -3.9). A small hole <1mm in the skull was drilled with a dentist's drill (K-control 4970 with K5 plus-tool holder, KaVo). The micro syringe (Nanofil syringe, WPI) including the needle (NF34BL, WPI) filled with rAAV8 hSyn-GFP-cre virus (purchased from: The Vector Core at the University of North Carolina at Chapel Hill) or control virus (own production) was brought carefully to the correct x, y and z position, therefore the needle was inserted through the hole in the skull manually. The injector (UMPIII with SYS-Micro4 controller, WPI) covering the micro syringe was used to deliver 0.7µl virus (100nl/s) into the area. 2-3 min after the injection the needle was withdrawn slowly to avoid backflow.

The scalp wound was sutured and disinfected with PVP-iodine. The mouse was given an intraperitoneal injection (IP) of analgesic. The recovery and expression time was 2 weeks.

3.6 Behavioral test

The behavioral experiments testing for spatial memory were performed due to the publication of Kleinknecht et al [50]. The animals were 7-8 weeks old. Two weeks prior the start of the experiments the mice got to use to an inverse 12h day- /night cycle (start of the light phase 7pm). So that the nocturnal animals were in the active phase while conducting the experiments. The water cross maze (WCM), using for this experiment consists of 4 arms, arranged crosswise. The four arms were marked as North, East, South and West arm in a clockwise manner. It was made of transparent acrylic glass, so that the visual orientation of the animals via external cues was possible. A removable separation enables it to block the arm opposite the starting arm (either North or South arm). That means the part accessible for the animals had a 'T' shape. A platform (8 x 8 cm), also made from acrylic glass was positioned permanently in the West arm approx. 1cm below the water surface. So it was invisible for the animals. The water was renewed regularly during the experiment. A rescue bar was used to bring the mice back in their home cage after each run. Animals were tested in cohorts of 7.

On every experimental day, directly prior to the test start the animals were transported from the holding room to the test room. For every run the mice were inserted carefully into the water in the start arm, the head facing the wall. The experimenter behaved quietly and stood still behind the experimental setup during the testing period. After having located the platform the animal was retrieved and put back into the home cage. The mice were dried under infrared light. If the animal was not able to find the platform within 30s, it was guided gently to the platform and after remaining 5s on the platform for orientation purposes it was put back into the cage. To exclude olfactory orientation as track aid, after every run the water was stirred thoroughly.

Every animal passed 6 trials a day for a period of 5 days. These runs served the mice to learn the platform location whereas the platform position did not change. However the starting position changed in a pseudorandom manner during the 6 runs between North and South

arm. The alternating starting position forced the animal to use external cues for orientation. This learning type makes use of the hippocampus-dependent place learning.

The learning efficiency was assessed by using 3 parameters: Latency, accuracy and the accurate learner criterion. The latency was defined as the time the animals needed to locate the platform. The latency was indicated as mean of all 6 trials a day. In case the animal was not able to locate the platform within 30s, the value of 31s was taken. Every entrance of the mouse into an arm was counted by the experimenter. It was assessed as entrance if the whole body of the mouse (tail excluded) was within the arm. A second entrance into the same arm was just counted if the mouse has completely left the arm before. A trial was evaluated as 'accurate' if the animal chose immediately the arm in which the platform was positioned and located the platform correctly. Every other behavior was counted as incorrect. The accuracy is the percentage of accurate trials per animal and per day. An animal reached the criterion of an accurate learner, if it accomplished more than 83% accurate trials per day (i.e., ≥5 out of 6 trials). The number of accurate learners was indicated as percentage of the sum of all animals exceeding the threshold on each day.

3.7 Statistics

Origin™ 6.1 (Originlab Corp.) was applied for the statistical analysis. The Two-Sample t-test was applied. A p-value < 0.05 was considered as significant and the results were indicated as mean +/- SEM.

4 Results

4.1 Electroencephalography (EEG)

In order to investigate the impact of HCN2 channels on the regulation of neuronal circuits an appropriate method had to be applied. Thus, in a first step EEG measurements suitable for estimating the overall brain activity were established and validated. A telemetric, wireless and invasive system was used to measure and analyze the voltage fluctuations resulting from ionic currents within the neurons. The following procedure, compromising the surgery of the transmitters, the recording and the analysis was installed in order to generate appropriate datasets.

4.1.1 EEG surgery

In order to implant the transmitters for recording EEG and EMG data into the animals the following surgical procedure was applied. To assure aseptic conditions all instruments and materials as well as the work bench were disinfected prior to surgery and during the operation the disinfection was repeated regularly. The appropriate surgical anesthesia was administered and eye ointment was applied to each eye (Fig. 7A). The body hair was removed liberally from all intended incision sites with the electric shaver. The incision sites were disinfected. The transmitter was removed from its sterile package and the serial number was noted because it was important to ensure that the device had been identified with the animal in which it was implanted. Two biopotential leads are attached to the transmitter, one for recording EEG data (blue, channel 1) and the other one for recording the EMG signal (orange, channel 2) (Fig. 7B). The leads of the transmitter were shortened to an appropriate length according to the size of the animal. For 6-8 week-old mice, weighing 20-25g the EEG lead was cut to approx. 40mm and the EMG lead to a length of approx. 35mm. The absence of the animal's pinch toe reflex was confirmed and the animal was put in ventral recumbence on a temperature controlled surgery pad set to 37°C. A 2-3cm incision through the skin along the neck was made by using small, blunt dissecting scissors. A subcutaneous pocket was formed by blunt dissection from the neck incision across the back and down along the animal's flank. The tunnel and the subcutaneous pocket were as small as possible to keep the transmitter in position. The tunnel

was irrigated with sterile saline and the transmitter was inserted into the subcutaneous pocket with the leads orientated cranially (Fig. 7C and D).

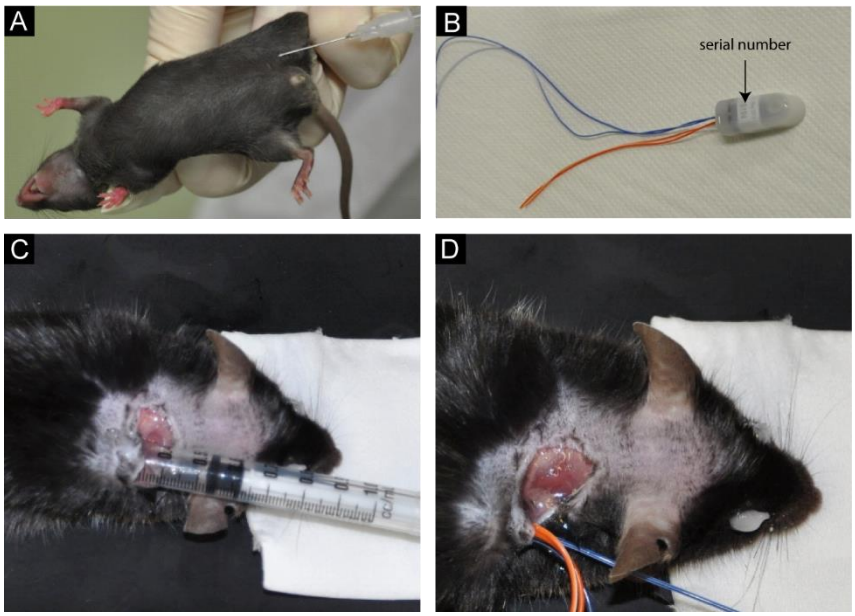

Figure 7 EEG surgery - preparation and placement of the transmitter

(A) Application of anesthesia IP (B) F20-EET transmitter with EMG (orange) and EEG (blue) electrodes (C) Incision and irrigation of the subcutaneous pocket with sterile saline (D) Transmitter and electrodes in subcutaneous pocket and orientation of electrodes.

The lead pair of channel 2 to monitor postural muscle EMG was retrieved. The cervical trapezius muscle in the dorsal region of the neck was located and an area of the muscle that could accommodate lead attachment was selected. Using two 21-gauge needles, it was tunneled through approx. 3mm of muscle tissue perpendicular to the long axis of the fiber bundles and through a second part of muscle tissue being 1-2mm apart from the first one along the same group of muscle fibers (Fig. 8A). The lead wire was passed into the lumen of the needle so that, as the needle was withdrawn, the lead wire was left embedded in the muscle (Fig. 8B). 4-5mm of the insulation from the terminal end of the lead was stripped by using a scalpel (Fig. 8C) and the saved piece of insulation was put onto the terminal end of the lead wire not covered by the muscle (Fig. 8D and E). The leads were secured with several suture ties (Fig. 8F). The open wound was moisturized with sterile saline (Fig. 8G).

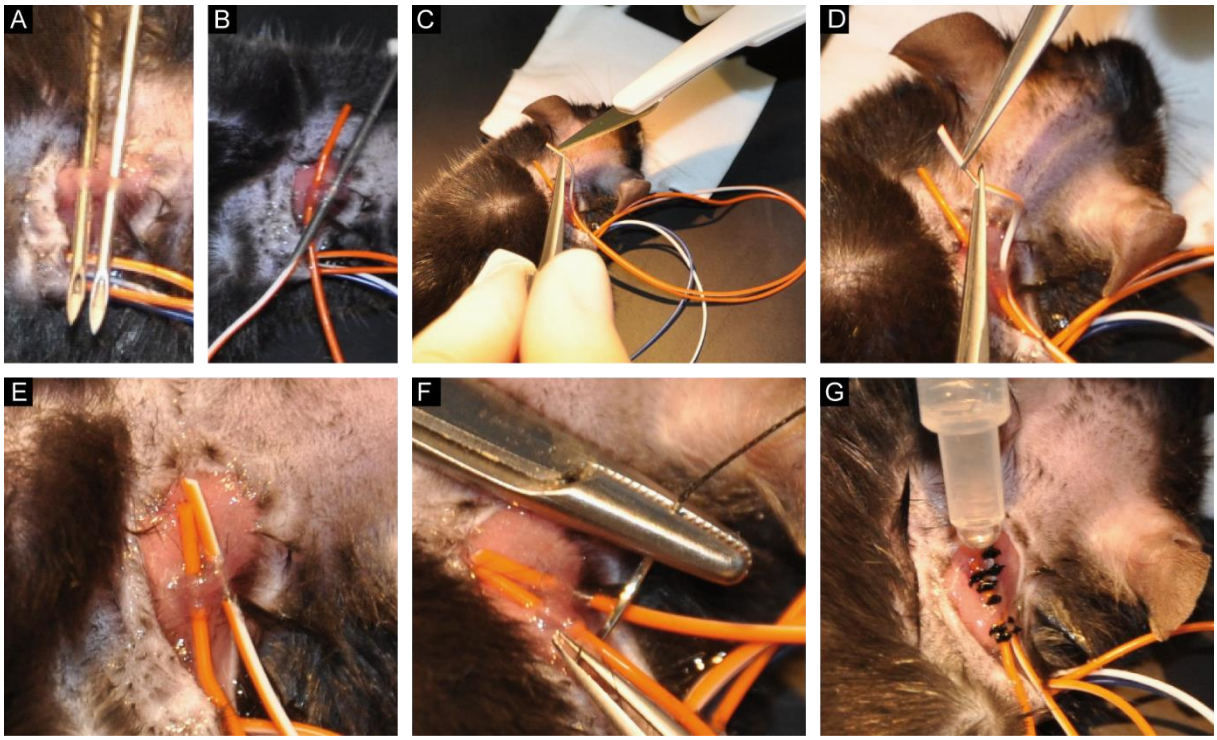

Figure 8 EEG surgery - EMG positioning

(A) The 21-gauge needles tunneled through musculus trapezius (B) The lead wire passed into the lumen of the needle (C) and (D) The insulation from the terminal end of the lead was stripped (E) The insulation putted on the terminal end (F) The wire secured with several suture ties (G) The finished suture moisturized with sterile saline.

Next the mouse was fixed in the stereotaxic apparatus in sternal recumbence in order to place the EEG leads (Fig. 9A). An approx. 2cm incision was made through the skin along the dorsal midline from the posterior margin of the eyes to a point midway between the scapulae. The skull was cleared of tissue down to the bone by using a cotton bud soaked in 3% hydrogen peroxide (Fig. 9B). The bone was dehydrated again with application of sterile saline. The correct positions (ML 1.8; AP 2.0 recording electrode and ML -0.5; AP 1.0 reference electrode) were identified and marked by using lambda and bregma as a reference (Fig. 9C and D). If the lambda to bregma distance was less than 4.0mm, the coordinates were adjusted. Using a 1.0mm micro drill bit, the skull was perforated at the marked locations (Fig. 9E). The holes passed completely through the skull but did not perforate the dura membrane. Care was taken to prevent bleeding (Fig. 9F).

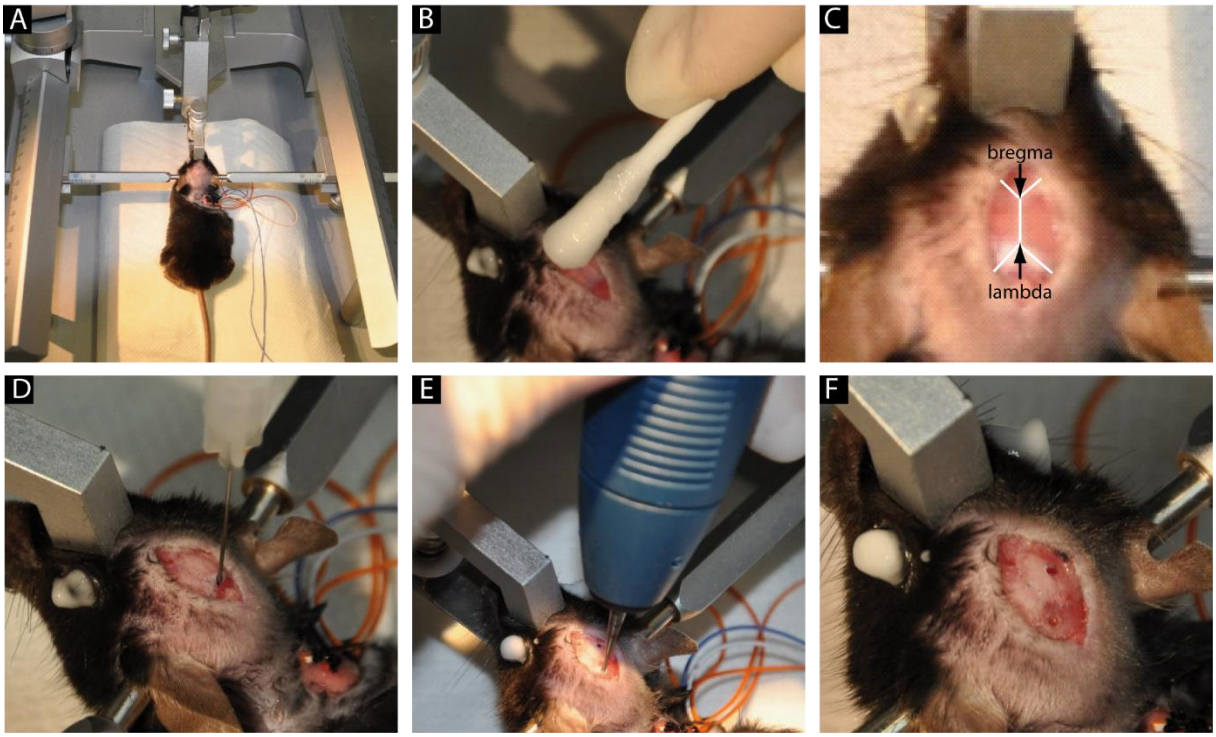

Figure 9 EEG surgery - EEG positioning

(A) Fixed mouse in stereotactic apparatus (B) Incision on the scalp and clearing skull with 3% hydrogen peroxide (C) Orientation points bregma and lambda are visible (D) Marking of identified correct position (E) Perforating the skull at marked positions (F) Drilled holes are visible.

The EEG leads were pervaded subcutaneously from the neck incision to the cranial one (Fig. 10A). 1mm of the insulation was stripped from the terminal end of the leads by using a scalpel (Fig. 10B). The wire coil were grasped between two pairs of fine forceps and the coil was gently stretched to a length of 3mm (Fig. 10C). With fine forceps, the lead wire was bend to a U-form. The bent loop portion of the wire was compressed and inserted into the skull perforation. The wire loop was advanced into the hole until the wire was in contact with the dura membrane. The compressed loop needed to expand and the spring tension held temporarily the bent wire in place (Fig. 10D and E). The procedure was repeated using the other EEG lead. The skull was dried with a cotton tip. The dental acrylic was blended and applied sparingly to the lead entry holes and the surrounding bone (Fig. 10F and G). The dental acrylic needed to cover all bare wire including the insulation of both lead wires (Fig. 10H). Once the dental acrylic was cured, the remaining leads were stored and the incisions were sutured and clipped (Fig. 10I).

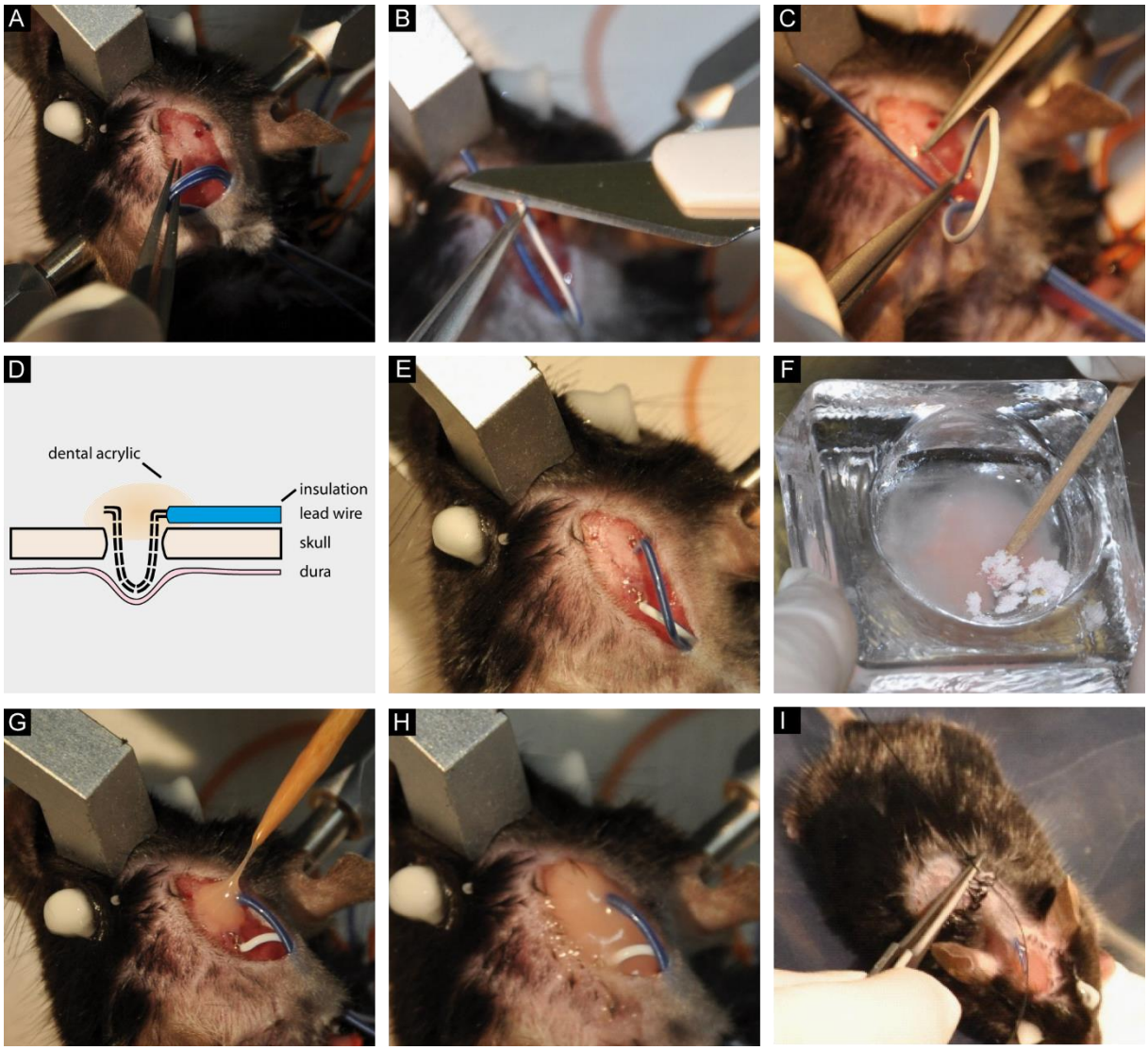

Figure 10 EEG surgery - EEG fixation

(A) Pervaded leads to the cranial incision (B) Stripped insulation from the terminal end (C) Wire coil is stretched (D) Schema how coil is inserted (E) Inserted wire into the cranium (F) Mixed cement for fixation (G) Cement put on wires (H) Cement covered on wires (I) All incisions were sutured.

Post-surgical analgesia and antiseptic PVP-iodine ointment were administered. The animal was placed back in a cage and put on a warm (37°C) platform until it was awake. It was transferred to a cage with one of its littermates to allow social interaction. The mouse was monitored closely during the recovery period of 4-10 days and parameters like wound healing, general health condition, body weight and vital parameters were assessed regularly. In addition, mice were maintained under a 12h light/dark cycle, with the light cycle beginning at

7pm. Animals were allowed approx. 14 days of recovery from surgery and habituation before the recording started.

4.1.2 EEG recording

The animals had been placed into a separate housing cage with free access to food and water several days before the recording started. The same number of wild type (WT) and mutant mice were included in one recording session to equally distribute the environmental variations. Four animals were recorded simultaneously in one session. In each session EEG, EMG, activity and video signals were recorded continuously for at least 24h that means at least a full 12h light period and a full 12h dark period without any disturbance and stored within the Dataquest A.R.T. ™ software. In order to improve the signal to noise ratio the receivers were placed directly under the animals' cages (Fig. 11). Before each recording every transmitter was configured within software system. The EMG and the EEG signals were sampled at 2 kHz while activity data was sampled at 0.1Hz.

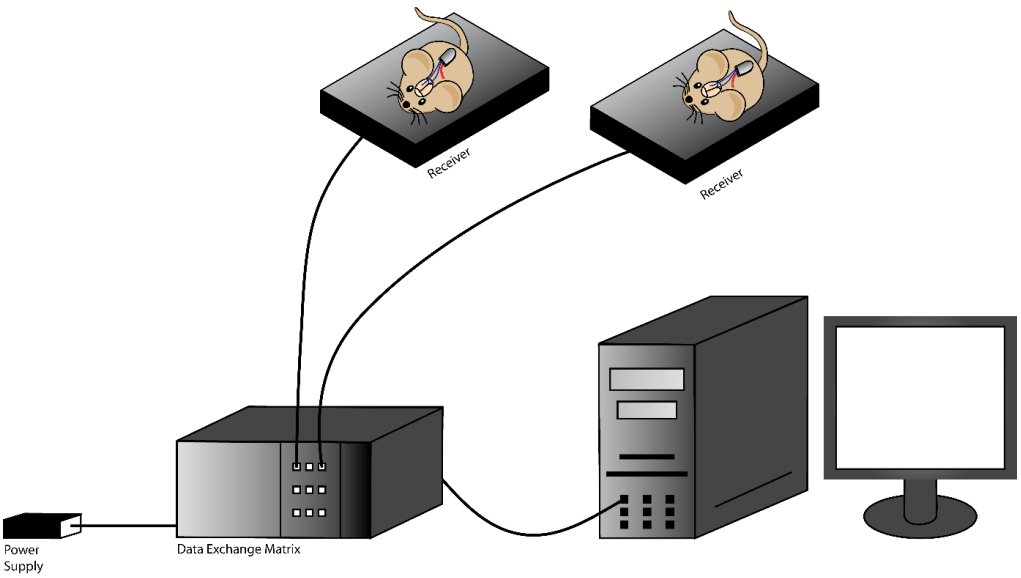

Figure 11 Radiotelemetric setup for EEG monitoring

The implanted probes transmit data from mice to the Receiver (RPC1-, DSI™), further processed to the Data Exchange Matrix, which serves as a multiplexer. Data is finally transferred to a data acquisition and then to an analysis system.

4.1.3 EEG analysis

NeuroScore™ and Matlab™ analysis software were used to analyze the neurophysiological data collected in the Dataquest A.R.T. ™ system. Recordings were analyzed with focus on seizures, oscillations and sleep staging. Vigilance states were scored by the manual, visual inspection of the traces. The whole recording was divided into 4s epochs. Each of these 4s epochs was scored as wake, NREM or REM sleep on the basis of the video, EEG, EMG and activity data due to general approved criteria [51]. Wake state includes a broad variety of behaviors (e.g. drowsiness, exploratory behavior, grooming), therefore it is characterized by an EEG pattern of various frequency contents and low-amplitude. Not only lower frequency components (delta waves during drowsiness) but also higher ones (theta waves during exploratory behavior) contribute. Muscle tone is present and can be highly variable, further the animal can show activity. NREM sleep is dominated by high-amplitude slow waves in the delta frequency range (1-4Hz). The muscle tone is low-mid and there is no activity recognizable. NREM sleep is intersected regularly by REM sleep episodes. Normal REM sleep is characterized by regular low-amplitude theta waves (4-12Hz) in the EEG. To clearly identify a REM sleep period, the theta ratio (quotient of theta power to delta power) is calculated. The theta ratio greater than approx. 3.2 indicates a REM sleep episode. Further hallmarks of a REM sleep period are muscle atonia and the animals displays no activity (Fig. 12).

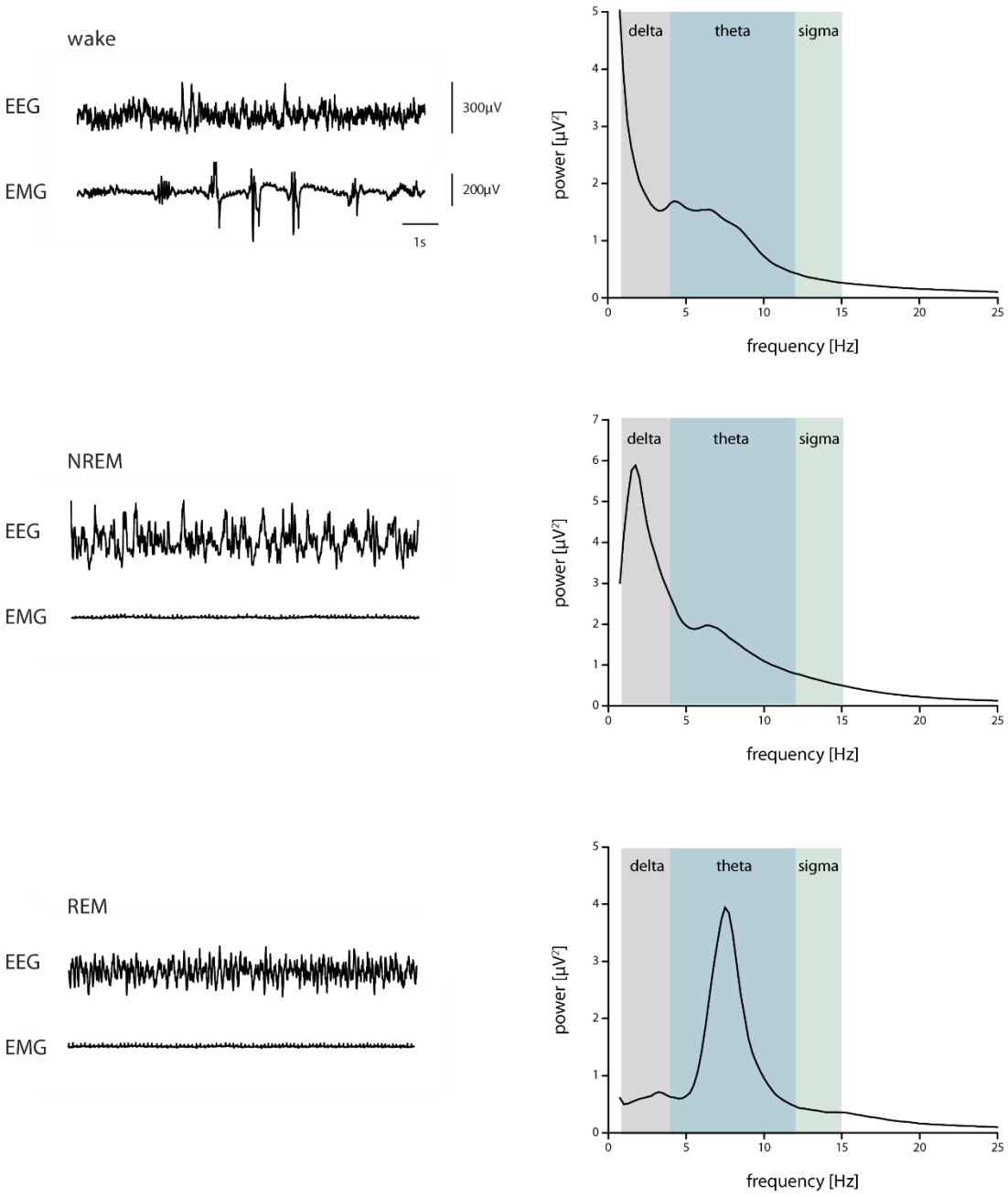

Figure 12 Representative EEG and EMG traces and appropriate power spectra for each vigilance state

Wake is characterized by a variable EEG and a variable EMG (upper panel). NREM sleep is characterized by a peak in the delta frequency range (1-4Hz) and by a low EMG (middle panel). REM sleep is dominated by a peak in the theta wave (4-12Hz) and a very low EMG (lower panel).

Each 4s epoch of the 24h recording was visually scored as wake, NREM and REM and artifacts were excluded from further analysis. All scoring data were saved in the database. The spectra including EEG and EMG signal, time stamps and sleep stages in the frequency range 0.75 to

25Hz were exported into Excel using Discrete Fourier Transform (DFT) and signal window Hamming or into Matlab™.

4.1.3.1 Time spent in behavioral states

All the epochs that had been scored as wake, NREM or REM were summed in three separate categories. The total recording time minus the artifact periods was calculated. The total time spent in each behavioral state in the light period, the dark period and the total recording time was calculated and normalized to the total recording time.

4.1.3.2 Mean episode duration

The artifacts were removed and then the mean of all individual bouts scored as wake, NREM or REM were calculated in three separate categories.

4.1.3.3 Transitions

The number of transitions from one behavioral state to another was determined and normalized to the total number of transitions within the total recording time.

4.1.3.4 Color-coded spectrograms

For determining the power change of each frequency bin over time, a 3-dimensional plot was created by using Matlab™ (see appendix for scripts). The power intensity was visualized by a color code while the time was plotted (x-axis) against the frequency (y-axis). The power intensity was calculated by using Fast Fourier transform (FFT).

4.1.3.5 Spectral analysis – power spectra

The raw EEG data was imported into Matlab™ (see appendix for scripts). For determining power spectra, every single 4s epoch of the EEG recording was subjected to DFT between 0.75 and 25Hz (0.25Hz bins, 4s epoch, signal window Hamming). If a 4s epoch of one vigilance state was adjacent to an epoch scored as a different state, it was excluded from spectral analysis. The mean power spectrum was calculated in total and separately for each vigilance state. To correct interindividual variations in overall EEG signal amplitude, absolute spectral values were normalized to the mean total EEG power for all frequency bins of the three vigilance states. The relative EEG spectral power was averaged over all mice. The relative spectral EEG power (x-axis) was plotted against die frequency (y-axis) in total and for each vigilance state.

4.1.3.6 EEG dynamics at state transitions

This analysis reveals the time course of the EEG changes immediately before and after a transition from one behavioral state to another. Based on the vigilance state scoring, at least 8 consecutive episodes of one behavioral state followed by at least 8 consecutive episodes of another vigilance state were identified using a Matlab™ based script (see appendix). All characteristic power values of selected transitions were aligned with respect to the time of transition (=time 0). The power values of selected frequency ranges of corresponding 4s-epochs were averaged and expressed as percentage of mean power scored as NREM 2min before or after the transition. The power values of the particular frequency range was plotted against the time (Fig. 13).

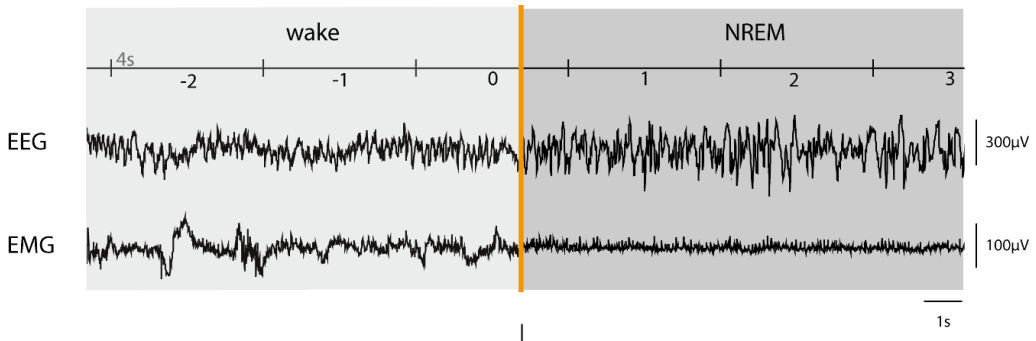

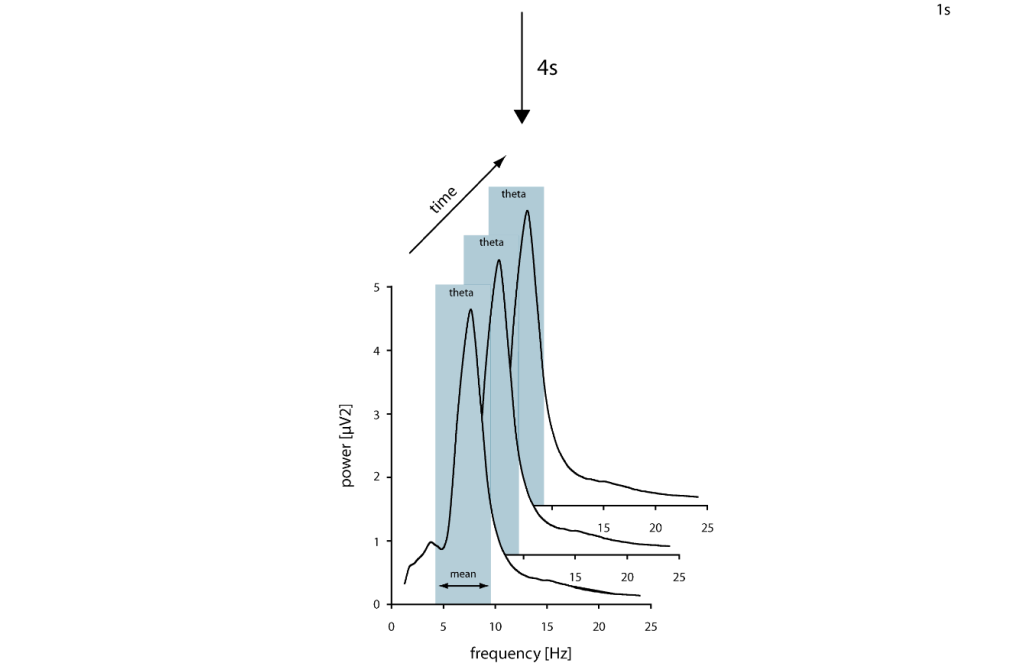

sleep stage	time [s]	epoch number	power [µV²]
wake	12	-3	3.2
	8	-2	3.8
	4	-1	3.5
transition	0	0	3.4
NREM	4	1	1.5
	8	2	1.8
	12	3	2.0

Figure 13 Schematic illustration of the EEG dynamics at state transition

Consecutive episodes of one behavioral state (e.g. wake state) followed by consecutive episodes of another vigilance state (e.g. NREM state) were identified. A DFT of every single 4s epoch was performed and all characteristic power values were aligned with respect to the time of transition (=time 0).

4.2 EEG recordings in HCN2 mutant mouse lines

To test whether and to what extent HCN2 channels and their regulation via cAMP are involved in neuronal rhythmicity, combined EEG and EMG measurements including an activity signal plus video data in freely moving mice were applied. The data provided information about the electrical activity of the brain because the EEG recording primarily detects the signal generated by the synchronized postsynaptic potentials which vary considerably between the different vigilance states and activities. In addition coherent signals from deeper brain layers, such as hippocampus, can also importantly contribute to the rodent's EEG [48]. The raw data analysis was focused on two major interests. Firstly, the occurrence of seizure events was assessed in every mouse line. Secondly, the EEG in combination with the EMG trace was used to distinguish between the different vigilance states and activities by their characteristic pattern, as a base for further analysis [51, 52].

4.2.1 HCN2 KO

To assess the consequences of the general lack of HCN2 channels on brain activity, EEG and EMG raw traces including activity data and derived signals were analyzed in global HCN2 KO and WT littermates (WT n=8; HCN2 KO n=9). Preexisting EEG data of global HCN2 KO animals [25] had been acquired with a non-telemetric method which meanwhile became obsolete. That is why the data was regathered using a state-of-the-art wireless, telemetric system.

As previously reported HCN2 KO mice display epileptiform activity including general SWDs, the neurological correlates of absence epilepsy, in the raw EEG trace [25]. These findings were confirmed and it was shown that the time within two seizure events is mostly shorter than 20s. In addition generalized seizures were detected in these animals (Fig. 14).

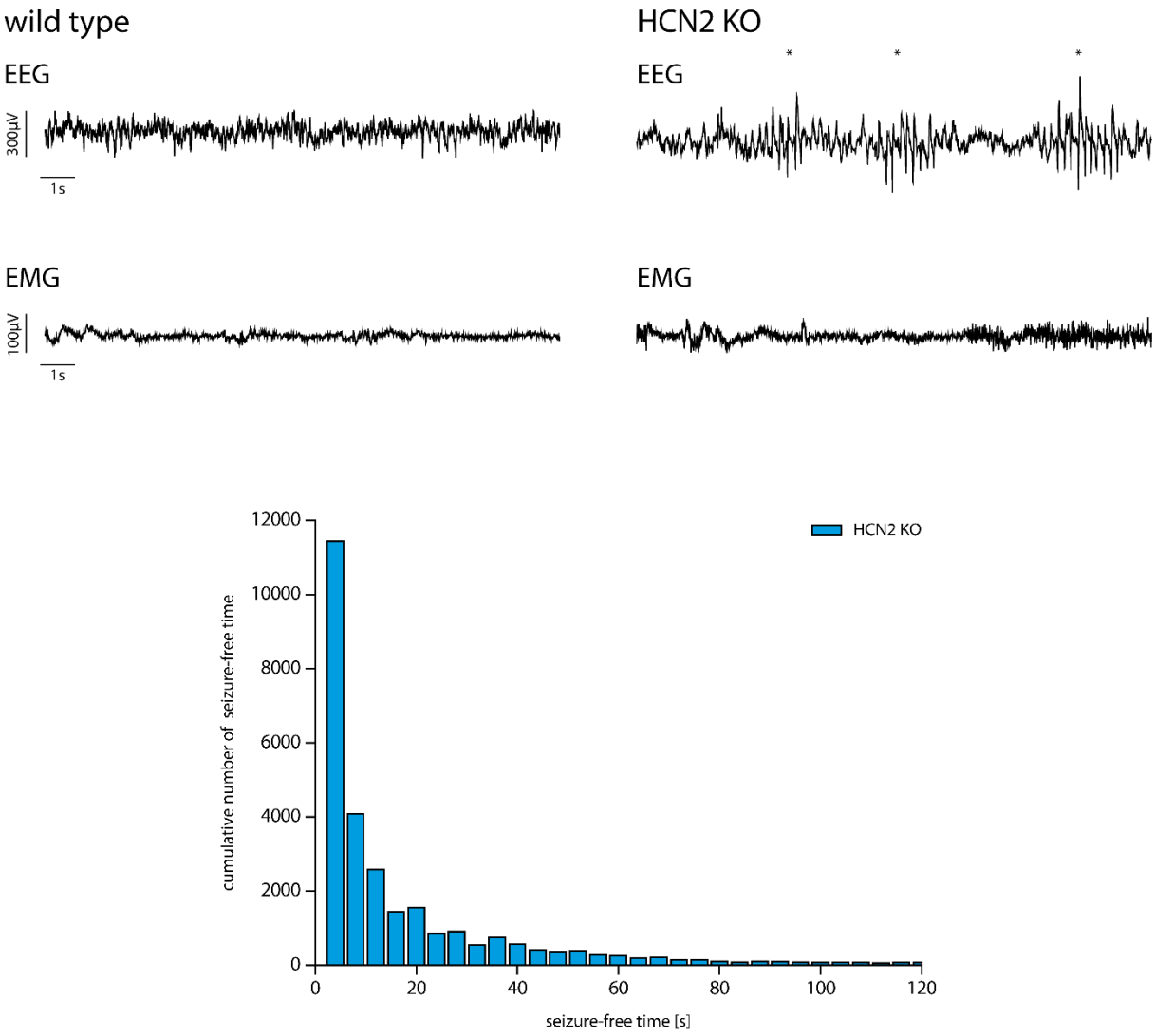

Figure 14 HCN2 KO - EEG and EMG raw traces

Representative raw EEG and EMG patterns of WT (left panel) and HCN2 KO (right panel) animals of 30s recordings. Asterisks indicate SWDs (top) and cumulative numbers of the seizure-free time between two absence epilepsy epochs in HCN2 KO animals (bottom).

To investigate whether there were changes of the frequency's content and its power, the global power spectrum between 0.75-25Hz was analyzed in order quantify the contribution of the various frequencies that constitute the EEG signal. The total KO spectrum showed an increase in low-frequency delta rhythms (1-4Hz), which are mainly of thalamic origin. In addition a drop down in the theta frequency band (4-12Hz) was remarkable. The theta wave is MS driven and partially generated in the hippocampus. The theta band decrease is overlaid by a power increase at around 5 Hz. This augmentation is likely a result of the absence seizures occurring in HCN2 KO animals, because the SWDs fire in this range [25] (Fig. 15). This multitude

of effects apparent in the global power spectrum was consistent with the fact that HCN2 is expressed in numerous brain regions [39, 40].

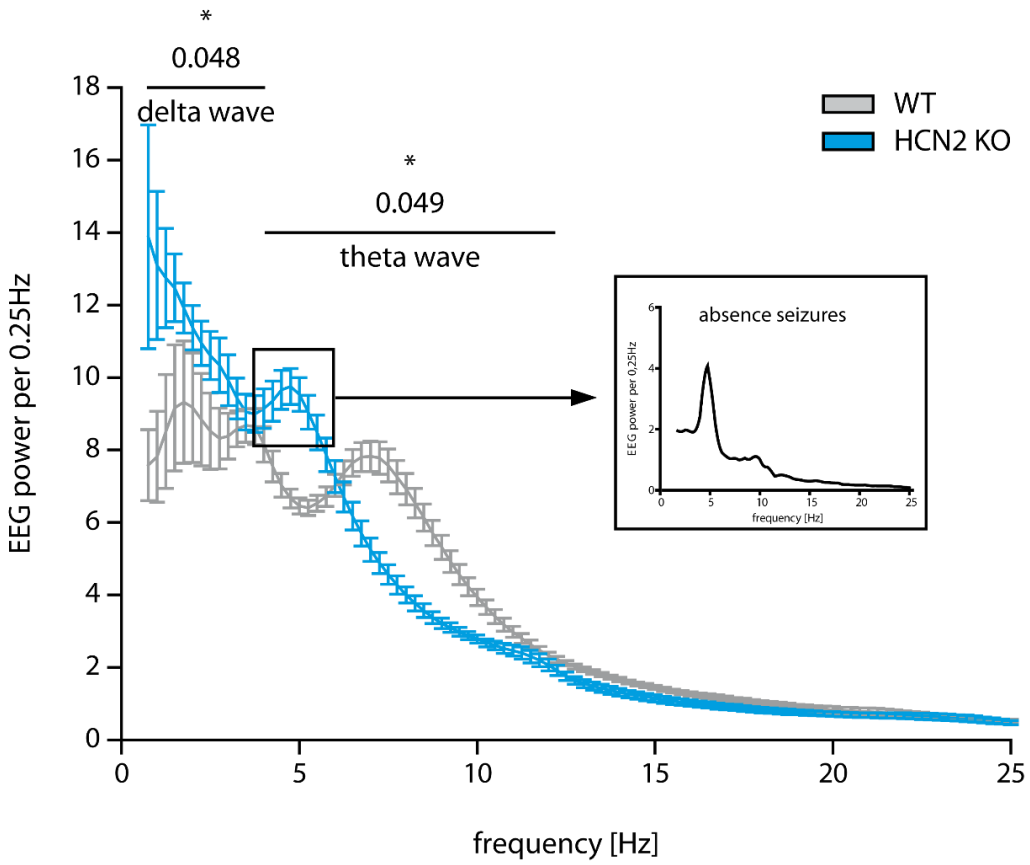

Figure 15 HCN2 KO - global power spectrum

Average total EEG power spectra of 24h recording time between 0.75 and 25Hz (0.25Hz bins, 4s epoch, Hamming) are shown in corresponding graphs. HCN2 KO spectrum shows an increase in the delta frequency range (1-4Hz) and a decrease in the theta frequency range (4-12Hz). Rectangle shows frequency content of absence seizures reflecting the peak at 5Hz in the global HCN2 KO spectrum. Asterisks indicate points with significant genotype differences ($p<0.05$, Two-Sample t-test).

To take a closer look at these findings the different vigilance stages should be analyzed in detail. The color-coded spectrogram (Fig. 16), indicating the power density of each frequency as a function of time showed that WT animals display a vigilance state pattern typical for rodents. During the wake state the EEG was rather variable, it consisted of slower (delta band range; 1-4Hz) and faster (theta band range; 4-12Hz) frequency components and it was characterized by a higher and variable EMG. The EEG of NREM sleep was dominated by a high delta frequency component while the EMG remained low. The NREM sleep was interjected by

REM sleep episodes characterized by a high theta frequency fraction and also a low EMG. (Fig. 16, left panel). Due to this criteria it was possible to distinguish clearly between the different vigilance states in WT animals. However, the HCN2 KO EEG and EMG color-coded heat maps seemed to be totally messed up thus a vigilance state classification was impossible. The EEG spectrogram allowed no real differentiation because many different frequencies were present throughout the whole recording (Fig. 16, right panel). Due to the impossibility of a vigilance state classification a general statement could not be made regarding the duration and the quality of the different arousal states. It is further conspicuous that there is an additional band visible in the HCN2 KO EEG spectrogram at around 13Hz and that the EMG is rather high throughout the recording. These phenomena are known from mice which experienced fear conditioning [53].

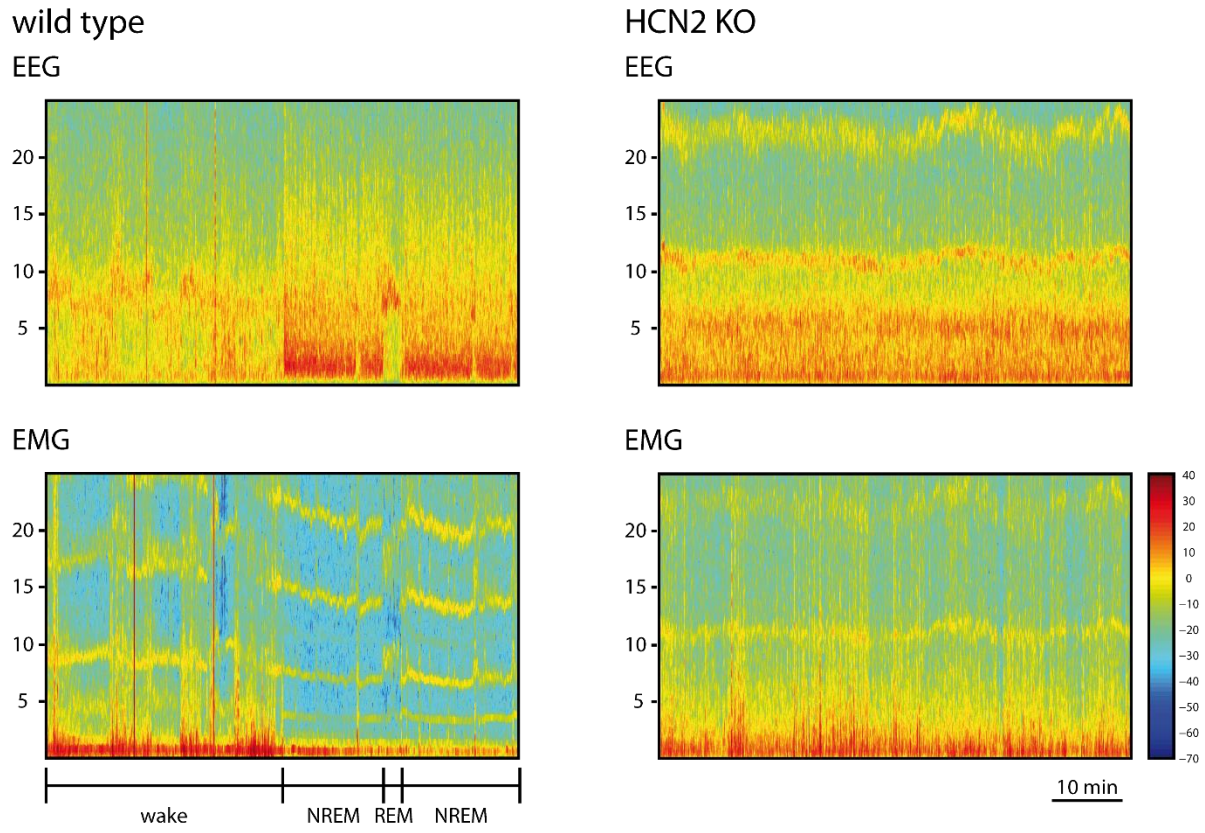

Figure 16 HCN2 KO - color-coded spectrogram

Representative sections of a color-coded heat map of EEG and EMG power between 0.75–25 Hz (0.25-Hz bins) as a function of time. WT animals show a normal distribution including wake, NREM and REM portions clearly distinguishable (left panel). However, HCN2 KO animals show a uniform frequency distribution thus a classification in different vigilance states was impossible (right panel). Scale indicates intensity showing red for high and blue for low intensity levels.

To further elucidate possible abnormalities in HCN2 KO animals which could be associated with the changes in the power spectrum, the activity level during light and dark phases was analyzed. During baseline conditions, WT mice yielded an activity pattern typical for nocturnal rodents, being more active during the dark phase and quieter during the light phase. The behavior of HCN2 KO mice was distinct from that of WT littermates, because the activity pattern differed barely between the 12h light and dark period (Fig. 17).

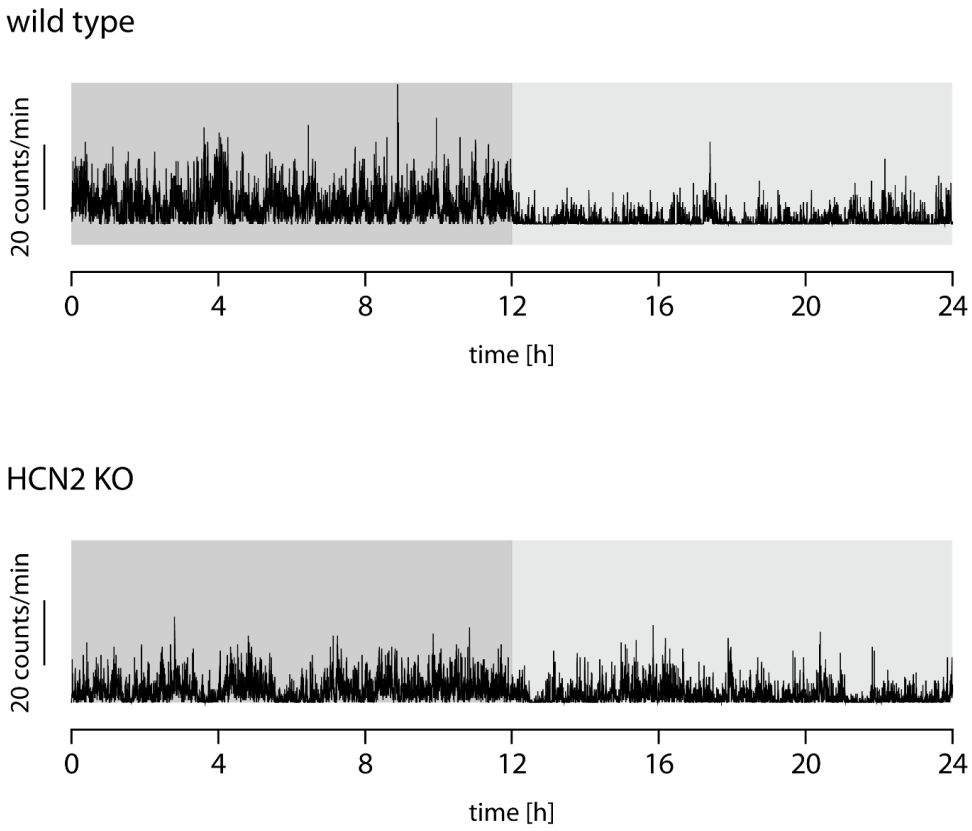

Figure 17 HCN2 KO - activity pattern

Comparison of the activity pattern of HCN2 KO and WT animals. WT mice show a behavior normal for nocturnal rodents, being more active during the dark phase (dark gray) and less active during the light phase (light gray). However, HCN2 KO animals show an activity pattern equal during dark and light period. Activity pattern is indicated as counts per minute over a period of 24h containing a 12 hour light and dark period respectively.

This effect could either be due to reduced locomotor activity and hypoactivity, which is known to occur in HCN2 KO mice [25] or it could be due to other dysfunctions e.g. a disturbed circadian rhythm.

In conclusion the data reveals that HCN2 channels contribute profoundly to the generation and regulation of the theta frequency but it remains unknown which nuclei, expressing HCN2 are actually involved.

4.2.2 Selective HCN2 KO

Preexisting evidence demonstrated a role for MS in controlling theta rhythms [54]. Predominant HCN2 expression on mRNA level in this brain area [39] leads to the hypothesis, that the loss of HCN2 channels in this brain area might be responsible for the attenuated theta power, observed in global HCN2 KO mice. First the HCN2 expression in MS neurons was confirmed on protein level. Therefore immunohistochemistry was performed on brain slices containing MS area using WT and HCN2 KO animals serving as negative control. A distinct HCN2 expression pattern was observed in MS area in WT slices while immunofluorescence staining for HCN2 was absent in HCN2 KO brain sections (Fig. 18B). To investigate the expression level of other HCN isoforms in this nucleus further staining was carried out. It was shown that both HCN1 and HCN4 were expressed much weaker than HCN2 whereas HCN4 showed a little higher expression level (Fig. 18C). These findings confirm that HCN2 is the major isoform expressed in MS and therefore might be crucially involved in theta regulation.

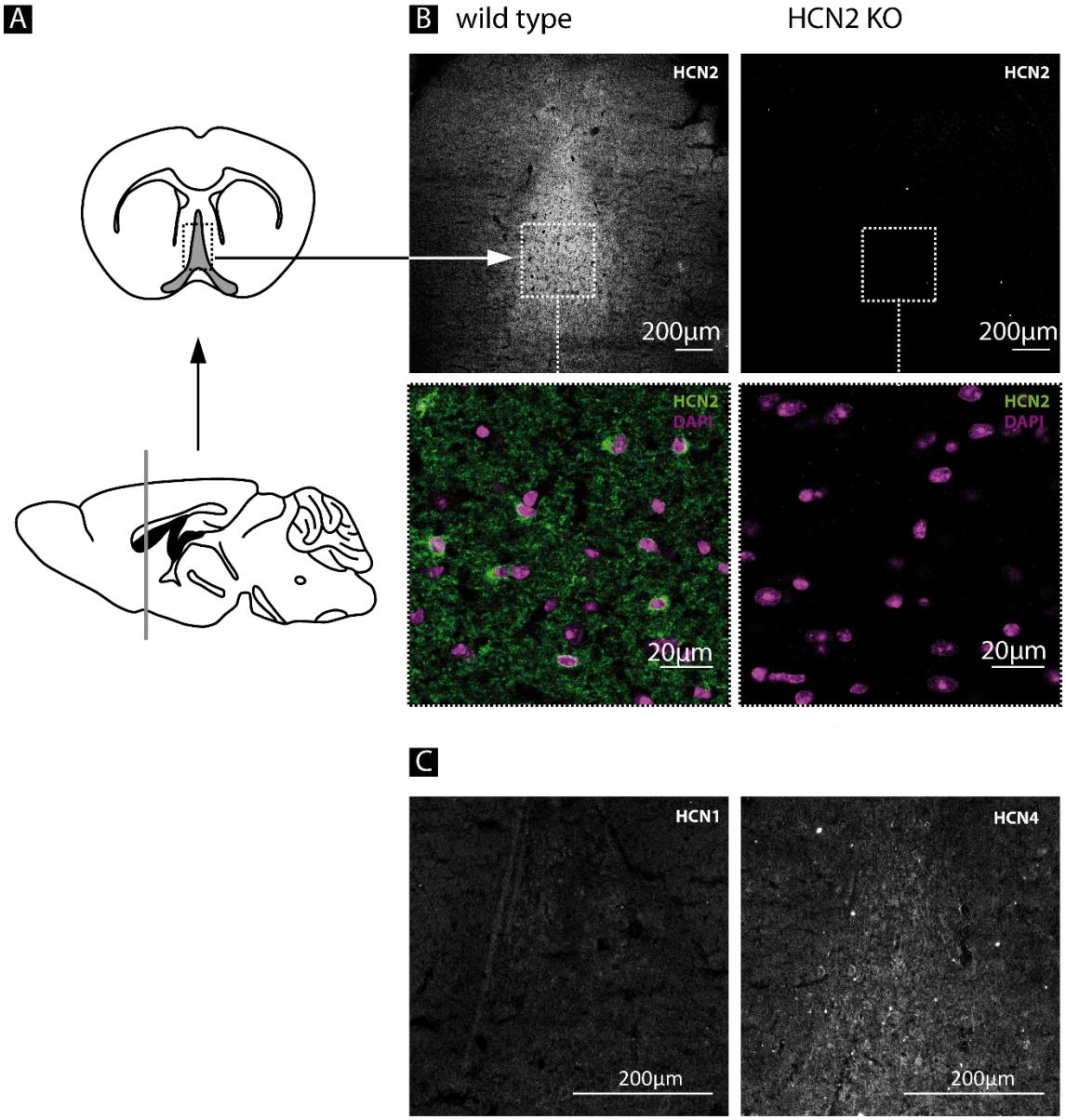

Figure 18 HCN2 staining in MS neurons

(A) Location of MS area (gray) in coronal (upper panel) and sagittal (lower panel) brain sections. (B) HCN2 expression in MS neurons in WT and HCN2 KO brain slices, rectangles show higher magnification; HCN2 staining in green and DAPI in magenta. Immunofluorescence staining of HCN2 is obvious in WT sections but absent in HCN2 KO slices in MS area. (C) HCN1 and HCN4 expression in MS neurons in WT slices.

To further investigate the causal relationship between a lack of HCN2 in MS neurons and the immense reduction of theta power, cre-mediated gene silencing using a floxed HCN2 (HCN2 L2) mouse line was applied. To locally knockdown HCN2 gene expression, simultaneously with the EEG surgery, 0.7µl of an adeno-associated virus (AAV) was delivered stereotactically into MS cells of 8-week-old HCN2 L2 mice. The virus contained either GFP-cre under the control of

the human Synapsin (hSyn) promoter, which transduces primarily neuronal cells (rAAV8/hSyn-GFP-cre, further referred as GFP-cre) or a control (control n=5; GFP-cre n=6). The GFP-cre virus showed a titer of $4.7x10^{12}$ virus molecules/ml and was dialyzed in w/350mM NaCl and 5% D-Sorbitol in PBS. After having finished the EEG measurements, approx. 4 weeks after surgery and injection, in postmortem examinations of brains immunohistochemistry staining for HCN2 was performed. It could be shown that just one population of the cells within the MS was positive for HCN2, indicated by the green loop structure around the nucleus in Fig. 19. These cells might be GABAergic neurons because former data reveal that just this population is positive for HCN2 [55]. It could be demonstrated that the cells, which express GFP-cre (cyan in Fig. 19), are negative for a HCN2 staining, indicating a successful knockdown (Fig. 19).

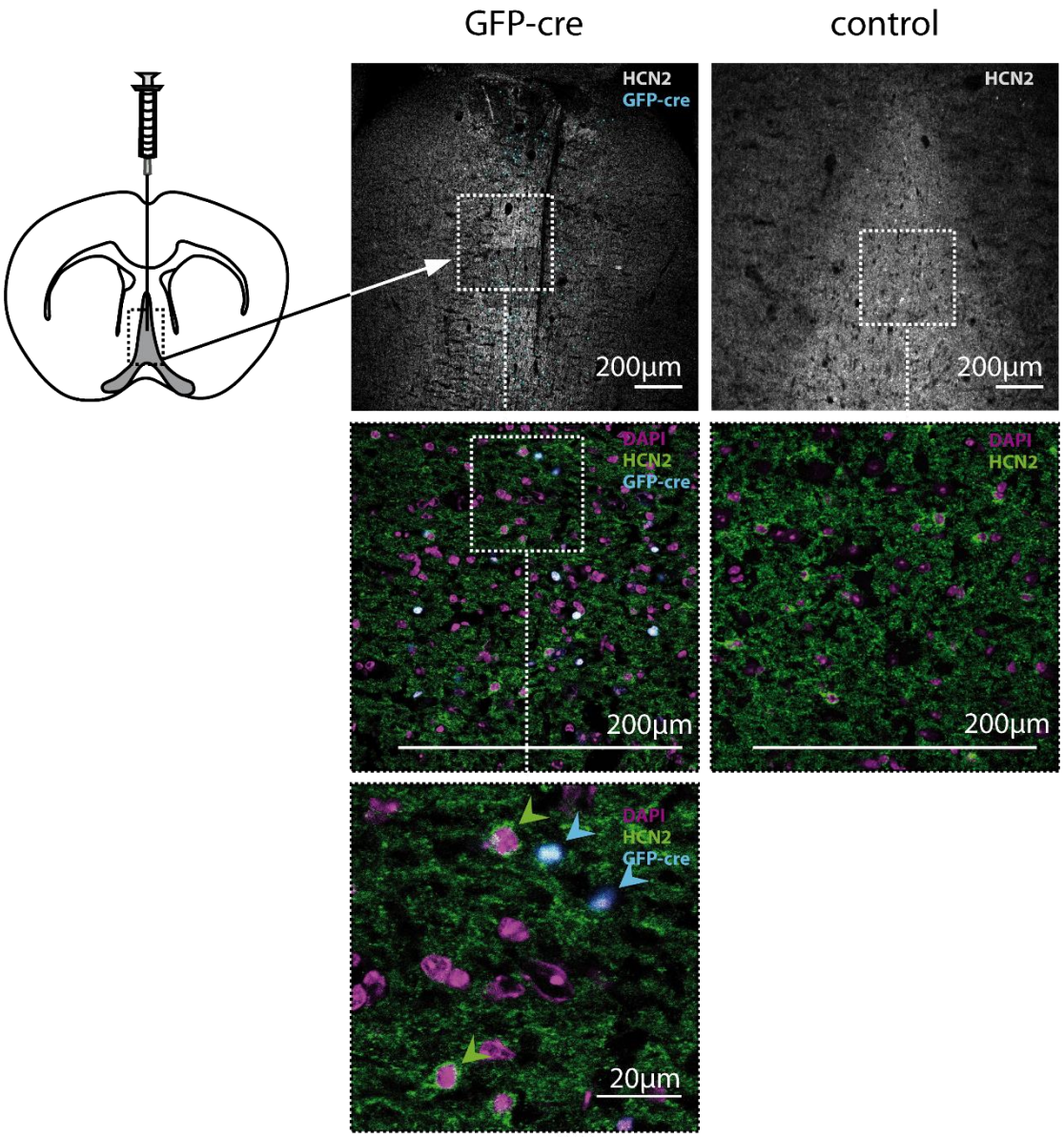

Figure 19 HCN2 expression in MS after GFP-cre injection

Stereotactic injections were used to deliver AAV-viruses containing GFP-cre or control into MS of 8-week old HCN2 L2 mice. The staining, performed approx. 4 weeks after injection, show that not only in the GFP-cre animals but also in control animals just a part of the cells are positive for HCN2 (green) suggesting that just the GABAergic population is HCN2-positive. The immunofluorescence staining for HCN2 (green) in MS area of GFP-cre injected cells (cyan) is diminished. Rectangles show higher magnification; HCN2 staining in green, DAPI in magenta and GFP-cre expression in cyan.

Analyzing the EEG and EMG recordings (control n=5; selective HCN2 KO n=6), it was investigated whether selective knockdown of HCN2 expression in MS neurons replicates the phenotype seen in HCN2 KO mice. Raw EEG traces looked normal and did not show any signs

of epileptiform activity, notably including the absence of SWDs, which were present in the global HCN2 KO mouse (Fig. 20).

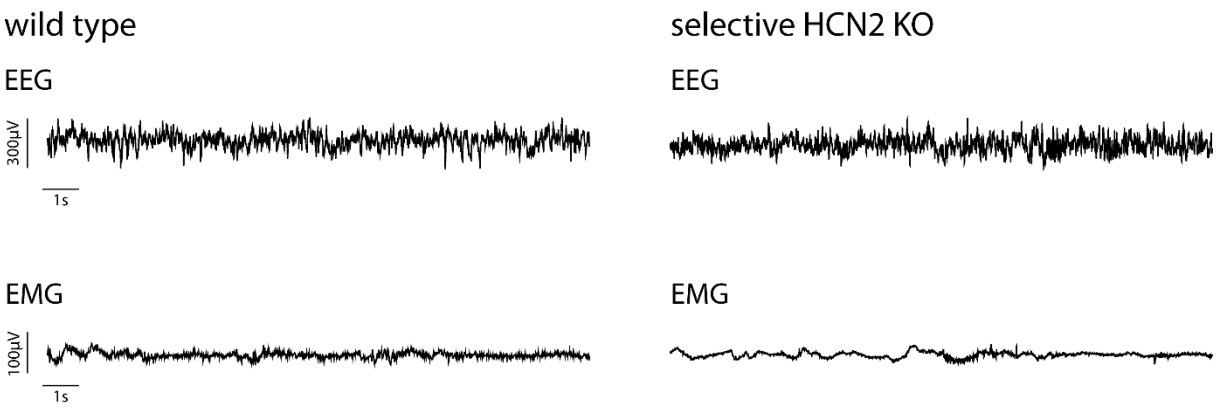

Figure 20 Selective HCN2 KO - EEG and EMG raw traces

Representative EEG and EMG patterns of WT and selective HCN2 KO animals of 30s recordings. Selective HCN2 KO trace does not show any abnormalities.

The total EEG spectral profile between 0.75 - 25 Hz was examined in selective HCN2 KO and control animals. In the selective HCN2 KO group, the total EEG power showed a reduction in theta power and an increase in delta power, similar to the pattern observed in HCN2 KO mice (Fig. 21A). Taking a closer look to the power spectra of the individual vigilance states, which were classified due to general approved criteria, it could be demonstrated that the absence of HCN2 channels in MS compromised the REM sleep EEG to the greatest extent. A significant drop down in the theta power (4–12Hz) was observed within this vigilance state. For the wake state a pronounced reduction was also noted in the theta frequency range. However, the NREM sleep power was unaltered in the theta frequency range in the selective HCN2 KO group (Fig. 21B).

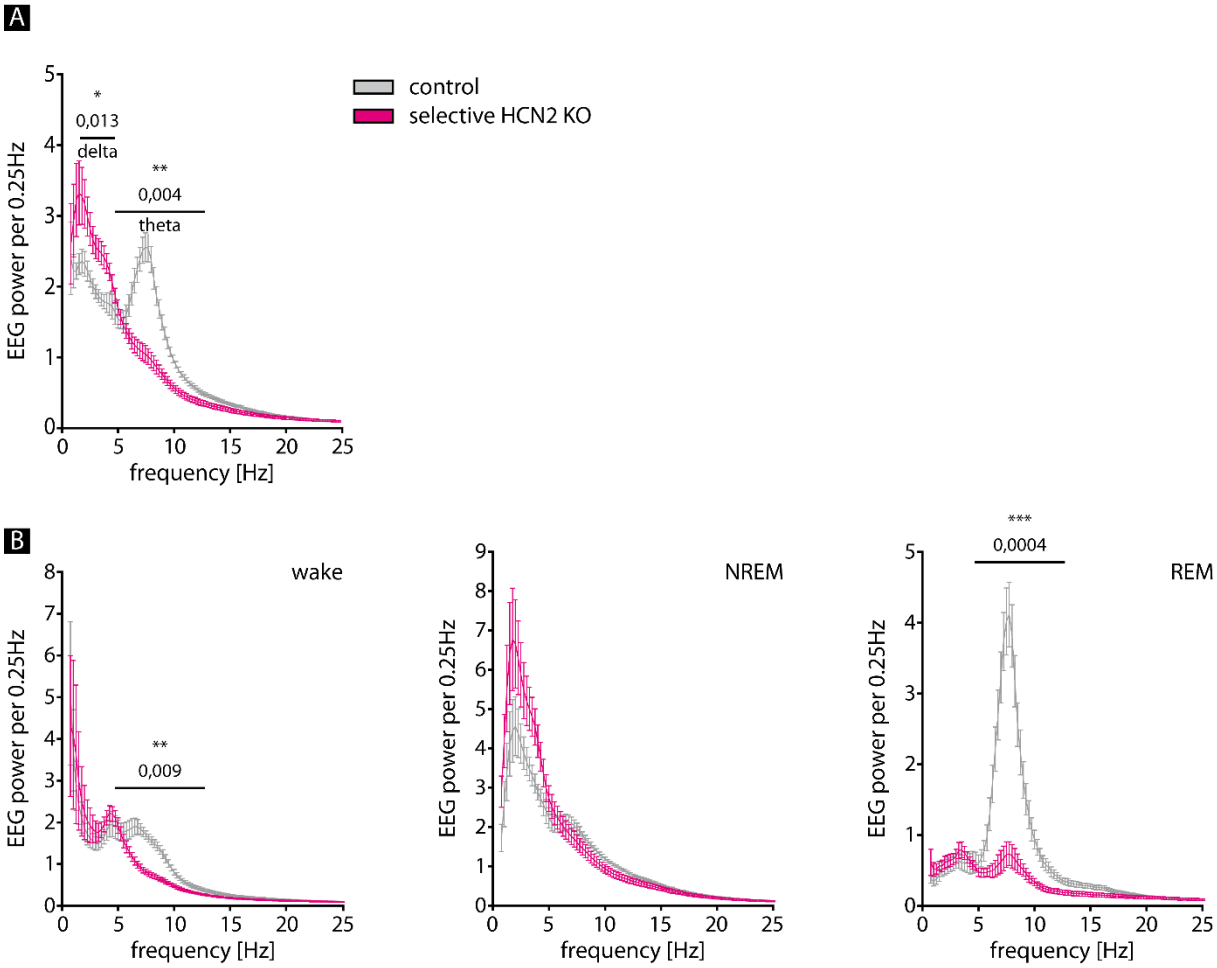

Figure 21 Selective HCN2 KO - power spectra

(A) Total power spectra of 24h recording time between 0.75 and 25Hz (0.25Hz bins, 4s epoch, Hamming) of control and selective HCN2 KO animals. (B) Mean spectral profiles for wake, NREM and REM sleep between 0.75 and 25Hz (0.25Hz bins, 4s epoch, Hamming) are shown in corresponding graphs. Selective HCN2 KO shows a decrease in theta power and an increase in delta power.

As the theta rhythm is a major hallmark of REM sleep and the theta power drop down is most prominent during this sleep stage, in a next analysis step it was investigated whether the quality and the duration of sleep is affected by a selective HCN2 KO in MS area. Initially the color-coded spectrogram of selective HCN2 KO and WT animals was analyzed. The spectrograms of both groups showed clearly that the NREM sleep is interrupted by REM sleep episodes (Fig. 22, blue bars). Normally, as it is the case in WT animals, at the transition from NREM sleep stage into REM sleep stage there is a change to a desynchronized EEG state. The delta waves, present during NREM sleep disappear and theta waves become the prevailing

oscillation during REM episodes. However, in the selective HCN2 KO spectrogram this theta band (peaking at around 8Hz) was clearly diminished during REM sleep.

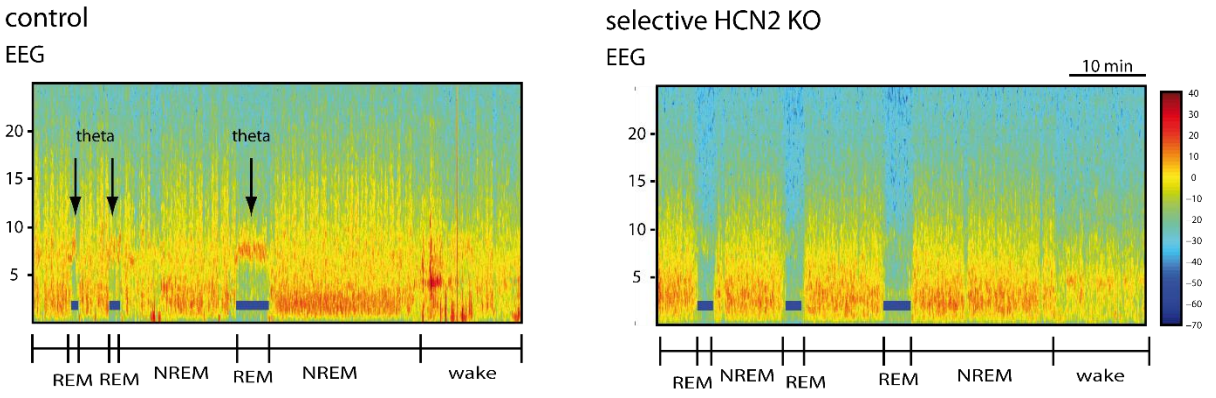

Figure 22 Selective HCN2 KO - color-coded spectrogram

Representative sections of a color-coded heat map of EEG power between 0.75 - 25Hz (0.25Hz bins) as a function of time. The control as well as the selective HCN2 KO animal show a normal NREM sleep interrupted by shorter REM sleep episodes (blue bars, arrows indicate theta). However, in the selective HCN2 KO animal the theta frequency oscillation is clearly reduced during REM sleep. Scale indicates intensity showing red for high and blue for low intensity levels.

To exclude further vigilance state specific effects, sleep-wake architecture was analyzed. Both animal groups showed a sleep-wake distribution typical for this nocturnal species with high and low sleep times during the light and the dark phase, respectively. There were no group-dependent differences in total NREM, REM or wake time during either light or dark phase (Fig. 23A). The mean episode duration of wake, NREM and REM bouts was comparable in the selective HCN2 KO and control group (Fig. 23B).

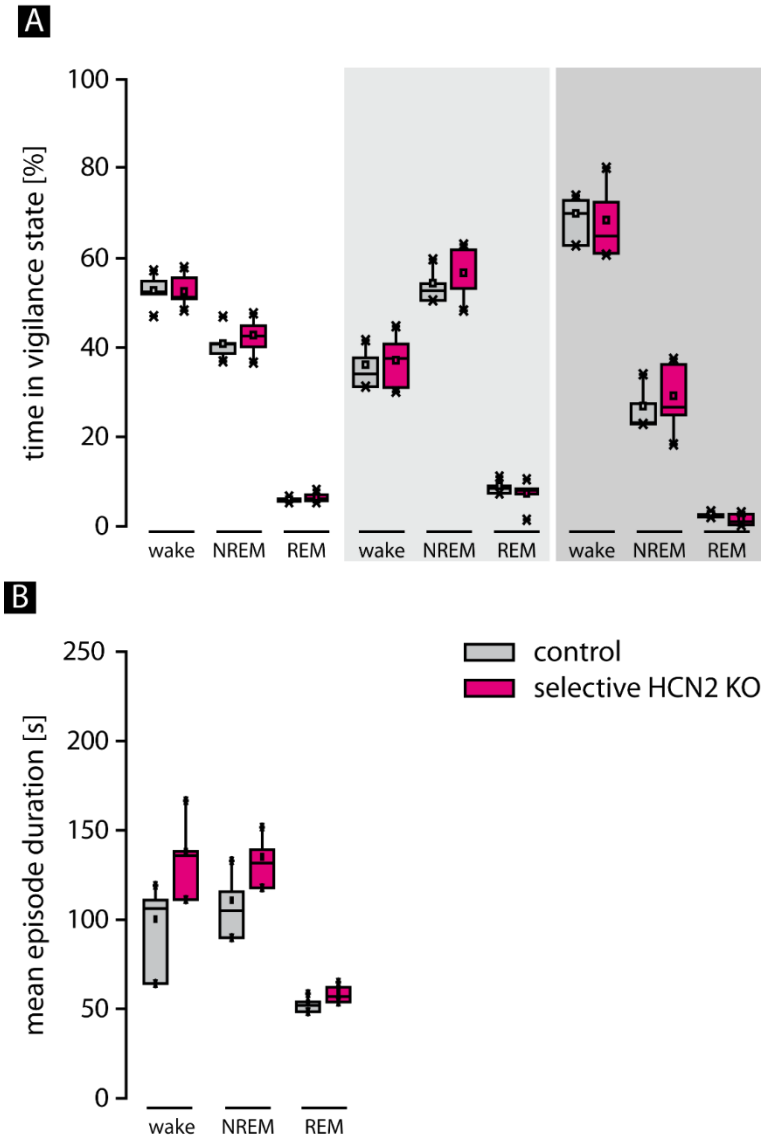

Figure 23 Selective HCN2 KO - time in different vigilance states

(A) Percentage of time spent in wake, NREM and REM sleep in total and separated for the 12h light/ dark periods. Selective HCN2 KO time spent in wake, NREM and REM sleep is similar to WT. (B) Mean episode duration of wake, NREM and REM sleep during total time is unchanged.

Also the relative transition from one behavioral state to another was unchanged and the total number of transitions was equal in both groups (Fig. 24A and B).

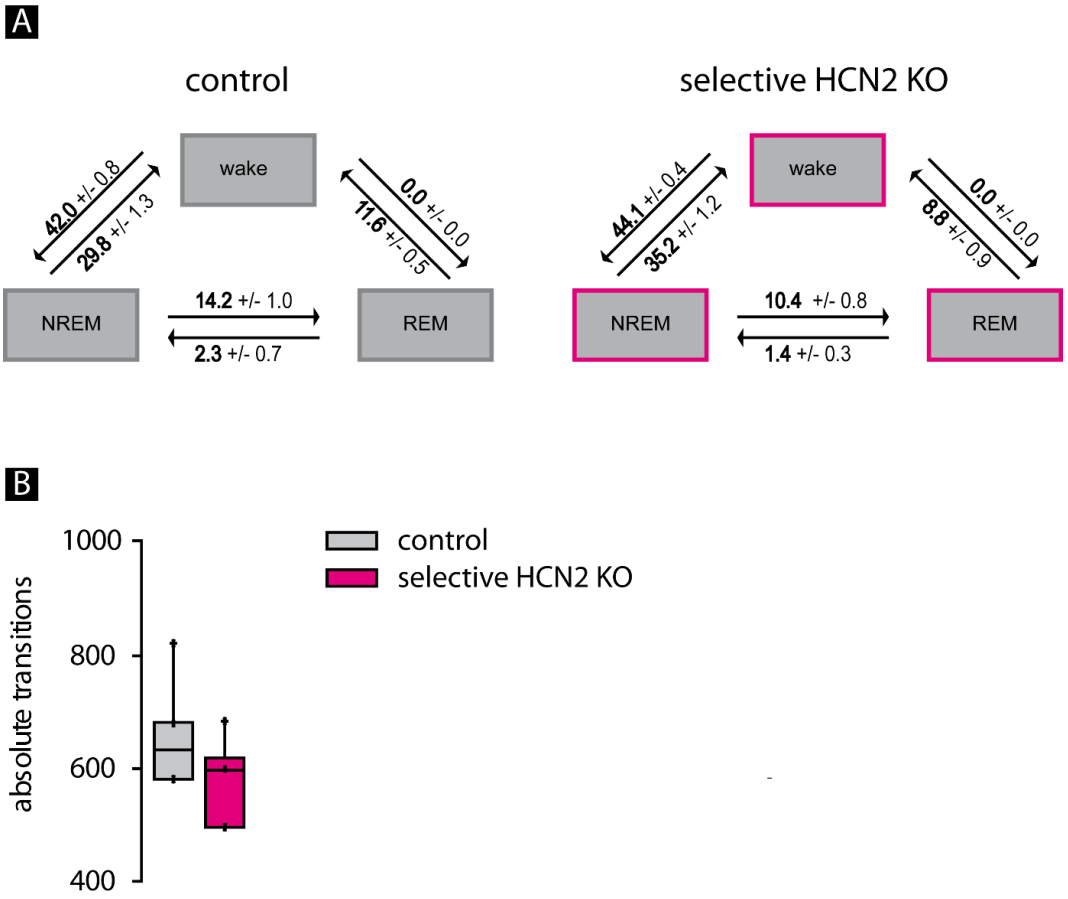

Figure 24 Selective HCN2 KO - transition

(A) Values indicate the relative number (mean +/- SEM) of transitions between wake, NREM and REM sleep per 24h for control and selective HCN2 KO animals. The relative number of transitions is unchanged (B) Absolute number of transitions within 24h is also unaffected.

Further analysis of the EEG theta power at the state transitions was carried out, in particular the transitions from NREM to REM sleep (NREM-REM) as well as from wake to NREM sleep (wake-NREM) and vice versa were examined. The control group showed the characteristic theta power peak at the NREM-REM sleep transition [51], while the selective HCN2 KO group revealed a steep decrease in theta power at the transition, which remained significantly lower during the subsequent REM sleep episode. Regarding the NREM-wake and wake-NREM transition respectively a similar phenomenon occurred. During the wake state, which was determined partly by its theta frequency content, the EEG theta power was significantly reduced in the HCN2 KO group (Fig. 25).

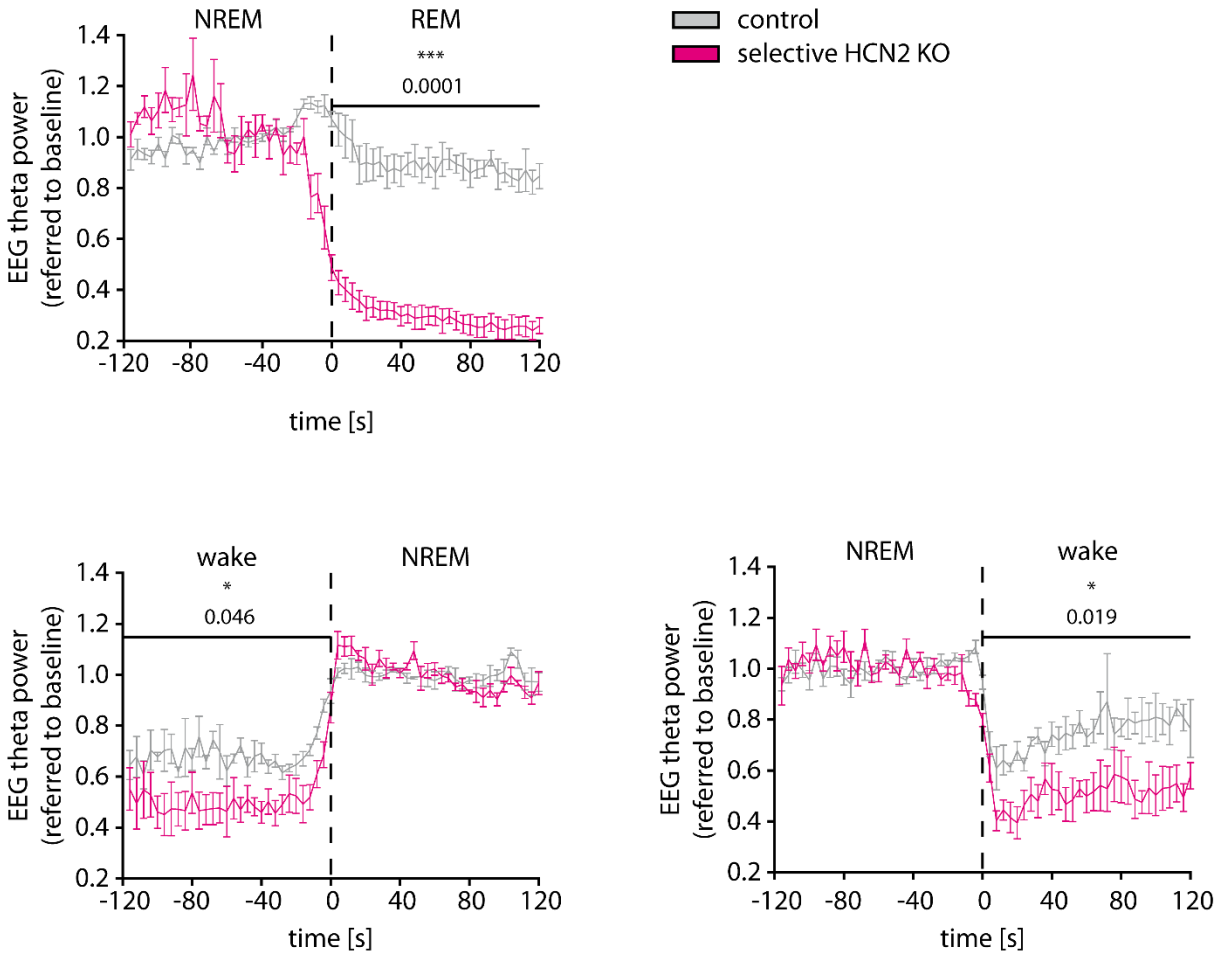

Figure 25 Selective HCN2 KO – spectral changes at state transition

Time course of EEG power in the theta frequency range (4-12Hz) at the transition between NREM and REM, wake and NREM and NREM and wake. Data were expressed as a percentage of baseline values during NREM sleep. Only data for the 2min before and after transition are shown. Vertical dashed line indicates transition at time 0. Selective HCN2 KO animals show a decrease in theta power.

These data indicate that the loss of HCN2 channels in MS contributes substantially to the generation of theta frequency, which is indeed a characteristic feature of normal REM sleep and also characteristic for the exploratory behavior of the wake state [51], but the REM sleep itself remains unaffected.

4.2.1 HCN2 EA and HCN2 FEA

To examine the impact of the cAMP-dependent HCN2 channel modulation on theta control mechanisms, mutants of the channel being insensitive towards cAMP, HCN2 EA (WT n=6; EA n=7) and HCN2 FEA (WT n=6; FEA n=7), were employed for telemetric EEG and EMG recordings

in freely moving mice. The HCN2 EA mutant shows two point mutations (R591E and T592A) in Exon 7 in the CNBD of the HCN2 channel. The resulting change in the CNBD abolished high affinity binding of cAMP leading to a suppression of the coactivaton of the channel. In addition the HCN2 FEA mutant was activated at voltages that are shifted to more positive values in comparison to WT in the absence of cAMP. In some native cells HCN channels are likely preactivated to some extent by basal cAMP [38]. To imitate a possible preactivation the additional F mutation (Y449F) in Exon 4, which encodes for the C-Linker of the channel was inserted (Fig. 26). This mutation leads to an activation curve shift to more positive values under basal conditions. As a consequence at the same potential more HCN2 channels are in the opening state than in WT control cells (mouse models were generated by Christian Gruner).

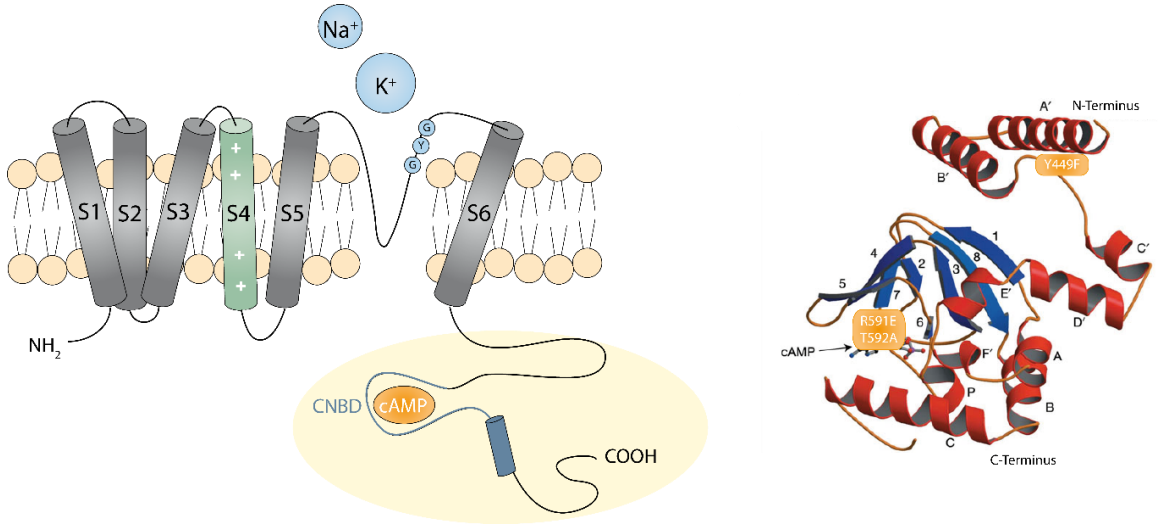

	$V_{0.5}$	ΔV_{max} cAMP
HCN2	-89.7 +/- 0.8 (19)	+ 18.7
HCN2 EA	-88.4 +/- 1.0 (3)	no shift
HCN2 FEA	-78.8 +/- 0.7 (11)	no shift

Figure 26 HCN2 EA and HCN2 FEA - point mutations in the C-Terminus of HCN2 channels

Transmembrane topology of HCN2 channels. The C-Terminus responsible for cAMP modulation is marked by a yellow circle (upper left). The mutated amino acids replaced in HCN2 EA and HCN2 FEA are indicated (upper right). $V_{0.5}$ values of heterologous expressed mutant HCN2 channels in HEK293 cells (lower left).

Schema adapted from [27] and chart shows unpublished data from Xiangang Zong

The raw EEG and EMG traces demonstrated that absence epilepsy was absent in HCN2 FEA mice while HCN2 EA mutant mice suffered from SWDs (Fig. 27).

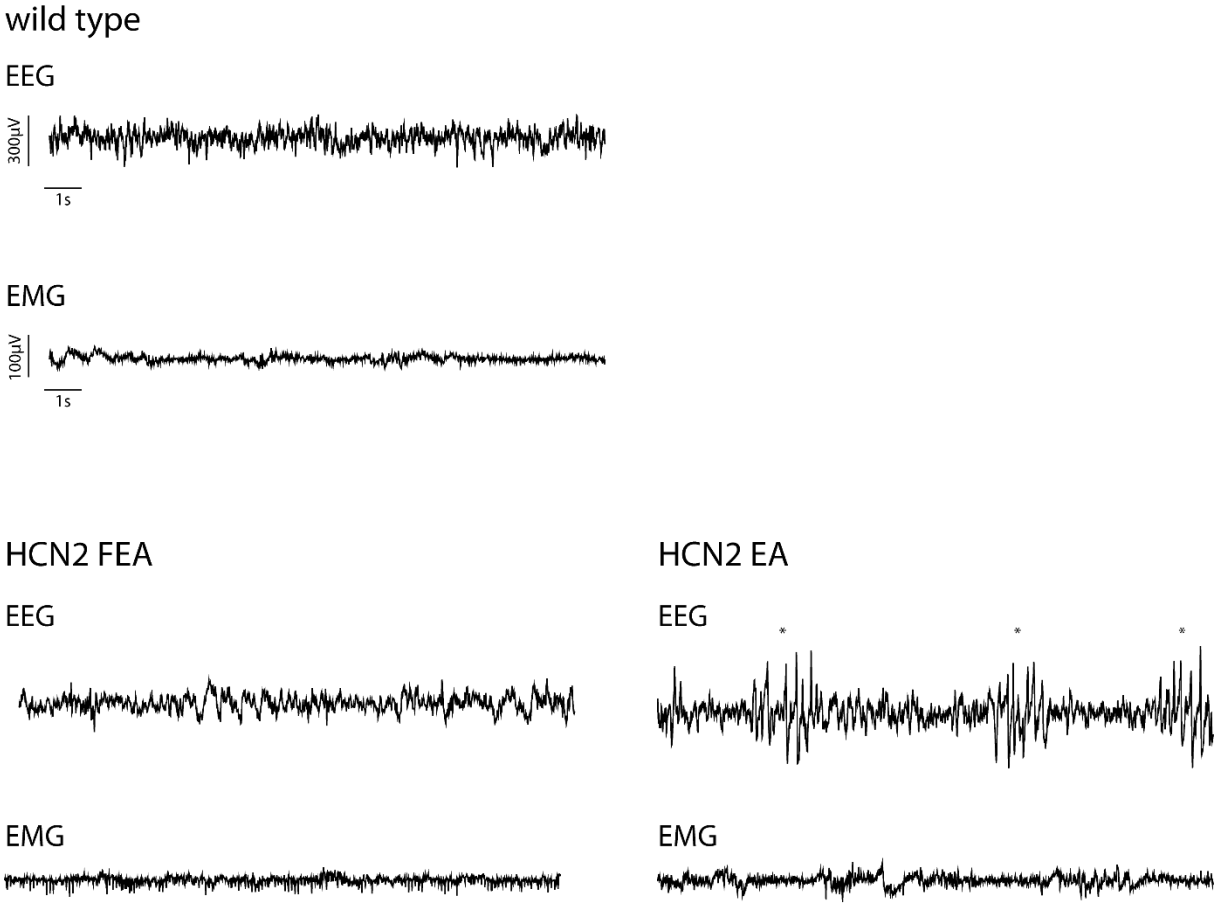

Figure 27 HCN2 FEA and HCN2 EA – EEG and EMG raw traces

Representative EEG and EMG patterns of HCN2 FEA, HCN2 EA and WT animals. Representative 30s recordings. Asterisks indicate SWDs. HCN2 FEA shows no abnormalities while HCN2 EA shows SWDs.

To investigate the impact of a cAMP insensitive channel on the frequencies' power, the total power spectrum and the power spectra of the three different vigilance states were assessed. The total power spectrum of the HCN2 FEA mice showed no significant difference in the broader theta frequency range (4-12Hz), but a slight decrease in the main theta frequency range (7-9Hz) compared to WT spectrum while the HCN2 EA spectrum was unchanged (Fig. 28A). During the wake stage the power in the 5Hz range was slightly increased in both mutants. The power spectra of the NREM sleep stage of the HCN2 FEA and HCN2 EA mutants respectively resembled the WT power spectrum, only the theta power seemed to be slightly

reduced in the HCN2 FEA mouse. Also during the REM sleep stage the theta power showed a reduction in the HCN2 FEA animals, while it was comparable to WT in the HCN2 EA mice (Fig. 28B).

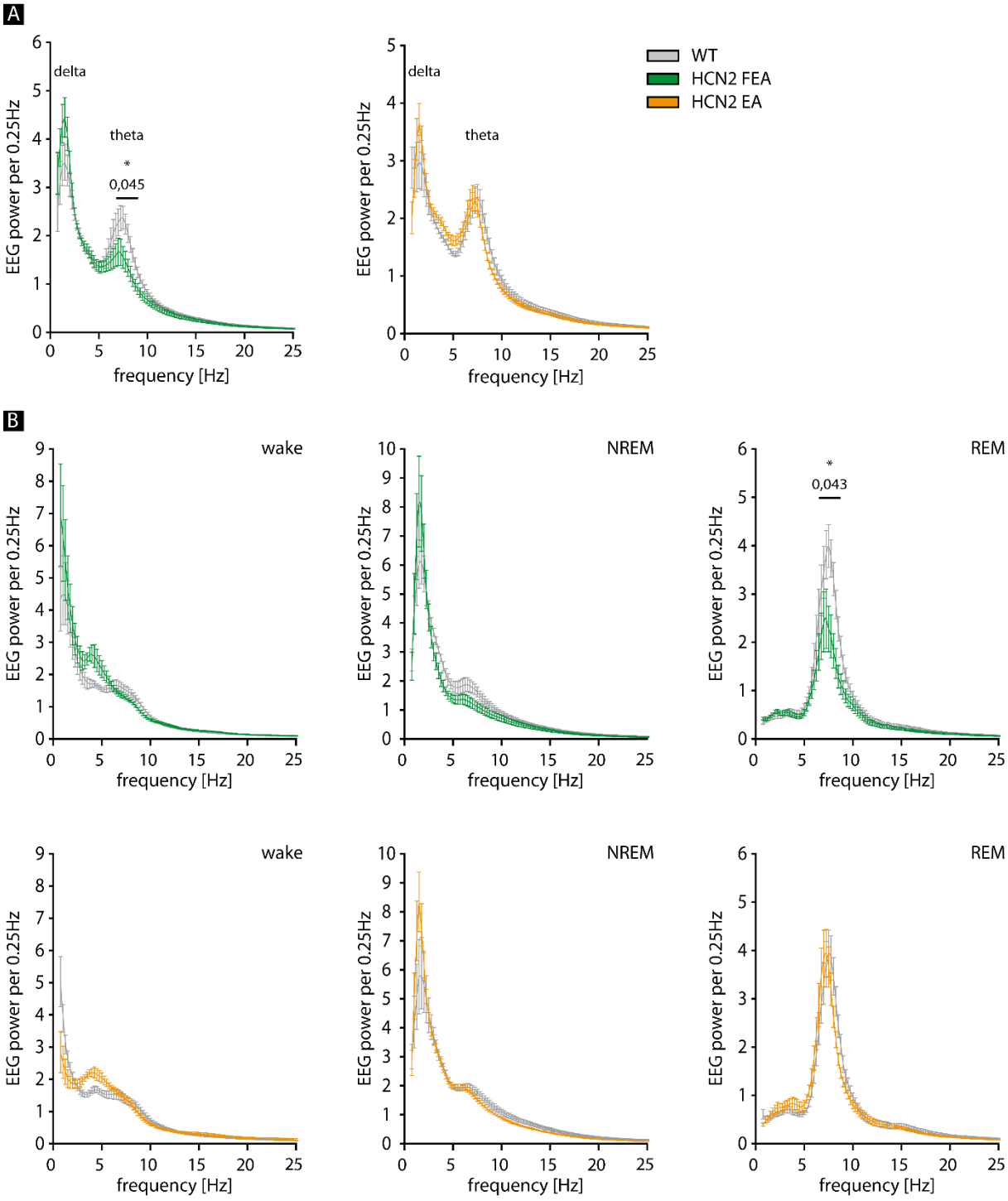

Figure 28 HCN2 FEA and HCN2 EA – power spectra

(A) Total power spectrum of 24h recording time between 0.75 and 25Hz (0.25Hz bins, 4s epoch, Hamming) for WT (gray), HCN2 FEA (green) and HCN2 EA animals (orange) (B) Mean spectral profiles for wake, NREM and REM sleep between 0.75 and 25Hz (0.25Hz bins, 4s epoch, Hamming) are shown in corresponding graphs.

As in HCN2 FEA animals the theta power is slightly affected it should be ruled out that the sleep architecture and quality was affected as a consequence, therefore the color-coded spectrogram of selective HCN2 FEA and EA animals with corresponding WT littermates was analyzed. The spectrograms of both groups showed clearly that the NREM sleep was interrupted by REM sleep episodes (blue bars) and the theta band (peaking at around 8Hz) was comparably present during REM sleep within all groups (Fig. 29).

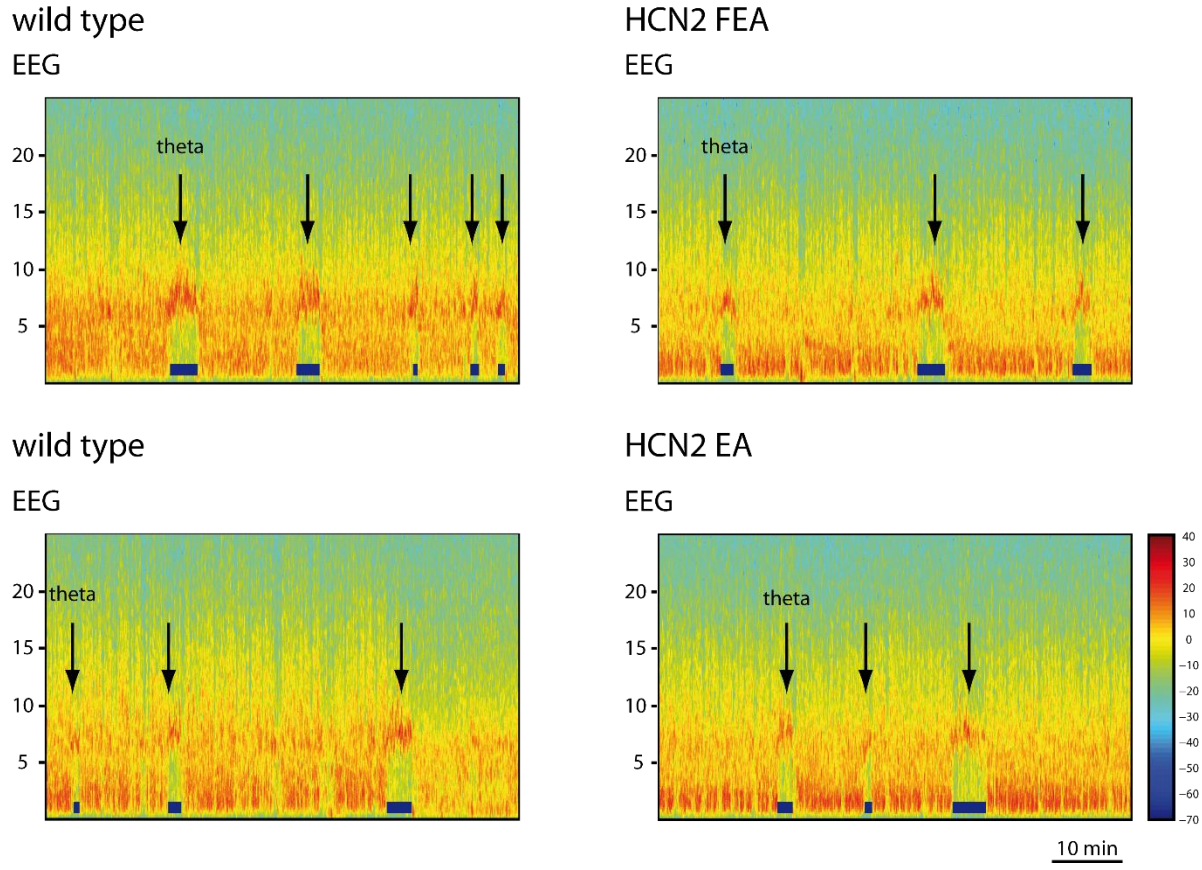

Figure 29 HCN2 FEA and HCN2 EA – color-coded spectrogram

Representative sections of a color-coded heat map of EEG power between 0.75.25Hz (0.25Hz bins) as a function of time. All groups show a normal NREM sleep interrupted by shorter REM sleep episodes (blue bars) and the theta frequency oscillation is clearly visible during REM sleep within all groups.

To assess the role of the cAMP insensitive channel for behavioral state duration, the time spent in the different vigilance states was analyzed. Both groups showed a sleep-wake pattern typically for nocturnal animals, they showed high sleep times during the light phase and low sleep times during the dark phase. The HCN2 FEA and HCN2 EA mice did not demonstrate any significant differences regarding the duration of the three different vigilance states. Both in the HCN2 FEA and the HCN2 EA mutants the duration of individual episodes spent in wake, NREM and REM sleep was unchanged (Fig. 30A and B).

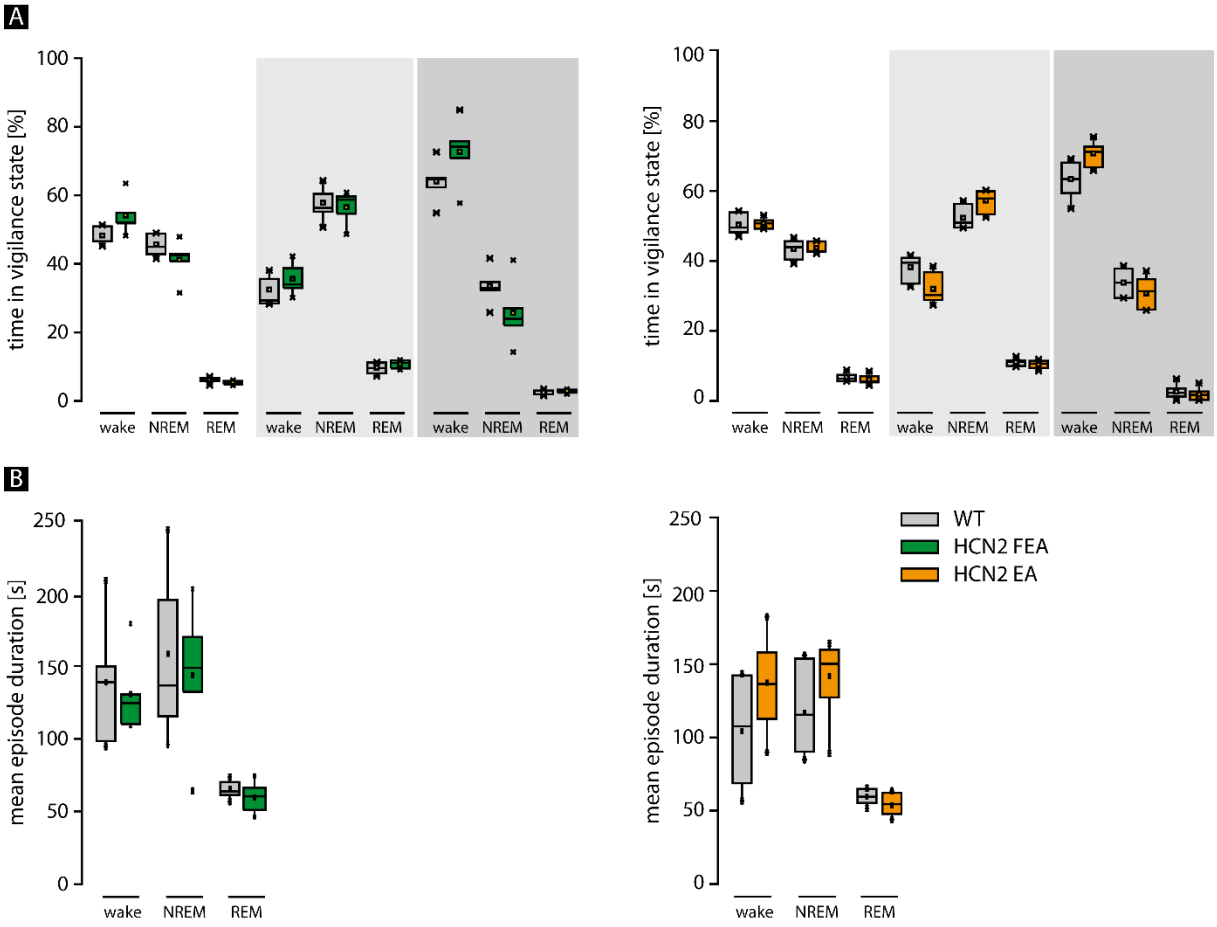

Figure 30 HCN2 FEA and HCN2 EA - time in different vigilance states

(A) Relative time spent in wake, NREM and REM sleep in total and separated for the 12h light/ dark periods for HCN2 FEA and HCN2 EA mice with corresponding littermates. Relative time is similar in all groups. (B) Mean episode duration during total time only in HCN2 FEA and HCN2 EA animals is unchanged.

The relative transition from one behavioral state to another was comparable to WT in HCN2 FEA and HCN2 EA and the total number of transitions was unchanged (Fig. 31A and B).

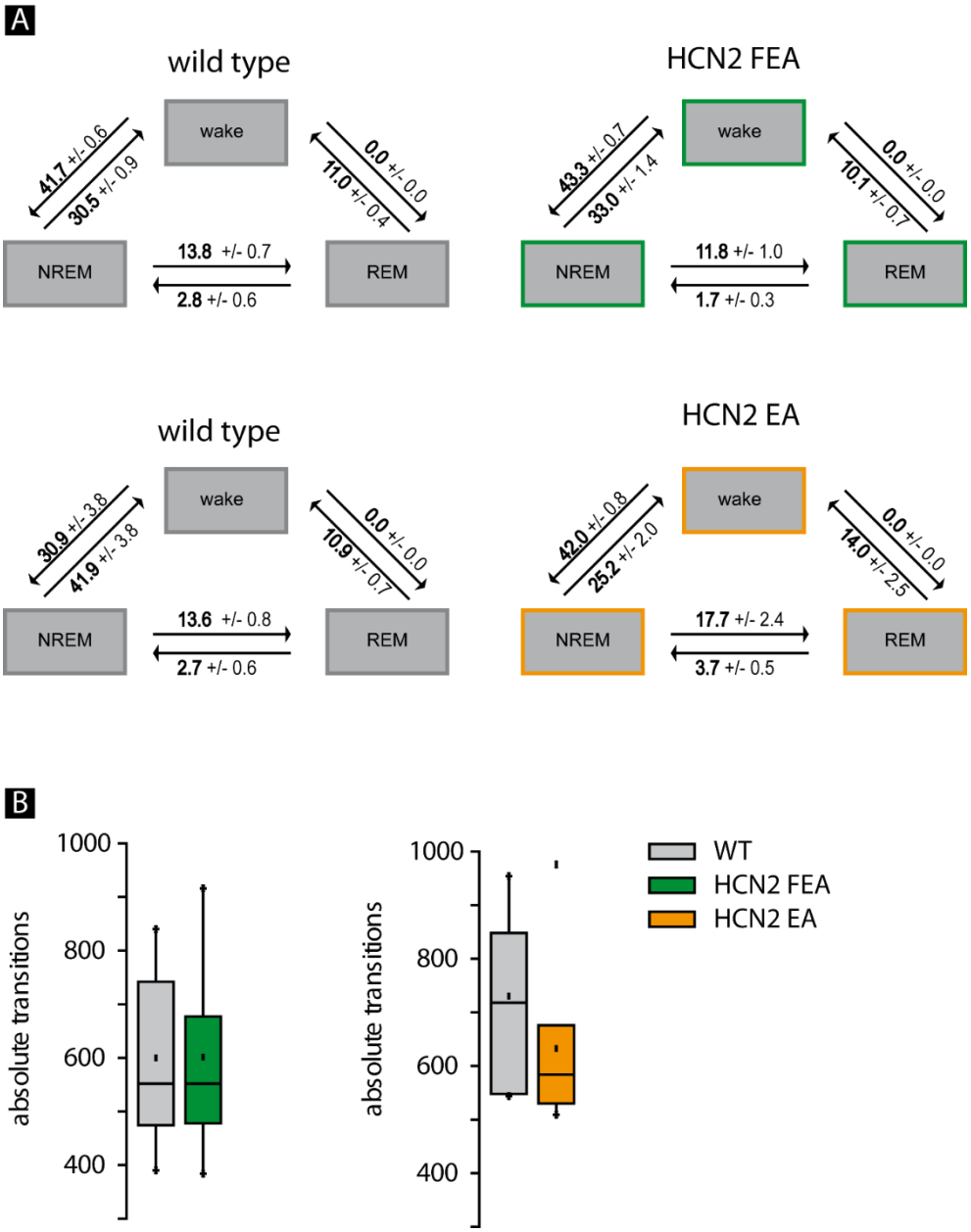

Figure 31 HCN2 EA and HCN2 FEA - transition

(A) Values indicate the relative number (mean +/- SEM) of transitions between wake, NREM and REM sleep per 24h for control and selective HCN2 KO animals. The relative number of transitions is unchanged. (B) Absolute number of transitions within 24h is also unaffected.

Regarding the NREM to REM transition it is evident that theta power increased to a marginally lesser extent at the transition in the HCN2 FEA mouse while the augmentation was comparable to WT in the HCN2 EA mouse line (Fig. 32).

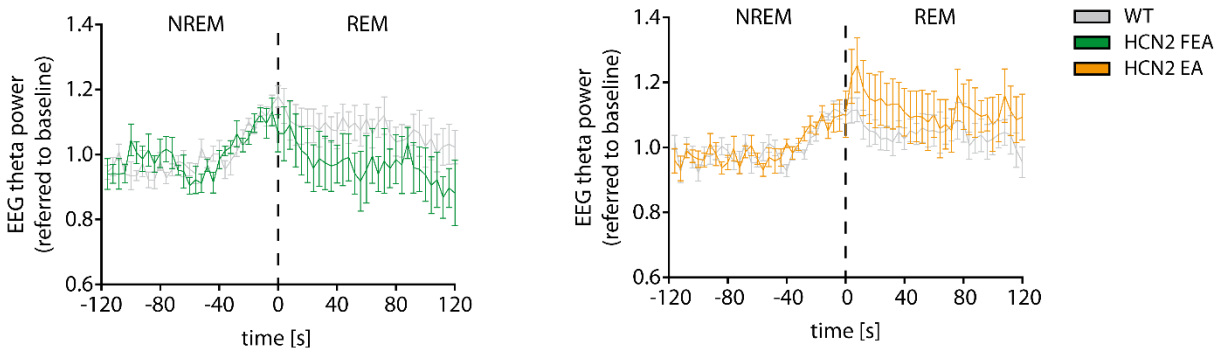

Figure 32 HCN2 EA and HCN2 FEA – spectral changes at state transition

Time course of EEG power in the theta frequency range at the transition between NREM and REM for HCN2 FEA (left panel) and HCN2 EA (right panel). Data were expressed as a percentage of baseline values during NREM sleep. Only data for the 2min before and after transition are shown. Vertical solid lines indicate transitions at time 0. Theta power is slightly reduced after the transition in HCN2 FEA animals while it is comparable to WT in HCN2 EA animals.

4.3 Hippocampus-dependent learning

To clarify whether the reduced theta power due to the loss of HCN2 channels in MS has an effect on the hippocampus-dependent place learning, a behavioral test using the water cross maze (WCM) was conducted [50]. For this experiment the selective HCN2 KO population was used, because the global HCN2 KO animals show severe physical impairments. The animals were 7-8 weeks old at the start of the experiment (selective HCN2 KO n=7; control n=7). The WCM used for this experiment consisted of 4 arms, arranged crosswise. The four arms were marked as North (N), East (E), South (S) and West (W) arm. A removable separation enabled to block the arm opposite the starting arm (either N or S arm), meaning that the part accessible for the animals had a 'T' shape. A platform was positioned permanently in the W arm below the water surface, invisible for the animals (Fig. 33). For every run the mouse was inserted carefully into the water in the start arm. After having located the platform the animal was retrieved and put back into the home cage. Every animal passed 6 trials a day for a period of 5 days. These runs served the mice to learn the platform location whereas the platform position did not change. However the starting position changed in a pseudorandom manner during the 6 runs between N and S arm. The alternating starting position forced the animal to use external cues for orientation. The learning efficiency was assessed by using three different parameters: Latency, accuracy and the accurate learner criterion. The latency was defined as the time the animals needed to locate the platform. A trial was evaluated as 'accurate' if the animal chose immediately the arm in which the platform was positioned and located the platform correctly. The accuracy resembled the percentage of accurate trials on every day for each animal. Animals have been rated as accurate learners if they succeeded in 5 out of 6 trials (83.3%), meaning they located the platform correctly in 83.3% of the cases.

Both groups, selective HCN2 and control littermates, showed no difference regarding the latency. However, the accuracy was significantly reduced in selective HCN2 KO animals. Hence, it can be concluded that the selective HCN2 KO group had more problems to locate the platform correctly than their control injected littermates. Assessing the accurate learners on day 5 this finding was even more obvious. The number of animals reaching the accurate learner criterion was significantly lower in the selective HCN2 KO group. That means the selective HCN2 KO leads to an impairment in learning the platform's location (Fig. 33).

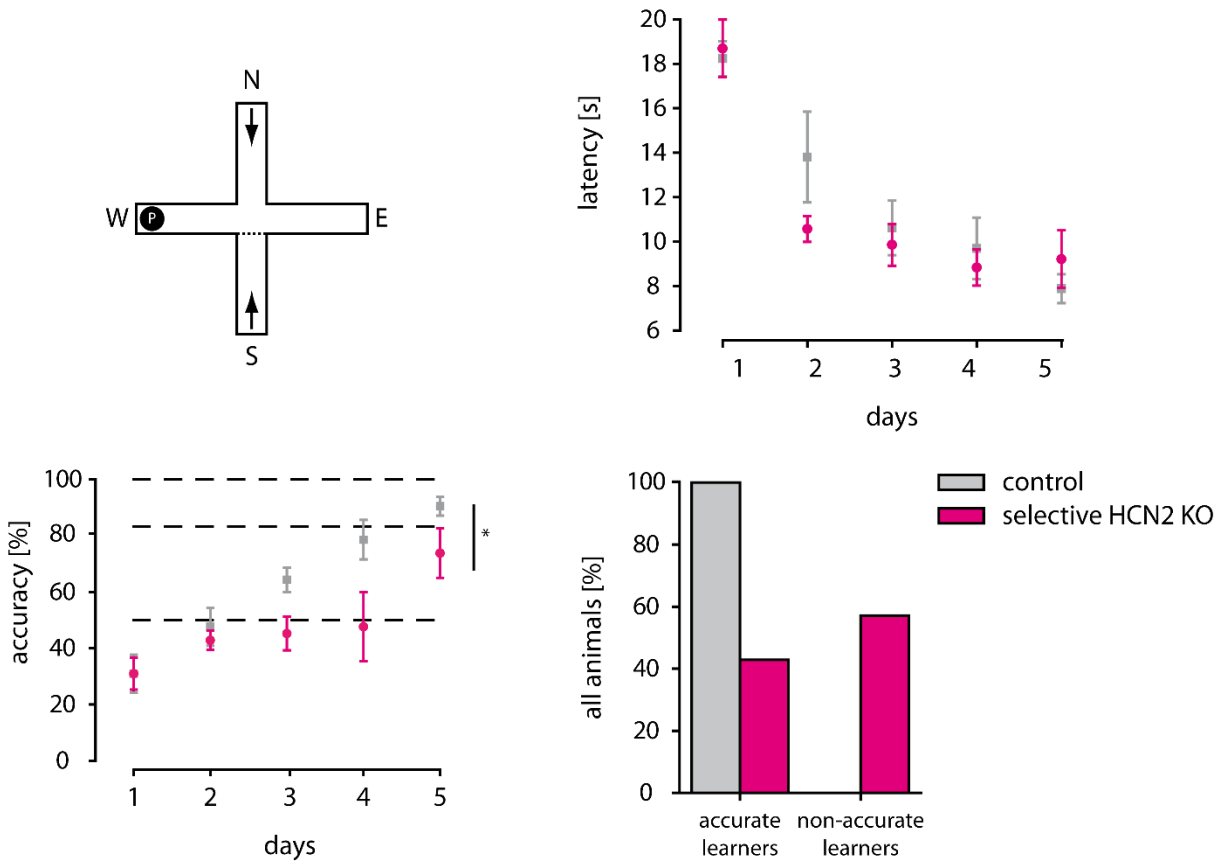

Figure 33 Selective HCN2 KO - place learning

Experimental setup: crosswise basin in which the northern (N) and southern (S) arm respectively is blocked by a Plexiglas barrier. The mice were trained 5 days long, 6 trials a day with alternating starting points (N or S). The hidden platform was located in the western arm. During the trials the latency (upper right panel), accuracy (lower left panel) and accurate learners (lower right panel) were calculated. Selective HCN2 KO group shows a significant reduction in accuracy and reached the accurate learner criterion rarer.

5 Discussion

Within the framework of the present thesis the electrical brain activity of various HCN2 mutants was assessed by applying EEG measurements. The main conclusion of the work is that correct HCN2 channel function is essentially involved in the control of neuronal rhythms both in the thalamo-cortical system and in the septo-hippocampal system.

As a first goal it could be demonstrated that not only a loss but also a cAMP insensitivity of HCN2 channels contribute to evoke SWDs, a major hallmark of absence epilepsy originating probably from the thalamo-cortical system.

Further the present work showed evidence that the activity of HCN2 channels, expressed in MS neurons, play a major role in regulating theta rhythm. A loss of HCN2 in MS area leads to a considerable drop down of theta power. Finally, in a behavioral test, checking the spatial navigation capabilities, MS-selective HCN2-deficient mice perform significantly worse in comparison to their WT littermates. Overall, an impairment or loss of HCN2 channel function in MS leads to a dysfunction of theta wave generation that finally results in an impairment of spatial memory. In the following sections the main conclusions were interpreted.

5.1 Influence of cAMP on SWDs

Within the context of this work it could be confirmed by using state-of-the-art methods that HCN2 KO animals show absence seizures assumably of thalamic origin [25]. In subsequent experiments the area of seizure origin needs to be confirmed, possibly by performing EEG measurements in selective thalamic HCN2 KO animals. These animals could be generated by employing the HCN2 cre/loxP system and a viral approach. It is likely that a dysfunction of the thalamo-cortical feedback loop is involved in seizure generation. The following model has been proposed for a proper function. Hyperpolarization activates I_h which leads to a depolarization of the membrane towards a threshold for a Ca^{2+} spike. The activation of the Ca^{2+} current (I_T), conferred by T-type Ca^{2+} channels, depolarizes the membrane towards a threshold for a burst of Na^+- and K^+-dependent action potentials. Repolarization caused by I_T inactivation is followed again by hyperpolarization (Fig. 34A, left panel). It is possible that the

time course of activation of HCN channels determines the frequency of membrane potential rhythms [7, 8]. A defect in this mechanism is highly associated with the occurrence of absence seizures. In HCN2-deficient thalamo-cortical rely neurons there is a hyperpolarizing shift in the resting membrane potential. This hyperpolarizing shift promotes recovery from inactivation of T-type Ca^{2+} channels and leads thereby to a facilitation of low-threshold burst firing in response to depolarizing inputs. This results in an increased oscillatory activity in the thalamo-cortical network contributing to SWDs [23] (Fig. 34A, right panel). In the present thesis it was investigated to what extent the channel modulation via cAMP plays a role for the seizure activity. Interestingly SWDs were detected in HCN2 EA animals but not in HCN2 FEA mice. Both mutants display an insensitivity towards cAMP whereas under basal conditions in the absence of cAMP the HCN2 FEA mutant shows an additional voltage shift to more positive values (e.g. in HEK 293 cells, Fig. 34B, left panel). By adding cAMP to the system the WT activation curve shifts to more positive values and as a result in cAMP preactivated systems WT and HCN2 FEA show similar $V_{0.5}$ values while the HCN2 EA activation curve is shifted to negative values (Fig. 34B, right panel). It is known that different cell types show different basal cAMP levels [56]. HEK293 cells show very low basal cAMP levels (approx. 0.1µM). Other cell types e.g. primary mouse cardiomyocytes demonstrate considerable higher basal cAMP levels (approx. 1 µM) whereas in thyroid cells the basal cAMP concentration is medium (approx. 0.5µM) [56]. It is possible that the basal cAMP levels differ not only between cell types but also within different brain regions. It is possible that during non-activated states the cAMP concentration is relatively high within the thalamo-cortical circuit. It might also be that the concentration of cAMP, which acts in discrete subcellular microdomains varies microdomain-specifically and is different from the cAMP levels in the cytosol [57]. Possible high subcellular cAMP microdomain concentrations could also contribute to the effect. In subsequent experiments these hypotheses need to be confirmed e.g. by expressing FRET-based cAMP sensors within this brain region and performing FRET measurements. The model of high cAMP leads to the hypothesis that in the thalmao-cortical system WT neurons are strongly preactivated by basal cAMP levels (Fig. 34B, right panel). According to this model the results identifying differences regarding the occurrence of SWDs in the different mutant models are explainable. In thalamo-cortical neurons in the basal state HCN2 FEA channels act like WT channels because the preactivation is mimicked by the positive voltage shift. Due its insensitivity towards cAMP a preactivation of HCN2 EA channels is not possible and consequentially in thalamo-cortical

relay neurons the $V_{0.5}$ values are more negative in comparison to WT. *In vivo* it is possible that the lower $V_{0.5}$ membrane potential values of HCN2 EA channels could not be reached in thalamo-cortical neurons resulting in a limited opening probability of the channel under physiological conditions. As the channel function is restricted in the thalamo-cortical area in HCN2 EA mice acting as a functional HCN2 KO, the inactivation of T-type Ca^{2+} channels is impaired. This leads to a facilitation of low-threshold burst firing, like it is the case in HCN2 KO animals and this augmented oscillatory activity is highly associated with SWDs (Fig. 34A, right panel).

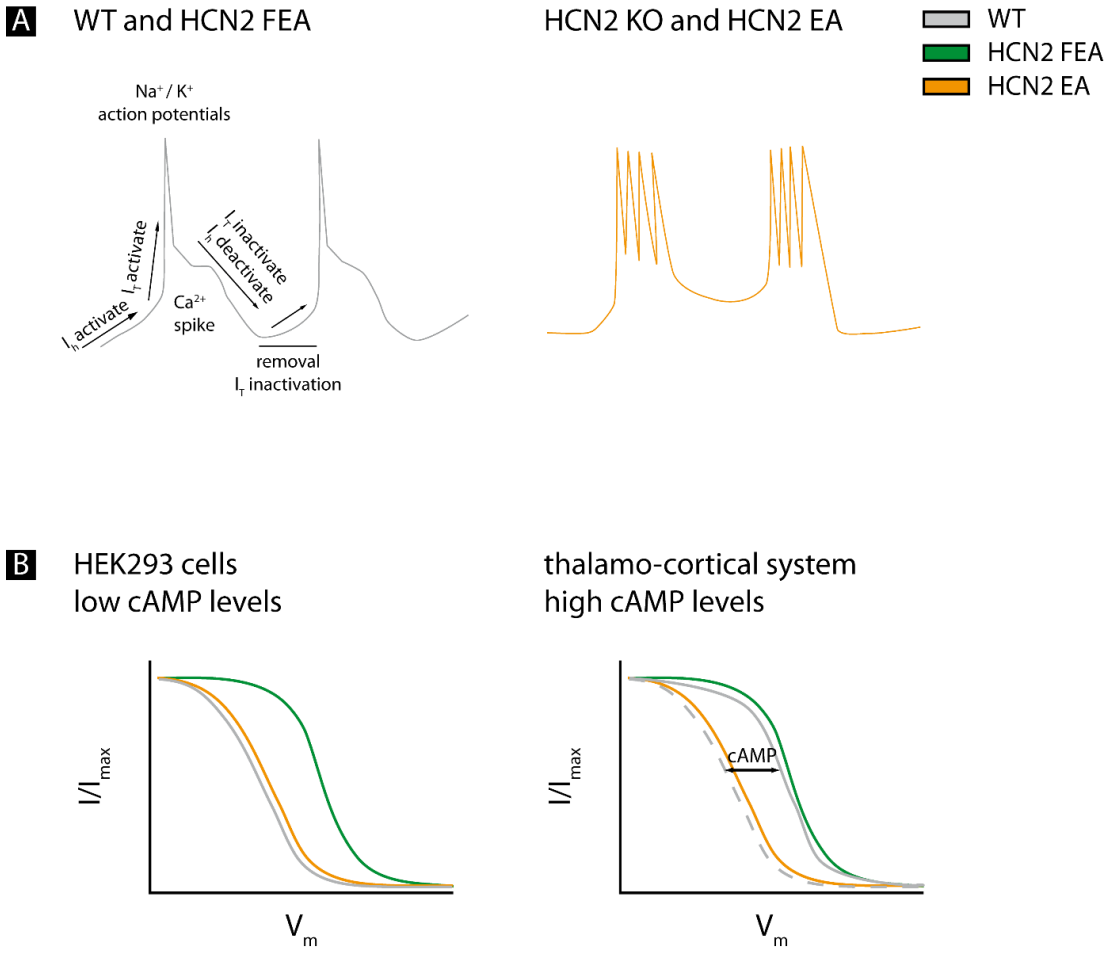

Figure 34 Burst mode in thalamo-cortical neurons of HCN2 mutants and activation curve in various cell types

(A) Shown is a schema of the burst firing mode of both WT, HCN2 FEA and HCN2 KO, HCN2 EA neurons. In HCN2 KO and EA neurons the inactivation of T-type Ca2+ channels is impaired. This leads to a promotion of low-threshold burst firing and the augmented oscillatory activity is highly associated with SWDs. (B) Shown are schemas of the activation curves of HCN2 mutants in HEK293 cells (left panel) and in the thalamo-cortical system (right panel). In HEK293 cells WT channels are barely preactivated by cAMP leading to similar $V_{0.5}$ values like in HCN2 EA cells and the activation curve of HCN2 FEA overexpressing

cells shows a positive shift. However in the thalamo-cortical system the basal cAMP levels are elevated and WT channels are preactivated leading to similar $V_{0.5}$ values like in HCN2 FEA cells.

5.2 Theta regulation via HCN2

To evaluate the role of HCN2 for theta control within the septo-hippocampal pathway it is essential to understand the mechanisms underlying theta wave generation. To switch the network state of the hippocampus from a resting state, occurring during immobile wake state and NREM sleep [61] into the theta mode, appearing during activated brain states and REM sleep, a trigger is necessary. This transition is facilitated and sustained by the pacemaker activity of MS neurons [62] which receive input from the HT and BS area and project to the hippocampal formation. The MS contains a large variety of distinct neurons. There are cholinergic [63], GABAergic [14, 64, 65] and glutamatergic [66, 67] cells. An inactivation of MS GABAergic neurons in mice reduces significantly theta power [69], suggesting that *in vivo* GABAergic neurons are the neuron type primarily involved in theta wave generation. Due to acknowledged theories, MS GABAergic projecting cells inhibit GABAergic interneurons of the hippocampal formation [3], triggering a disinhibitory action on pyramidal cells and MS GABAergic neurons receive intraseptal regulating inputs from both cholinergic and glutamatergic neurons [58] (Fig. 35).

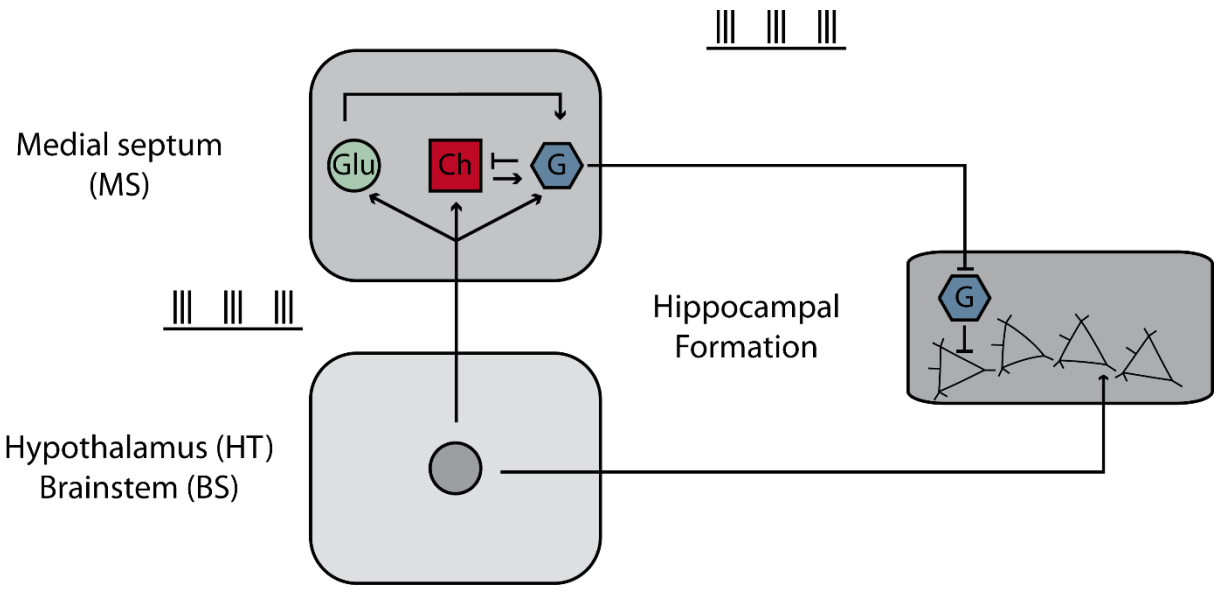

Figure 35 Ascending system of theta rhythm control

The theta rhythm of the hippocampal formation is mainly controlled and regulated by the cholinergic (Ch), glutamatergic (Glu) and GABAergic (G) neurons of MS, which receive inputs from deeper BS and HT areas.

Modified from [59]

The present study revealed that HCN2 channels expressed in MS neurons have a major effect on theta band generation. It could be shown that the pacemaker channel HCN2 is the major isoform expressed throughout MS nucleus and HCN1 and HCN4 are expressed considerably weaker. Electrophysiological recordings in acute brain slices in MS confirmed largely the expression data because the I_h inward currents were significantly lower in HCN2 KO cells in this nucleus (experiments performed by Henrik Huelle, data not shown). There are data indicating that HCN2 immunoreactive cells are primarily GABAergic and that the hippocampus is among the targets of these projections neurons [55]. In consecutive experiments these data need to be confirmed either by performing immunohistochemistry co-staining with GABA- and HCN2-antibodies or by creating a selective GABA-specific MS HCN2 KO expressing a GFP-cre virus under a selective GABAergic promoter (e.g. GAD65 promoter [60]) in HCN2 L2 animals.

Due to the theory that HCN2-positive cells are GABAergic, it is possible that these neurons fire rhythmically at theta frequencies and act as impulse generator for theta rhythms in the hippocampal formation [61]. HCN2 pacemaker channels can trigger action potentials. Neurons, expressing HCN2, could pass through a cycle, consisting of an action potential, afterhyperpolarization and depolarization followed again by another action potential. A prominent role for HCN2 channels in contributing to the rhythmic firing of theta frequency in MS neurons could be proofed by the genetic deletion of HCN2 leading to a disruption of theta frequency membrane potential oscillations.

It is possible that the timing of the theta frequency oscillations in hippocampal formation neurons may be determined by the time course of activation and deactivation of I_h currents, which means faster time constants lead to theta rhythms of higher frequencies [62, 63]. These findings suggest that HCN2 subunits could be also involved in determining and maintaining place cell firing in the hippocampus and grid spacing the EC, which underlay intact theta wave firing [64]. EC grid cells show periodic firing locations that scale up within the EC. This

expansion is in accordance with changes in cellular properties depending on HCN channels [45]. HCN2 channels expressed in MS, projecting to EC and hippocampus, contribute possibly to the scale change in grid firing. The results that MS-selective HCN2 KO animals showed an impairment in spatial learning consolidates the hypothesis that navigation and orientation, which requires intact grid and place cell firing might be impaired in these animals.

Although the relation between theta and REM sleep is clearly established in rodents [65], no abnormalities regarding REM sleep duration and architecture could be detected in all HCN2 mutant animals. To interpret these results it is necessary to focus on the neuronal circuits responsible for switching between NREM and REM sleep. Recent findings propose a BS flip–flop switch, consisting of coordinated inhibitory REM-off, which fire when the brain is not in a REM state and REM-on areas, which fire during REM sleep in the mesopontine tegmentum. The REM-on area consists of two different neuron populations, one projecting to the basal forebrain (BF) including MS which regulates the EEG components of REM sleep. The other one projects to the BS and spinal cord (SC) and regulates atonia and eye movement during REM sleep, another important hallmark [66]. Due to this model it is explainable that the REM sleep itself is not affected. Because the actual trigger location for REM sleep, the mesopontine tegmentum seems to be not affected by an absence of HCN2 likely due to the weak expression in this area [40]. However the EEG components of REM sleep, the theta oscillations are compromised in consequence of a HCN2 loss in theta regulating brain areas, the basal forebrain implying MS neurons. Further at the transition from NREM to REM sleep the theta power decreases more rapidly in selective HCN2 KO animals suggesting that the BS is incapable to execute the frequency shift correctly (Fig. 36).

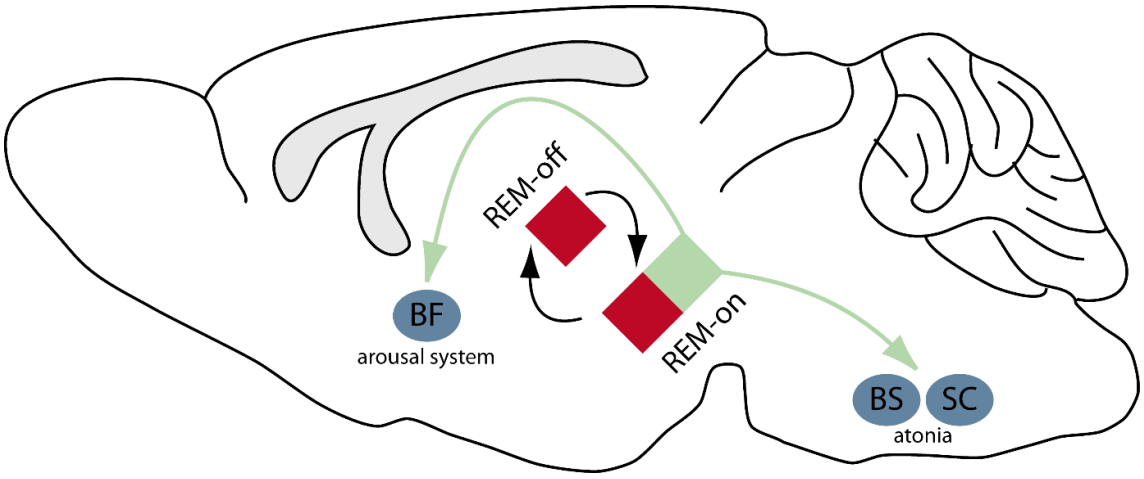

Figure 36 The flip-flop switch for control of REM sleep

A schema indicating the REM sleep flip-flop switch in the mesopontine tegmentum. Neurons in the mesopontine tegmentum (red and green squares) are REM-off and REM-on neurons which act as mutual antagonists. Projecting neurons (green arrows) originating from the REM-on zone lead to the basal forebrain (BF) to cause EEG desynchronization. Other neurons send axons to the BS and spinal cord (SC), where they control eye movements and muscle tone.

5.3 Theta regulation via cAMP

To investigate to what extent a cAMP insensitivity of HCN2 influences theta regulation, the mutant mouse models HCN2 FEA and HCN2 EA were used. The HCN2 FEA mutant displays an insensitivity towards cAMP caused by the EA mutation and a positive voltage shift in systems with low basal cAMP levels provoked by the F mutation. The HCN2 EA mutant shows just an insensitivity towards cAMP. Surprisingly the power analysis of the EEG spectra showed a reduction of the theta power in HCN2 FEA and no change in HCN2 EA animals. To interpret these results it is assumed that within the septo-hippocampal circuitry the basal cAMP levels are low or that there are at least low subcellular cAMP microdomain concentrations preventing that possible high cytosolic cAMP levels could reach the target [56]. These hypotheses need to be clarified in further FRET-based experiments. As a consequence HCN2 channels are barely preactivated leading to similar activation curves of WT and HCN2 EA but to a positive activation curve shift of HCN2 FEA due to the F mutation (Fig. 37A). To explain the results within this context it is necessary to consider the effects of an increasing membrane conductance on the excitability of a neuron (Fig. 37B). Activation of HCN channels by hyperpolarization leads to an opening of the channels and consequently Na^+ inflow, which depolarizes the membrane further and additional channels are opened which results in a rapid

increase of the conductance. In conclusion the excitability elevates with increasing conductance until a maximum is reached, which reflects the pacmaking activity of HCN2 channels and the ascending part of the curve in Fig. 37B. The value of the maximum depends critically on the balance between HCN2 and other channels. After having exceeded maximal values, the excitability decreases again with a further increase in conductance. This is probably due to shunting inhibition that means a reduction of the amplitude and the duration of excitatory postsynaptic potentials (EPSPs) by increasing the membrane conductance [67] or due to an inactivation of Na^+ channels. This condition simulates the descending part of the curve in Fig. 37B.

It is evident that in global HCN2 KO animals the conductance is minimal and as a consequence ion flow is vanished due to the absence of the channel. Consequently the excitability of neurons is marginal leading to a limited generation of a theta oscillation. Thus, in HCN2 KO animals the greatest effect on theta power was monitored. In WT and HCN2 EA animals the channels act as pacemaker, because at a defined conductance value a corresponding excitability value on the ascending part of the curve is given (Fig. 37B). However, in HCN2 FEA mutant mice the opening probability of the channel at a defined membrane potential is higher than in WT and HCN2 EA because the basal activation curve is shifted to more positive values, that means the conductance is increased. At this point the excitability already exceeded the peak, so that the excitability in HCN2 FEA neurons is lower than in WT cells and thus leading to a diminished theta power (Fig. 37B).

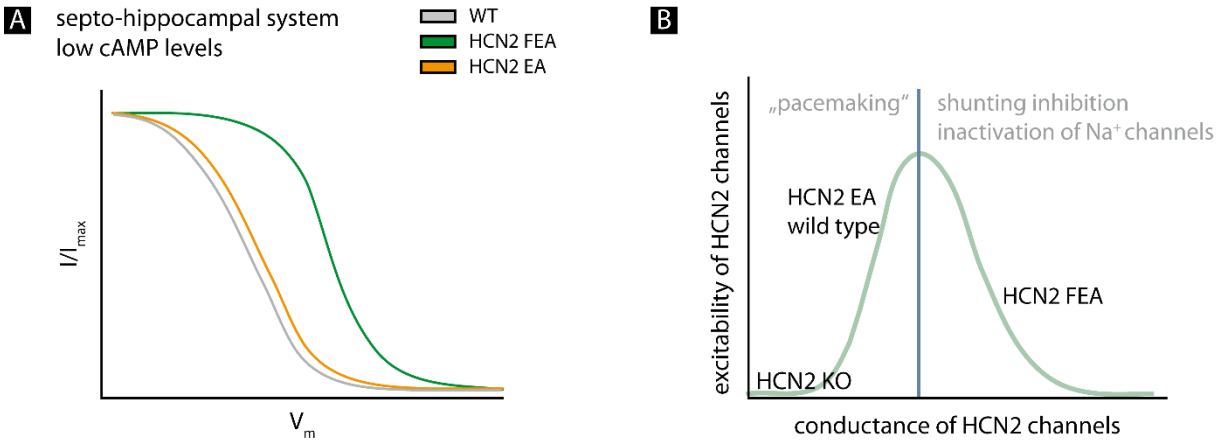

Figure 37 Activation curve in septo-hippocampal system and excitability-conductance-diagram

(A) Shown is a schema of the activation curve of HCN2 mutants in the septo-hippocampal system. Within this system there are low cAMP levels and WT channels are barely preactivated by cAMP leading to similar $V_{0.5}$ values like in HCN2 EA cells and the activation curve of HCN2 FEA cells shows a positive voltage shift. (B) Activation of HCN channels by hyperpolarization leads to a depolarization of the membrane and an increase of the conductance. The excitability elevates with increasing conductance until a maximum is reached. The ascending part of the curve reflects the pacemaking activity of HCN2 channels. After having exceeded maximal values, the excitability decreases with a further increase in conductance. This is probably due to shunting inhibition or due to an inactivation of Na^+ channels. This condition simulates the descending part of the curve.

6 Summary

Rhythmic oscillations of various frequencies are essential for signal transmission within neuronal networks and for the communication between different brain areas. An important neuronal rhythm is the theta rhythm which occurs primarily during REM sleep and active wake states. In addition there is strong evidence that the theta rhythm is involved in spatial learning and navigation by influencing the firing of place and grid cells. It has been suggested that the medial septal (MS) nucleus acts as pacemaker and controls the theta rhythm. There is initial evidence that hyperpolarization-activated cyclic nucleotide-gated (HCN) channels in MS neurons play a role in regulating these oscillations. The HCN channel family comprises four isoforms (HCN1-4) which are gated by voltage and by the direct binding of cAMP. In the context of this thesis it was shown that HCN2, expressed within the MS, is the main isoform involved in theta control mechanisms. To characterize the specific role of HCN2 channels for the regulation of the theta rhythm global and MS-selective HCN2 KO animals were used for EEG measurements. The MS-restricted KO was generated by using an *in vivo* adeno-associated virus mediated cre-dependent gene silencing approach in floxed HCN2 mice. The EEG data revealed that not only a global lack of HCN2 but also a MS-specific absence of the channel lead to an impairment of theta oscillations. The theta power was significantly reduced in these animals. In addition, EEG recordings were performed with two HCN2 knockin mouse models, HCN2 FEA and HCN2 EA. In both mutants the channel is insensitive towards cAMP. Within the MS the activation curve of the FEA mutant is probably shifted to more positive values in comparison to WT while it is similar to WT in the EA mutant. The FEA animals showed a slight decrease in theta power while the power spectra of the EA mutant was unchanged. Furthermore MS-specific HCN2-deficient mice showed an impairment in spatial learning behavior. Future experiments need to investigate the causal link between the theta drop down and the impairment of spatial navigation in HCN2-deficient animals. As it is known that grid and place cell firing depend critically on intact theta rhythm, it is likely that a loss of HCN2 leads to an impairment of grid and place cell function and thus to defects in spatial learning.

Within this study it was further demonstrated that also in other neuronal systems HCN2 channels contribute to oscillation control. In global HCN2 KO as well as in HCN2 EA animals spike and wave discharges, a hallmark of absence epilepsy, were detected. It has been

suggested that these spike and wave discharges possibly originate from the thalamo-cortical system.

In conclusion, the present thesis shows evidence that HCN2 is of crucial importance for controlling und regulating neuronal oscillations *in vivo* in rodents.

7 Bibliography

1. Vanderwolf, C.H., *Hippocampal electrical activity and voluntary movement in the rat.* Electroencephalogr Clin Neurophysiol, 1969. **26**(4): p. 407-18.
2. Colgin, L.L. and E.I. Moser, *Hippocampal theta rhythms follow the beat of their own drum.* Nat Neurosci, 2009. **12**(12): p. 1483-4.
3. Freund, T.F. and M. Antal, *GABA-containing neurons in the septum control inhibitory interneurons in the hippocampus.* Nature, 1988. **336**(6195): p. 170-3.
4. Pignatelli, M., A. Beyeler, and X. Leinekugel, *Neural circuits underlying the generation of theta oscillations.* J Physiol Paris, 2012. **106**(3-4): p. 81-92.
5. Luthi, A., T. Bal, and D.A. McCormick, *Periodicity of thalamic spindle waves is abolished by ZD7288,a blocker of Ih.* J Neurophysiol, 1998. **79**(6): p. 3284-9.
6. Luthi, A. and D.A. McCormick, *H-current: properties of a neuronal and network pacemaker.* Neuron, 1998. **21**(1): p. 9-12.
7. Dickson, C.T., et al., *Properties and role of I(h) in the pacing of subthreshold oscillations in entorhinal cortex layer II neurons.* J Neurophysiol, 2000. **83**(5): p. 2562-79.
8. Thoby-Brisson, M., P. Telgkamp, and J.M. Ramirez, *The role of the hyperpolarization-activated current in modulating rhythmic activity in the isolated respiratory network of mice.* J Neurosci, 2000. **20**(8): p. 2994-3005.
9. Xu, C., et al., *Hippocampal theta rhythm is reduced by suppression of the H-current in septohippocampal GABAergic neurons.* Eur J Neurosci, 2004. **19**(8): p. 2299-309.
10. Wahl-Schott, C. and M. Biel, *HCN channels: structure, cellular regulation and physiological function.* Cell Mol Life Sci, 2009. **66**(3): p. 470-94.
11. Biel, M., et al., *Hyperpolarization-activated cation channels: from genes to function.* Physiol Rev, 2009. **89**(3): p. 847-85.
12. Brown, H.F., D. DiFrancesco, and S.J. Noble, *How does adrenaline accelerate the heart?* Nature, 1979. **280**(5719): p. 235-6.
13. DiFrancesco, D., P. Ducouret, and R.B. Robinson, *Muscarinic modulation of cardiac rate at low acetylcholine concentrations.* Science, 1989. **243**(4891): p. 669-71.
14. Fenske, S., et al., *Sick sinus syndrome in HCN1-deficient mice.* Circulation, 2013. **128**(24): p. 2585-94.
15. Dossi, R.C., A. Nunez, and M. Steriade, *Electrophysiology of a slow (0.5-4 Hz) intrinsic oscillation of cat thalamocortical neurones in vivo.* J Physiol, 1992. **447**: p. 215-34.
16. Leresche, N., et al., *Pacemaker-like and other types of spontaneous membrane potential oscillations of thalamocortical cells.* Neurosci Lett, 1990. **113**(1): p. 72-7.
17. Leresche, N., et al., *Low-frequency oscillatory activities intrinsic to rat and cat thalamocortical cells.* J Physiol, 1991. **441**: p. 155-74.
18. Soltesz, I., et al., *Two inward currents and the transformation of low-frequency oscillations of rat and cat thalamocortical cells.* J Physiol, 1991. **441**: p. 175-97.
19. McCormick, D.A. and J.R. Huguenard, *A model of the electrophysiological properties of thalamocortical relay neurons.* J Neurophysiol, 1992. **68**(4): p. 1384-400.
20. McCormick, D.A. and H.C. Pape, *Properties of a hyperpolarization-activated cation current and its role in rhythmic oscillation in thalamic relay neurones.* J Physiol, 1990. **431**: p. 291-318.

21. DiFrancesco, D. and P. Tortora, *Direct activation of cardiac pacemaker channels by intracellular cyclic AMP.* Nature, 1991. **351**(6322): p. 145-7.
22. Wang, J., et al., *Activity-dependent regulation of HCN pacemaker channels by cyclic AMP: signaling through dynamic allosteric coupling.* Neuron, 2002. **36**(3): p. 451-61.
23. Coulon, P., T. Budde, and H.C. Pape, *The sleep relay--the role of the thalamus in central and decentral sleep regulation.* Pflugers Arch, 2012. **463**(1): p. 53-71.
24. Steriade, M., D.A. McCormick, and T.J. Sejnowski, *Thalamocortical oscillations in the sleeping and aroused brain.* Science, 1993. **262**(5134): p. 679-85.
25. Ludwig, A., et al., *Absence epilepsy and sinus dysrhythmia in mice lacking the pacemaker channel HCN2.* Embo j, 2003. **22**(2): p. 216-24.
26. Doyle, D.A., et al., *The structure of the potassium channel: molecular basis of K+ conduction and selectivity.* Science, 1998. **280**(5360): p. 69-77.
27. Zagotta, W.N., et al., *Structural basis for modulation and agonist specificity of HCN pacemaker channels.* Nature, 2003. **425**(6954): p. 200-5.
28. Vaca, L., et al., *Mutations in the S4 domain of a pacemaker channel alter its voltage dependence.* FEBS Lett, 2000. **479**(1-2): p. 35-40.
29. Yu, F.H. and W.A. Catterall, *The VGL-chanome: a protein superfamily specialized for electrical signaling and ionic homeostasis.* Sci STKE, 2004. **2004**(253): p. re15.
30. DeBerg, H.A., et al., *Structural mechanism for the regulation of HCN ion channels by the accessory protein TRIP8b.* Structure, 2015. **23**(4): p. 734-44.
31. Santoro, B., et al., *Identification of a gene encoding a hyperpolarization-activated pacemaker channel of brain.* Cell, 1998. **93**(5): p. 717-29.
32. Ludwig, A., et al., *A family of hyperpolarization-activated mammalian cation channels.* Nature, 1998. **393**(6685): p. 587-91.
33. Ishii, T.M., et al., *Molecular characterization of the hyperpolarization-activated cation channel in rabbit heart sinoatrial node.* J Biol Chem, 1999. **274**(18): p. 12835-9.
34. Ludwig, A., et al., *Two pacemaker channels from human heart with profoundly different activation kinetics.* Embo j, 1999. **18**(9): p. 2323-9.
35. DiFrancesco, D., *Pacemaker mechanisms in cardiac tissue.* Annu Rev Physiol, 1993. **55**: p. 455-72.
36. Pape, H.C., *Queer current and pacemaker: the hyperpolarization-activated cation current in neurons.* Annu Rev Physiol, 1996. **58**: p. 299-327.
37. Cao-Ehlker, X., et al., *Up-regulation of hyperpolarization-activated cyclic nucleotide-gated channel 3 (HCN3) by specific interaction with K+ channel tetramerization domain-containing protein 3 (KCTD3).* J Biol Chem, 2013. **288**(11): p. 7580-9.
38. Moosmang, S., et al., *Differential distribution of four hyperpolarization-activated cation channels in mouse brain.* Biol Chem, 1999. **380**(7-8): p. 975-80.
39. Santoro, B., et al., *Molecular and functional heterogeneity of hyperpolarization-activated pacemaker channels in the mouse CNS.* J Neurosci, 2000. **20**(14): p. 5264-75.
40. Notomi, T. and R. Shigemoto, *Immunohistochemical localization of Ih channel subunits, HCN1-4, in the rat brain.* J Comp Neurol, 2004. **471**(3): p. 241-76.
41. Kocsis, B. and S. Li, *In vivo contribution of h-channels in the septal pacemaker to theta rhythm generation.* Eur J Neurosci, 2004. **20**(8): p. 2149-58.
42. Fitch, T.E., et al., *Dopamine D1/5 receptor modulation of firing rate and bidirectional theta burst firing in medial septal/vertical limb of diagonal band neurons in vivo.* J Neurophysiol, 2006. **95**(5): p. 2808-20.

43. Bassant, M.H., et al., *Medial septal GABAergic neurons express the somatostatin sst2A receptor: functional consequences on unit firing and hippocampal theta.* J Neurosci, 2005. **25**(8): p. 2032-41.
44. Nolan, M.F., et al., *The hyperpolarization-activated HCN1 channel is important for motor learning and neuronal integration by cerebellar Purkinje cells.* Cell, 2003. **115**(5): p. 551-64.
45. Giocomo, L.M., et al., *Grid cells use HCN1 channels for spatial scaling.* Cell, 2011. **147**(5): p. 1159-70.
46. Giocomo, L.M. and M.E. Hasselmo, *Knock-out of HCN1 subunit flattens dorsal-ventral frequency gradient of medial entorhinal neurons in adult mice.* J Neurosci, 2009. **29**(23): p. 7625-30.
47. Heys, J.G., L.M. Giocomo, and M.E. Hasselmo, *Cholinergic modulation of the resonance properties of stellate cells in layer II of medial entorhinal cortex.* J Neurophysiol, 2010. **104**(1): p. 258-70.
48. Hussaini, S.A., et al., *Increased size and stability of CA1 and CA3 place fields in HCN1 knockout mice.* Neuron, 2011. **72**(4): p. 643-53.
49. Mironov, S.L., et al., *Imaging cytoplasmic cAMP in mouse brainstem neurons.* BMC Neurosci, 2009. **10**: p. 29.
50. Kleinknecht, K.R., et al., *Hippocampus-dependent place learning enables spatial flexibility in C57BL6/N mice.* Front Behav Neurosci, 2012. **6**: p. 87.
51. Franken, P., A. Malafosse, and M. Tafti, *Genetic variation in EEG activity during sleep in inbred mice.* Am J Physiol, 1998. **275**(4 Pt 2): p. R1127-37.
52. Mang, G.M. and P. Franken, *Sleep and EEG phenotyping in mice.* Current Protocols in Mouse Biology, 2012: p. 55-74.
53. Steenland, H.W., X.Y. Li, and M. Zhuo, *Predicting aversive events and terminating fear in the mouse anterior cingulate cortex during trace fear conditioning.* J Neurosci, 2012. **32**(3): p. 1082-95.
54. Bland, B.H., *The physiology and pharmacology of hippocampal formation theta rhythms.* Prog Neurobiol, 1986. **26**(1): p. 1-54.
55. Varga, V., et al., *The presence of pacemaker HCN channels identifies theta rhythmic GABAergic neurons in the medial septum.* J Physiol, 2008. **586**(16): p. 3893-915.
56. Borner, S., et al., *FRET measurements of intracellular cAMP concentrations and cAMP analog permeability in intact cells.* Nat Protoc, 2011. **6**(4): p. 427-38.
57. Sprenger, J.U., et al., *In vivo model with targeted cAMP biosensor reveals changes in receptor-microdomain communication in cardiac disease.* Nat Commun, 2015. **6**: p. 6965.
58. Hajszan, T., M. Alreja, and C. Leranth, *Intrinsic vesicular glutamate transporter 2-immunoreactive input to septohippocampal parvalbumin-containing neurons: novel glutamatergic local circuit cells.* Hippocampus, 2004. **14**(4): p. 499-509.
59. Vertes, R.P., W.B. Hoover, and G. Viana Di Prisco, *Theta rhythm of the hippocampus: subcortical control and functional significance.* Behav Cogn Neurosci Rev, 2004. **3**(3): p. 173-200.
60. Weller, M.L., et al., *894. Selective Targeting of GABAergic Neurons Using rAAV: The Potential Role of EAAC1 in Seizure Susceptibility.* Molecular Therapy, 2006. **13**: p. S344-S345.
61. Hangya, B., et al., *GABAergic neurons of the medial septum lead the hippocampal network during theta activity.* J Neurosci, 2009. **29**(25): p. 8094-102.

62. Giocomo, L.M., et al., *Temporal frequency of subthreshold oscillations scales with entorhinal grid cell field spacing.* Science, 2007. **315**(5819): p. 1719-22.
63. Giocomo, L.M. and M.E. Hasselmo, *Time constants of h current in layer ii stellate cells differ along the dorsal to ventral axis of medial entorhinal cortex.* J Neurosci, 2008. **28**(38): p. 9414-25.
64. Koenig, J., et al., *The spatial periodicity of grid cells is not sustained during reduced theta oscillations.* Science, 2011. **332**(6029): p. 592-5.
65. Steriade, M.M. and R.W. McCarley, *Brain control of wakefulness and sleep*. 2007: Springer Science & Business Media.
66. Lu, J., et al., *A putative flip-flop switch for control of REM sleep.* Nature, 2006. **441**(7093): p. 589-94.
67. Pavlov, I., et al., *I(h)-mediated depolarization enhances the temporal precision of neuronal integration.* Nat Commun, 2011. **2**: p. 199.

8 List of figures

9 List of abbreviations

AAV ..... Adeno-associated virus

AP ..... *Anterior - posterior*

approx. ..... approximately

BF ..... *Basal forebrain*

BS ..... *Brainstem*

Ca^{2+} ..... *Bivalent calcium ion*

cAMP ..... Cyclic adenosine monophosphate

CNBD ..... Cyclic nucleotide binding domain

C-terminal ..... *Carboxy-terminal*

Cy3 ..... *Cyanine dye 3*

DFT ..... Discrete Fourier transform

DV ..... *Dorsal - ventral*

EEG ..... Electroencephalography

EMG ..... Electromyography

EPSP ..... *Excitatory postsynaptic potential*

FFT ..... Fast Fourier transform

GFP ..... Green fluorescent protein

GYG ..... Glycine-tyrosine-glycine

HCN channel ..... Hyperpolarization-activated cyclic nucleotide-gated cation channel

HEK293 ..... Human Embryonic Kidney 293

hSyn ..... *Human Synapsin*

HT ..... *Hypothalamus*

I_h ..... *Current produced by HCN channels*

IP ..... Intraperitoneal

I_T ..... *Current produced by calcium channels*

K^+ ..... *Monovalent potassium ion*

KCl ..... Potassium chloride

KH_2PO_4 ..... Dipotassium phosphate

KO ..... *Knockout*

L1 ..... *Line 1*

L2 ..... *Line 2*

ML ..... *Medial - lateral*

mRNA ..... Messenger ribonucleic acid

MS ..... *Medial septum*

N ..... *North*

Na^+ ..... *Monovalent sodium ion*

Na_2HPO_4 ..... Disodium phosphate

NaCl ..... Sodium chloride

NGS ..... *Normal goat serum*

NREM ..... Non-rapid eye movement

N-terminal ..... *Amino-terminal*

PBS ..... Phosphate-buffered saline

PCR ..... Polymerase chain reaction

REM ..... *Rapid Eye Movement*

S ..... *South, Segment*

SC ..... *Spinal cord*

SEM ..... Standard error of mean

SWDs ..... *Spike and wave discharges*

UV ..... Ultraviolet

WCM ..... *Water cross maze*

10 Appendix

10.1 Primer

10.1.1 HCN2 genotyping

Primer	Sequence
HCN2 14F	5‘-GGTCCCAGGCACTTCCATCCTTT-3‘
HCN2 15bR	5‘-GGAAAAATGGCTGCTGAGCTGTCTC-3‘
HCN2 16F	5’CAGCTCCCATTTGCCCTTGTGC-3‘

10.1.2 HCN2 EA and HCN2 FEA genotyping

Primer	Sequence
HCN2Genolxpfor	5’-AGTTGTACTCAACCAGTGGC-3’
HCN2Genolxprev	5’-TAGTCACGGTCACTGCCAAG-3’

10.2 Matlab™ scripts

10.2.1 EEG spectrogram plotting for staging purpose

Contents


```
function varargout = EEG(varargin)
```

GUI initializing code

```
gui_Singleton = 1;
gui_State = struct('gui_Name',       mfilename, ...
                   'gui_Singleton',  gui_Singleton, ...
                   'gui_OpeningFcn', @EEG_OpeningFcn, ...
                   'gui_OutputFcn',  @EEG_OutputFcn, ...
                   'gui_LayoutFcn',  [] , ...
                   'gui_Callback',   []);
if nargin && ischar(varargin{1})
    gui_State.gui_Callback = str2func(varargin{1});
end

if nargout
    [varargout{1:nargout}] = gui_mainfcn(gui_State, varargin{:});
else
    gui_mainfcn(gui_State, varargin{:});
end
```

Function will be executed when pushbutton is pressed

```
function pushbutton 'plot'_Callback(hObject, eventdata, handles)

tic
eeg = EbmRead('EEG.ebm');
emg=EbmRead('EMG.ebm');
```

Calculate spectrogram from EEG

```
[y, f, t, FStats]=mtcsglong(eeg ,4096*4,2000);
[ym, fm, tm, FStatsm]=mtcsglong(emg ,4096*4,2000);
```

Plot normalized spectra

```
subplot(2,1,1)
```

```
imagesc(t,f,20*log10(abs(sq(y(:,:,1))')));axis xy; colormap(jet)
colorbar
caxis([-70 40])
title('EEG')

subplot(2,1,2)
imagesc(tm,fm,20*log10(abs(sq(ym(:,:,1))')));axis xy; colormap(jet)
colorbar
caxis([-70 40])
title('EMG')

toc
```

Executes just before EEG is made visible

```
function EEG_OpeningFcn(hObject, eventdata, handles, varargin)
```

Choose default command line output for EEG

```
handles.output = hObject;
```

Update handles structure

```
guidata(hObject, handles);
```

Outputs from this function are returned to the command line

```
function varargout = EEG_OutputFcn(hObject, eventdata, handles)
```

Get default command line output from handles structure

```
varargout{1} = handles.output;
```

```
function Untitled_1_Callback(hObject, eventdata, handles)
```

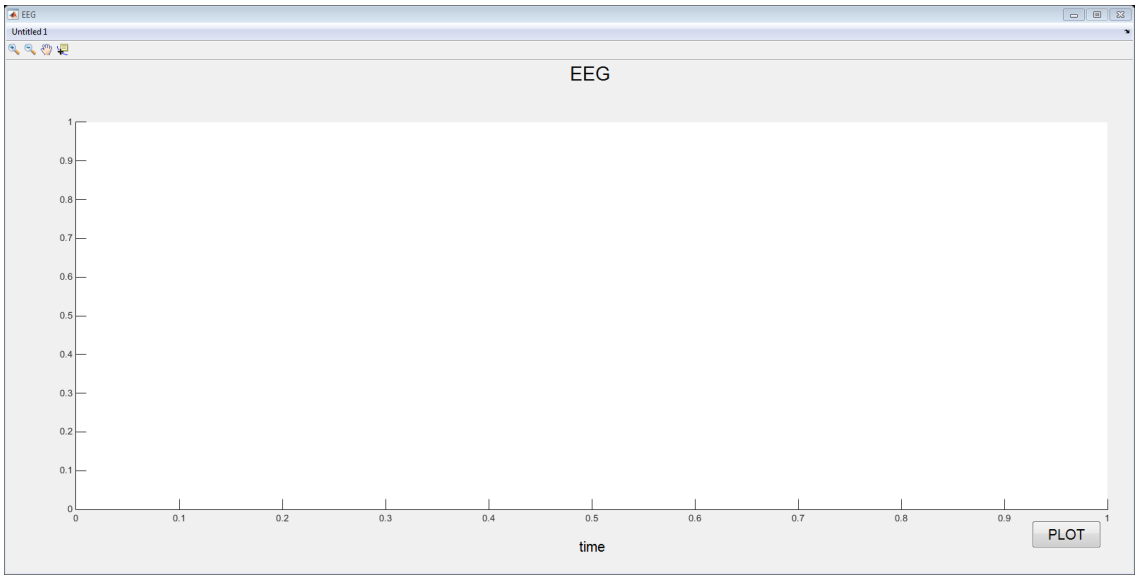
EEG
Untitled 1
EEG
1
0.9
0.8
0.7
0.6
0.5
0.4
0.3
0.2
0.1
0
0
0.1
0.2
0.3
0.4
0.5
0.6
0.7
0.8
0.9
1
time
PLOT

10.2.2 REM sleep staging

Contents


```
function [a,tot_rem]=REM(g);
```

Input: g = cell with REM data

REM duration

```
rem1 = zeros(1,0.5*length(g));
rem2 = zeros(1,0.5*length(g));

k=0;
for i=1:2:length(g)

k=k+1;
```

Extract values from cell; first 12h and second 12h (= light and dark phase)

```
if g(1,i).Position(1) <= 43200
rem1(k) = g(1,i).Position(1) - g(1,i+1).Position(1);

else
rem2(k) = g(1,i).Position(1) - g(1,i+1).Position(1);

end
end

rem1 =rem1(rem1~=0);
rem2 =rem2(rem2~=0);
tot_rem = [rem1 rem2]./60;


R_1 = sum(rem1);
R_2 = sum(rem2);

R=R_1 + R_2;
```

Calculate REM duration in min

```
rem_duration = R/60;
rem_dur1 = R_1/60;
rem_dur2 = R_2/60;
```

Calculate number of REM episodes

```
episodes = length(rem1) + length(rem2);
mean_rem_duration = (mean([ rem1 rem2]))/60; % min



a={'total REM', 'REM light', 'REM dark','number of REM Episodes', 'mean duration';...
 rem_duration rem_dur1 rem_dur2 episodes mean_rem_duration };

figure
hist(tot_rem,10)
```

10.2.3 REM sleep plot

Contents


```
function plotREM(g);

eeg = EbmRead('EEG.ebm');
```

Calculate and plot spectrogram

```
[y, f, t, FStats]=mtcsglong(eeg ,4096*4,2000);

Figure(1)
imagesc(t,f,20*log10(abs(sq(y(:,:,1))')));axis xy; colormap(jet)
colorbar
caxis([-70 40])
hold on
```

Plot REM phases

```
for i=1:2:length(g)

   x=[g(1,i).Position(1) g(1,i+1).Position(1)];
   y=ones(1,length(x));
   figure(1)
    plot(x,y,'b','LineWidth',8);
    hold on
end
```

10.2.4 Total sleep staging

Contents


```
function [a,tot_nrem]=NREM(h);
```

Input: h = cell with sleep data

Sleep duration

```
sleep1 = zeros(1,0.5*length(h));
sleep2 = zeros(1,0.5*length(h));

k=0;
for i=1:2:length(h)

k=k+1;
```

Extract values from cell; first 12h and second 12h (= light and dark phase)

```
if h(1,i).Position(1) <= 43200
sleep1(k) = h(1,i).Position(1) - h(1,i+1).Position(1);

else
sleep2(k) = h(1,i).Position(1) - h(1,i+1).Position(1);

end
end

sleep1 =sleep1(sleep1~=0);
sleep2 =sleep2(sleep2~=0);
tot_sleep = [sleep1 sleep2]./60;

R_1 = sum(sleep1);
R_2 = sum(sleep2);

R=R_1 + R_2;
```

Calculate Sleep duration in min

```
sleep_duration = R/60;
sleep_dur1 = R_1/60;
sleep_dur2 = R_2/60;

a={'total sleep', 'sleep light', 'sleep dark';...
 sleep_duration sleep_dur1 sleep_dur2};
```

```
figure
hist(tot_sleep,10)
```

10.2.5 NREM sleep plot

Contents


```
function plotNREM(g,h);
```

Input: g = cell with REM data

h = cell with sleep data

```
eeg = EbmRead('EEG.ebm');
```

Calculate and plot spectrogram

```
[y, f, t, FStats]=mtcsglong(eeg ,4096*4,2000);

figure(1)
imagesc(t,f,20*log10(abs(sq(y(:,:,1))')));axis xy; colormap(jet)
colorbar
caxis([-70 40])
hold on

a=[g,h];
```

Extract values from cell

```
for i=1:length(a)

    points(i)= a(1,i).Position(1);
end
```

Sort them

```
sleep=sort(points);
```

Calculate duration of NREM

```
for i=1:2:length(a)

    nrem (i)= sleep(i+1)-sleep(i);
```

```
end

for i=1:2:length(a)

   x=[sleep(i) sleep(i+1)];
   y=ones(1,length(x));
   figure(1)
    plot(x,y,'k','LineWidth',8);
    hold on
end
```

10.2.6 Wake vigilance staging

Contents


```
function [f,wake_power]=wake_EEG()
```

Calculate power of wake stage with medium – high activity

```
act=EbmRead('activity.ebm');
act_1=nan(1,8640);

t_act=linspace(0,86400,8640);
```

Moving average of activity

```
mov_av=tsmovavg(act,'s',18,1);

for i=1:1:8640
    if (mov_av(i)>=3)
        act_1(i)=1;
    end

end
```

Plot activity, moving average and analyzed wake phases

```
figure
plot(t_act,act,'k','LineWidth',1)
hold on
plot(t_act,act_1,'g','LineWidth',6)
hold on
plot(t_act,mov_av,'r','LineWidth',2)


title('Activity')
legend('activity','wake', 'Moving average')
```

Find indices of medium and high activity phases

```
indices=find(act_1==1);

low=round(indices.*10);

eeg = EbmRead('EEG.ebm');
```

```
[tot_power,f] = pwelch(eeg,4096,2048,4096,2000);
```

Mean power for normalization

```
meanPower = mean(tot_power);
```

Calculate power

```
k=0;
for j=1:length(low)-1
    k=k+1;
ab= eeg((low(j)*2000-6000):((low(j)*2000+6000)));

[Pxx,f]=pwelch(ab,4096,2048,4096,2000);
Pxx=Pxx/meanPower;
powi(k,1:length(Pxx))=Pxx;

end


wake_power = mean(powi);
```

10.2.7 Power spectra calculation in total and for each vigilance state

Contents


```
function [power]=EEG_Power(g,h)
```

Input: g = cell with REM data
h = cell with sleep data

Total power

Load EEG data

```
eeg = EbmRead('EEG.ebm');
```

Calculate total power using Welch´s method

```
[tot_power,f] = pwelch(eeg,4096,2048,4096,2000);
```

Normalize to mean power

```
meanPower = mean(tot_power);

total_power=tot_power/meanPower;
```

REM Power

```
points_rem=ones(1,length(g));
```

Extract indices

```
for i=1:length(g)

    points_rem(i)= g(1,i).Position(1);

end
```

```
len=length(g);
k=0;
```

```
for j=1:2:length(g)

k=k+1;
```

Calculate REM power two sec after REM starts and two sec before it ends

```
 [Pxx,f]=pwelch(eeg((points_rem(j+1)*2000+4000):(points_rem(j)*2000-
4000)),4096,2048,4096,2000);
```

Normalize to total power

```
Pxx=Pxx/meanPower;
```

Write power in matrix

```
rem_power(k,1:length(Pxx))=Pxx;
warning('off','all')
end
```

Calculate mean REM power in all REM episodes

```
REM_power = mean(rem_power);
```

NREM power

Combine REM and sleep data cells

```
a=[g,h];
```

Extract indices

```
for i=1:length(a)

    points_nrem(i)= a(1,i).Position(1);
end

sleep=sort(points_nrem);
```

If the first value equals zero replace it by 1/2000 (1/2000 * Fs =1)

```
if sleep(1) ==0
    sleep(1)=1/2000;
```

```
end
```

```
k=0;
for j=1:2:length(sleep)

k=k+1;
```

Calculate power of NREM episodes two seconds before NREM starts and two seconds before it ends

```
if ((sleep(j+1)*2000)-(sleep(j)*2000)) >= 4096
[Pxx,f]=pwelch(eeg((sleep(j)*2000+4000):(sleep(j+1)*2000-
4000)),4096,2048,4096,2000);
```

Normalize to total power

```
Pxx=Pxx/meanPower;
```

Write power in matrix

```
nrem_power(k,1:length(Pxx))=Pxx;
else
    k=k-1;
end
warning('off','all')
end

NREM_power = mean(nrem_power);
```

Wake power

```
[f,WAKE_power]=wake_EEG;
```

Figures

Plot power of REM, NREM, wake phases and total power

```
figure
subplot(2,2,1)
plot(f,REM_power,'k')
xlim([0 25])
ylim([0 300])
xlabel('Frequency');
ylabel('Power');
title('REM power')
```

```
subplot(2,2,2)
plot(f,NREM_power,'k')
xlim([0 25])
ylim([0 300])
xlabel('Frequency');
ylabel('Power');
title('NREM power')

subplot(2,2,3)
plot(f,WAKE_power,'k')
xlim([0 25])
ylim([0 200])
xlabel('Frequency');
ylabel('Power');
title('WAKE power')

subplot(2,2,4)
plot(f,total_power,'k')
xlim([0 25])
ylim([0 200])
xlabel('Frequency');
ylabel('Power');
title('total power')


power=[f REM_power' NREM_power' WAKE_power' total_power];
value = ['Frequency' 'REM power'  'NREM power'  'wake power' 'total power'];
```

10.2.8 Power spectra plot

Contents


```
function [REM, NREM, wake, total]=powerPlot(varargin)
```

Input: matrices with REM, NREM, wake and total power

```
l=length(varargin);

varargin{l+1}=zeros(length(varargin{1}'),5);
varargin{l+2}=zeros(length(varargin{1}'),5);
varargin{l+3}=zeros(length(varargin{1}'),5);
varargin{l+4}=zeros(length(varargin{1}'),5);
varargin{l+5}=zeros(length(varargin{1}'),5);

a=varargin{1};
b=varargin{2};
c=varargin{3};
d=varargin{4};
e=varargin{5};
f=varargin{6};
g=varargin{7};
```

REM power

```
REM=[a(:,2) b(:,2) c(:,2) d(:,2)  e(:,2)  f(:,2)  g(:,2)];
REM=REM(:,1:l);
meanREM = mean(REM');
REM_SEM = std(REM')/sqrt(l);
```

NREM power

```
NREM=[a(:,3) b(:,3) c(:,3)  d(:,3)  e(:,3)  f(:,3) g(:,3)];
NREM=NREM(:,1:l);
meanNREM = mean(NREM');
NREM_SEM = std(NREM')/sqrt(l);
```

wake power

```
wake=[a(:,4) b(:,4) c(:,4)  d(:,4)  e(:,4)  f(:,4) g(:,4)];
wake=wake(:,1:l);
```

```
meanWake = mean(wake');
Wake_SEM = std(wake')/sqrt(l);
```

total power

```
total=[a(:,5) b(:,5)  c(:,5) d(:,5)  e(:,5)  f(:,5) g(:,5)];
total=total(:,1:l);
meantotal = mean(total');
total_SEM = std(total')/sqrt(l);
```

Extracting frequency

```
f=a(:,1);
```

Figures

```
figure(1)
title ('REM Power')
hold on
errorbar(f(1:53),meanREM(1:53),REM_SEM(1:53),'r');
hold on
xlim([0 25]);
xlabel ('Frequency')
ylabel('Power % total power');
hold on


figure(2)
title ('NREM Power')
hold on
errorbar(f(1:53),meanNREM(1:53),NREM_SEM(1:53),'r');
hold on
xlim([0 25]);
xlabel ('Frequency')
ylabel('Power % total power');
hold on

figure(3)
title ('wake Power')
hold on
errorbar(f(1:53),meanWake(1:53),Wake_SEM(1:53),'r');
hold on
xlim([0 25]);
xlabel ('Frequency')
ylabel('Power % total power');
hold on


figure(4)
title ('total Power')
```

```
hold on
errorbar(f(1:53),meantotal(1:53),total_SEM(1:53),'r');
hold on
xlim([0 25]);
xlabel ('Frequency')
ylabel('Power % total power');
hold on
```

10.2.9 Identification of state transitions

Contents

Load stages (= variable I)

```
load 'stage_45217_EA.mat'
I=I';
```

Preallocate variables

```
Z1=ones(1,8);
Z2=ones(1,8).*2;
min=7;
max=30;
index=1;
Location=[];
numofone = [];
numoftwo = [];
```

```
for i=(min+1):length(I)-8
```

Find transitions from one vigilance stage to another

```
    if I(i)==1 & I(i+1)==2
```

Check if at least 8 epochs before transition = 1 and at least 8 epochs after transition = 2

```
        if I(i-min:i)==Z1 & I(i+1:i+min+1)==Z2
```

Safe location of transition

```
            Location(index)=i;
            numofone(index)=0;
            numoftwo(index)=0;
```

Count number of ones (max. 30) before transition

```
            for j=i:-1:i-(max-1)
                if I(j) == 1
```

```
                    numofone(index) = numofone(index) + 1
                else
                    break
                end
            end
```

Count number of twos (max. 30) after transition

```
            for j=i+1:i+max
                if I(j) == 2
                    numoftwo(index) = numoftwo(index) + 1
                else
                    break
                end
            end
               index=index+1;
        end

    end
end
```

10.2.10 Calculation of power values at state transitions

Contents

Load theta power values (= variable C)

```
load ('theta_45217_EA.mat')
C=C';
    Location
data = {};
```

Extract power data at location of transition

```
for j=1:length(Location)
    data{j}{1} = C(Location(j):-1:Location(j)-numofone(j)+1);
    data{j}{2} = C(Location(j)+1:Location(j)+numoftwo(j));
end
```

Preallocate of variables

```
means_ones = {};
means_twos = {};

for i=1:30
    means_ones{i} = zeros(1,length(numofone));
    means_twos{i} = zeros(1,length(numoftwo));
end
```

Length of data equals number of transitions

```
for block = 1:length(data)
```

Rewrite cells with power (adjust dimensions)

```
    for position = 1:length(data{block}{1})
        means_ones{position}(block) =  data{block}{1}(position);
    end
    for position = 1:length(data{block}{2})
        means_twos{position}(block) =  data{block}{2}(position);
    end
end

merke = means_twos;
```

Remove zeros and take mean of power

```
for position = 1:length(means_ones)
    means_ones{position} = mean(means_ones{position}(means_ones{position} ~= 0));
end
for position = 1:length(means_twos)
    means_twos{position} = mean(means_twos{position}(means_twos{position} ~= 0));
end
```

10.3 Publication

Peer reviewed article

- Grimm, C., Holdt, L. M., Chen, C. C., Hassan, S., Muller, C., Jors, S., Cuny, H., Kissing, S., Schroder, B., Butz, E., Northoff, B., Castonguay, J., Luber, C. A., Moser, M., **Spahn, S.**, Lullmann-Rauch, R., Fendel, C., Klugbauer, N., Griesbeck, O., Haas, A., Mann, M., Bracher, F., Teupser, D., Saftig, P., Biel, M. and Wahl-Schott, C. , *High susceptibility to fatty liver disease in two-pore channel 2-deficient mice.* Nat Commun, 2014. **5**: p. 4699.

10.4 Acknowledgments

Ich möchte **Herrn Prof. Biel** danken für die Möglichkeit, diese Arbeit in seinem Arbeitskreis durchführen zu können und für das schnelle Korrekturlesen meiner Doktorarbeit.

Ich danke **Herrn Prof. Christian Wahl** für die Aufnahme in den Arbeitskreis, für die Bereitstellung meines Themas, die Betreuung und die wissenschaftlichen Ratschläge.

Bedanken möchte ich mich auch bei **PD Dr. Carsten Wotjak**, dafür dass er als mir TAC Member immer mit Rat und Tat zur Seite stand.

Ich danke Herrn **Prof. Sirota** für seinen Input und seine Unterstützung bei der Matlab Auswertung.

Dankbar für die finanzielle Unterstützung und die Möglichkeit an vielen Seminaren teilnehmen zu können, bin ich der **Graduate School for Systemic Neuroscience**.

Mein Dank allen, die mich während meiner Zeit unterstützt haben und viel Freude in den Alltag gebracht haben.

Verena, vielen Dank für deine tatkräftige Unterstützung bei allen EEG-OPs. **Melli**, die Geno-Göttin, vielen Dank, ohne dich wäre so manche KO-Maus nicht von einem WT unterscheidbar gewesen. **Vanessa**, vielen Dank, dass ich deine Kamera für die tollen Bilder nutzen konnte. **Elisabeth**, danke, dass du mich unterstützt hast, bisweilen Licht ins T1/T1 Neuronen Chaos zu bringen. **Paparazos**, danke, für die vielen witzigen Momente mir dir im Elite Lab. **Prakti**, danke für deine Geduld, die du in meiner ersten Zeit mit mir aufbringen musstest und **Rasmus**, danke, einfach für deine unglaubliche Art.

Ganz speziell hervorheben möchte ich fünf wunderbare Freunde, die immer für mich da waren und mit denen ich während meiner Zeit unendlich viel Lachen aber auch Leid teilen konnte.

Franz, dir bin ich zu größtem Dank verpflichtet. Dein Einsatz bei der Cyto-Optimierung und deine Matlab-Hilfe, um nur zwei kleine Beispiele zu nennen, war überragend. Es ist sehr toll, dich auf meinen letzten Metern noch als Freundin gewonnen zu haben. Herzlichen Dank.

Kika, Mitstreiterin und Nachbarin der (fast) ersten Stunde. Dir danke für die vielen lustigen, aber auch manchmal leidvollen täglichen Momente im Elite Lab. Du hast meine Launen und

Motzereien immer ertragen müssen und wurdest in schwierigen Zeiten nicht müde mich zu trösten. Es war immer schön, dich neben mir zu wissen. Tausend Dank.

Henne, mein Partner auf dem Neuro Sektor, dir danke ich für den regen wissenschaftlichen Austausch und das Austüfteln unserer Geschichte bis hin zur „Cell Story". Und noch viel wichtiger für die vielen spaßigen Abende und dein jederzeit offenes Ohr. Vielen Dank.

Dr. Hassaaan, bei dir bedanke ich mich für deine Ausdauer mich immer zu Höchstleistungen anspornen zu wollen und dafür, dass du bei Bedarf stets zur Stelle warst, um mich zu kritisieren, konstruktive Vorschläge zu machen und vor allem, um mit mir zu Lachen. Vielen Dank für die meist tolle und lustige Zeit mit dir, ohne dich hätte ich alles nicht halb so gut überstanden.

Krauso, bei dir möchte ich mich bedanken für die vielen erheiternden und amüsanten Momente und für alle bewährten Krause - Tipps & Tricks, ich denke mit Schrecken an unsere erste Maushaus-Session zurück. Schön, dass es dich gibt.

Mein letzter und wichtigster Dank gilt den Besten. **Niels**, **Mama & Papa** und **Tobias** einfach Danke für alles!